PATHOBIOLOGY OF NEUROINFLAMMATION AND BASAL GANGLIA CIRCUITRY IN PARKINSON'S DISEASE

by

Jonathan Matthew Wilson

A Dissertation

Submitted to the Faculty of Purdue University

In Partial Fulfillment of the Requirements for the degree of

Doctor of Philosophy

Department of Biological Sciences

West Lafayette, Indiana

May 2017

THE PURDUE UNIVERSITY GRADUATE SCHOOL
STATEMENT OF DISSERTATION APPROVAL

Dr. Cynthia V. Stauffacher, Chair
Department of Biological Sciences
Dr. Teri L. Belecky-Adams
Department of Biological Sciences
Dr. Kalpana M. Merchant
Department of Biological Sciences
Dr. Hong Wang
Department of Biological Sciences
Dr. Anthony J. Baucum II
Department of Biological Sciences
Dr. Ellen A. G. Chernoff
Department of Biological Sciences
Dr. Xianzhong Wang
Department of Biological Sciences

Approved by:

Dr. Stephen F. Konieczny (PWL) and Dr. Stephen K. Randall (IUPUI)
Head of the Departmental Graduate Program

This is dedicated to Jenny and Louie

ACKNOWLEDGMENTS

I would like to express my deepest gratitude to Dr. Teri Belecky-Adams. I am grateful for her constant encouragement, guidance and willingness to continue training me through the years. In the same way, I would like to sincerely thank Dr. Kalpana Merchant for her instructive guidance and the confidence she has in me as a scientist. The work presented in this dissertation would not have been possible without their unending support. I would also like to extend my sincere appreciation to my committee chair, Dr. Cynthia Stauffacher, for her involvement and time she has invested in me during the completion of this dissertation. I offer a heartfelt thank you to my committee members, Dr. AJ Baucum, Dr. Ellen Chernoff and Dr. Hong Wang for countless beneficial discussions relating to their seemingly endless background knowledge and expertise, their wisdom regarding experimental details and their overall insight relating to my Ph.D. projects. I greatly appreciate and value the numerous scientists I have interacted and collaborated with on these projects. I hope to continue working with you and show my appreciation to you all.

TABLE OF CONTENTS

LIST OF TABLES

LIST OF FIGURES

LIST OF ABBREVIATIONS

α-synuclein	Alpha-synuclein
ANOVA	Analysis of variance
BAC	Bacterial artificial chromosome
BCA	Bicinchoninic acid
BSA	Bovine serum albumin
cAMP	Cyclic adenosine monophosphate
cGMP	Cyclic adenosine monophosphate
ChIP	Chromatin immunoprecipitation
CNS	Central nervous system
COMT	catechol-O-methyl transferase
DBS	Deep brain stimulation
DLS	Dorsal lateral striatum
DMEM	Dulbecco's modified eagle medium
DMS	Dorsal medial striatum
E16.5	Embryonic day 16.5
ELISA	Enzyme linked immunosorbent assay
FDR	False discovery rate
FPKM	Fragments per kilobase per of transcript per million mapped reads
GABA	Gamma-Aminobutyric acid
Gapdh	Glyceraldehyde 3 phosphate dehydrogenase
GPCR	G-protein-coupled receptor

GWAS	Genome-Wide Association Study
IBA1	Ionized calcium binding adapter molecule 1
IL-1β	Interleukin-1 beta
IP	intraperitoneal
KO	Knock-out
LDH	Lactate dehydrogenase
L-DOPA	Levodopa
LPS	Lipopolysaccharide
MAO-B	monoamine oxidase B
Mm9	Mus musculus 9
MSD	Mesoscale discovery
MSN	Medium spiny neuron
MWCO	Molecular weight cut-off
NG2	Neuron-glial antigen 2
OCT	Optimal cutting temperature compound
P0	Postnatal day 0
PBS	Phosphate buffer saline
PD	Parkinson’s disease
PDE	Phosphodiesterase
PDE10i	Phosphodiesterase 10A inhibitor
PDL	Poly-d-lysine
PE	Phycoerytherin
PMSF	phenylmethylsulfonyl fluoride

PO	by mouth
PVDF	Polyvinylidene fluoride
RIN	RNA integrity number
RPM	Rotations per minute
RT-qPCR	Reverse transcription-quantitative polymerase chain reaction
SDS-PAGE	Sodium dodecyl sulfate polyacrylamide gel electrophoresis
SN	Substantia nigra
SNARE	Soluble NSF Attachment Protein Receptor
TBST	Tris-buffered saline, 0.05% Tween
TEM	Transmission electron microscopy
TLR2	Toll like receptor 2
TNFα	Tumor necrosis factor alpha
Trem2	Triggering receptor expressed on myeloid cells 2

ABSTRACT

Author: Wilson, Jonathan, M. Ph.D.
Institution: Purdue University
Degree Received: May 2017
Title: Pathobiology of Neuroinflammation and Basal Ganglia Circuitry in Parkinson's Disease.
Major Professor: Teri L. Belecky-Adams

Parkinson’s disease (PD) is the second most common neurodegenerative disease worldwide and the most common movement disorder. A defining pathologic feature of PD is the progressive death of dopaminergic neurons in a basal ganglia nucleus termed the substantia nigra (SN). Another hallmark feature of PD pathology is the presence of Lewy bodies and Lewy neurites, which are cellular inclusions with aggregated protein depositions, representing pathology in neuronal cell bodies and neuritic processes. Recently, epidemiological and genetic studies support roles for neuroinflammation in the progression of PD. Two types of cells that play a critical role in regulating neuroinflammation are microglia and astrocytes, which are activated in the basal ganglia of PD patients. Studies within this dissertation characterized activation of microglial cells by alpha-synuclein (α-synuclein), the most abundant protein in Lewy bodies, which has been implicated in PD pathogenesis. To garner insights into molecular mechanisms associated with astrocyte proliferation and activation, genomic alterations during developmental stages of astrocytes were examined since they are likely to recapitulate the reactivity associated with gliosis in PD brain. The activation of these glial cells and pathology of neurons in the basal ganglia causes the hallmark symptoms of PD. The symptoms of PD are termed parkinsonism. These are thought to result, at least in part, from alterations in the balance of output of the neostriatal efferent neurons, due to the

loss of dopaminergic neuronal innervation of these cells. Phosphodiesterase 10A (PDE10A) is preferentially expressed in neostriatal efferent pathways and PDE10A inhibitors (PDE10i) have been shown to target dopamine signaling mechanisms. Studies here have utilized PDE10i to understand the balance of activation of medium spiny neurons in the indirect pathway versus activation of the direct pathway, since recent findings show PDE10i lead to a decrease in thalamic drive to the motor cortex, a primary symptom of PD. In conclusion, the aims of this dissertation sought to identify neuroinflammatory mechanisms within activated microglia in response to α-synuclein and proliferating astrocytes. Also, this work evaluated an inhibition of PDE10A in neurons within a region important to the progression of PD.

CHAPTER 1: INTRODUCTION

Objectives

The purpose of studies described here is to enable the characterization of neuroinflammation mediated by alpha-synuclein (α-synuclein), a pathological molecule in Parkinson's disease (PD). Several lines of evidence implicate α-synuclein in this disease; however few experiments have identified key signatures of the direct toxic effect of α-synuclein in microglial cells while incorporating appropriate monomeric controls. Also, while it is known that astrocytes undergo de-differentiation and proliferation during reactive gliosis, it is not understood whether reactive gliosis has a representative expression profile or genomic modifications of a particular stage of development or if signaling pathways labeled "inflammatory" play a role in astrogenesis. Since current studies in the literature relating to astrogenesis analyses have many technical caveats, further systematic analyses of radial glial cells and astrocytes during proliferation and differentiation stages are warranted. Lastly, phosphodiesterase 10A (PDE10A) inhibitors (PDE10i) have been shown to activate cells within the neostriatum, a region of the brain associated with PD pathology. Studies here utilize PDE10i as a tool to further characterize the basal ganglia circuitry affected by PD pathology.

The central hypothesis of this dissertation is that aggregated α-synuclein initiates an inflammatory cascade via activation of microglial cells and astrocytes that result in a feed-forward pathogenic mechanism. The feed-forward, dysregulated inflammatory cascade, in turn, results in de-differentiation of the astrocyte cells, causing further

propagation of pathophysiology. Ultimately, this process contributes to cell death, including the loss of dopaminergic cells in the substantia nigra (SN), which define PD. This results in an overall decrease of motor circuitry causing the symptoms of PD. Specifically, an increase in the activity of the indirect pathway leads to a decrease in thalamic drive to the motor cortex. Inhibition of PDE10A enzyme will preferentially activate the indirect pathway, with a relatively smaller activation of the direct pathway because of a differential inhibition of PDE10A in the medium spiny neurons (MSNs) (Figure 1).

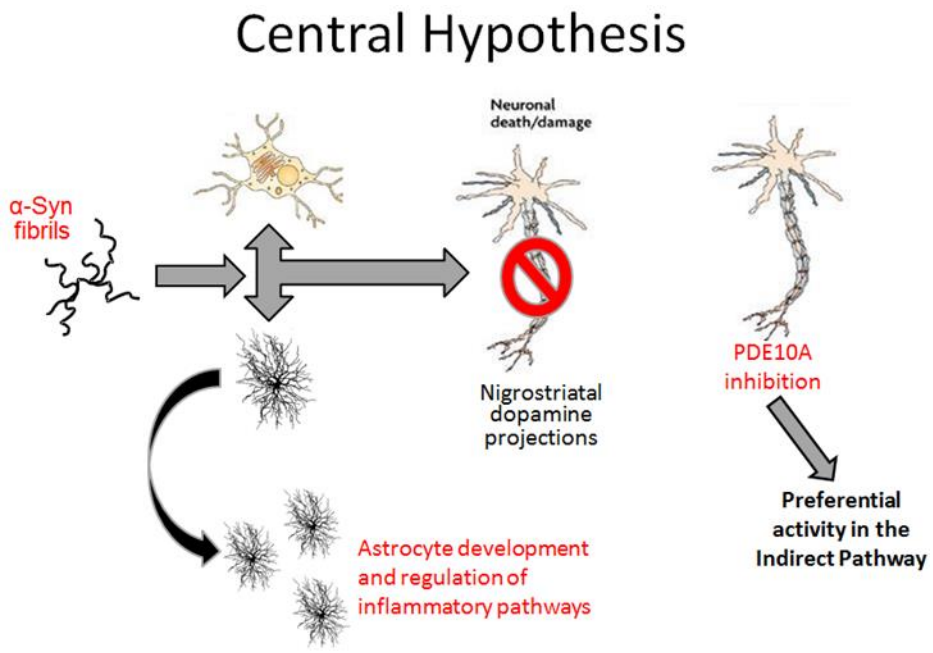

Figure 1: Central Hypothesis

To test this hypothesis, the following objectives were defined:

1. Determine the inflammatory effects of α-synuclein on microglia and astrocytes

2. Determine gene transcripts in proliferative astrocytes / radial glia and astrocyte precursor cells to understand genes and pathways that are important when astrocytes are proliferating and differentiating
3. Determine genes associated with acetylated histones in proliferating astrocytes / radial glia and astrocyte precursor cells to understand one of the aspects of gene regulation associated with the proliferation and differentiation of astrocytes
4. Determine acute PDE10i effects on neuronal activation in the brain to better understand activation within the motor cortex
5. Determine the role of PDE10i in the D1 direct and D2 indirect pathway to better understand the overall decrease in motor cortex activation

This set of objectives represents a unique exploration of the downstream effects of molecules abundantly expressed in the CNS, and the resulting dataset has helped define hypotheses for future therapeutic agents targeting α-synuclein and PDE10A.

Organization

This dissertation provides a literature review (Chapter 2) to orient the reader to the field of neuroinflammation and basal ganglia circuitry as it pertains to PD. Materials and methods used in this research are described in Chapter 3. Data acquired throughout this research are presented in the ensuing four chapters, each of which contains an independent introduction and discussion. Chapter 4 summarizes data describing the role of α-synuclein related effects in microglia and astrocytes, with emphasis on the context of

inflammation. Chapter 5 describes transcriptomic findings related to astrogenesis, while Chapter 6 describes histone acetylation modifications related to astrogenesis. Chapter 7 summarizes the effects of PDE10i on neuronal activation within the neostriatum. Chapter 8 articulates future directions based on the current work and how this data along with current literature is foundational for future experiments.

CHAPTER 2: LITERATURE REVIEW

Parkinson's Disease

Parkinson's disease (PD) is second only to Alzheimer's disease as the most common neurodegenerative disease worldwide. Conservatively estimated, not accounting for the undiagnosed population, PD prevalence is approximately 0.3% of the general population in the United States (US). These rates decrease to 0.02% of people younger than 45 and increase to 1.2% of people older than 70, indicating that age is the major risk factor of PD. An estimated 630,000 people in the US have been diagnosed with PD in 2010, which is approximately 10% of the worldwide PD population. Projections that account for demographic changes and an aging population suggest that the US diagnosed patients will reach 819,000 by 2020, 1.06 million by 2030, 1.24 million by 2040, and 1.34 million by 2050, if no disease modifying treatment is found (Kowal et al, 2013). Therefore, it is critical to understand PD pathophysiology and thereby identify disease modifying therapeutic approaches.

Pathology of Parkinson's Disease: Dopamine Neuronal Cells, Inflammation and Lewy bodies

A defining pathologic feature of PD is death of dopaminergic neurons in a basal ganglia nucleus termed the substantia nigra (Ehringer & Hornykiewicz, 1960; Hirsch et al, 1988). These neurons project to the neostriatum, which helps to regulate the voluntary movement via the extrapyramidal motor system (Figure 2, Young & Penney, 1984). The precise cause of cell death is unknown, however inflammation and protein clearance

deficits, such as proteosomal and lysosomal dysfunction, have been implicated (Zhou & Lim, 2009).

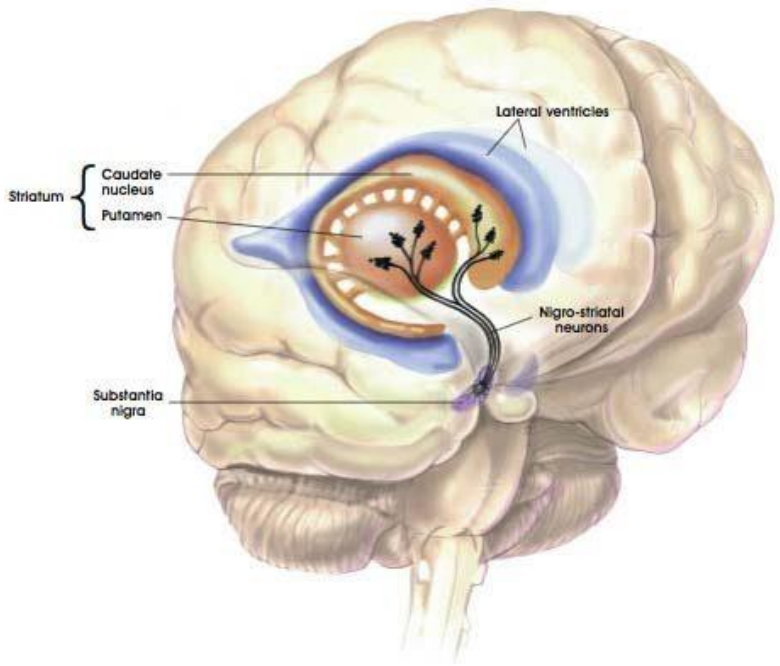

Figure 2: Dopamine neurons in the substantia nigra project to the neostriatum Substantia nigra regions (purple) at the base of the brain contain cells that project nigrostriatal projections (black arrows) into the collective striatum regions (red), made up of the caudate nucleus and the putamen

Imaging studies of PD patients using a positron emission tomography tracer, PK11195, have provided the evidence of activated resident immune cells throughout the basal ganglia including the SN (Bartels & Leenders, 2007; Gerhard et al, 2006). Further support for neuroinflammation associated with PD comes from post-mortem brain studies that have shown higher levels of neuroinflammatory cytokines associated with the presence of activated microglia in the SN (Brooks, 2005; Tansey & Goldberg, 2010). The current belief is that inflammatory processes during microglia polarization contribute to

the progression of PD through increased NFκβ activity and the apoptosis pathway (Gardet et al, 2010; Wang et al, 2015).

Another hallmark feature of PD pathology is the presence of Lewy bodies and Lewy neurites, which are cellular inclusions with aggregated protein depositions, representing pathology in neuronal cell bodies and neuritic processes, respectively (Figure 3, Spillantini et al, 1998; Toulorge et al, 2016).

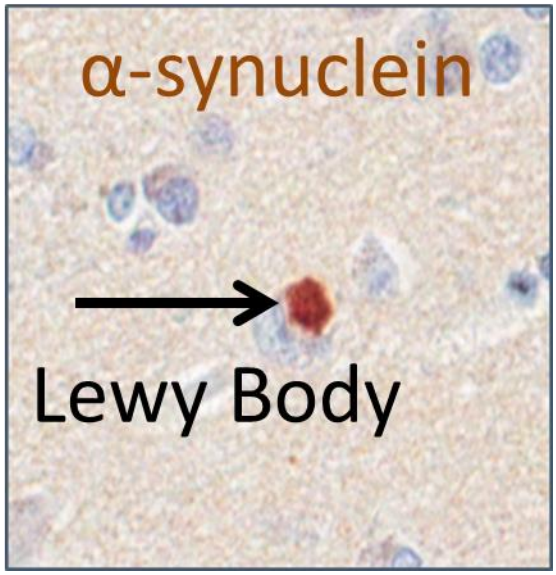

Figure 3: Lewy body
The black arrow points to a Lewy body (round dense inclusion) labeled with alpha-synuclein immunohistochemistry (brown) and nuclear counterstain using hematoxylin (blue).

The regional propagation pattern of Lewy bodies has been mapped and used by Braak *et al*. (Braak et al, 2003) to define 6 different, slowly progressing, pathological stages of PD. Lewy bodies may contain as many as 156 unique proteins (Leverenz et al, 2007), the most abundant being a protein termed alpha-synuclein (α-synuclein) which aggregates when misfolded. A deficit in protein clearance mechanisms is believed to underlie the

accumulation of misfolded proteins in Lewy bodies and Lewy neurites. Recent studies have uncovered a prion-like pathological mechanism of α-synuclein, which can be released, then taken up by nearby cells as a mechanism to propagate new Lewy body formation (Luk et al, 2012a; Luk et al, 2012b; Mougenot et al, 2012).

Etiology and the Genetics of Parkinson's Disease

Idiopathic PD accounts for more than 90% of all PD cases (Gilgun-Sherki et al, 2004). A number of loci and specific gene mutations causing familial PD have been identified in recent years, which have begun to provide insights into the etiologic mechanisms of PD (reviewed by Cookson et al, 2008). On the other hand, the biologic mechanisms underlying idiopathic PD remain hypothetical. One hypothesis states aggregated protein deposition is toxic to neurons, while the other hypothesis proposes mitochondrial dysfunction and oxidative stress as the key neurodegeneration event (reviewed by Dauer & Przedborski, 2003). The major risk factor for idiopathic PD is age, but recent genome-wide association studies (GWAS) have been shedding light on genetic risk factors. Polymorphic variants in the *SNCA* gene, that encodes for α-synuclein, are genetic risk factors of PD identified by multiple GWAS (Klein & Ziegler, 2011; Simon-Sanchez & Singleton, 2008). An interaction between genetic susceptibility and environmental factors, such as age and pesticide exposures, may explain the majority of idiopathic PD etiology (Gao & Hong, 2011). Interestingly, point mutations (A30P, E46K and A53T), duplications and triplication in the *SNCA* gene cause PD that has an earlier age of onset (Singleton et al, 2003). By and large, the mutated forms of α-synuclein aggregate at a higher rate (Taschenberger et al, 2012). The convergence of the presence of aggregated

α-synuclein in Lewy body pathology of PD and genetic etiology impinging on α-synuclein mutations and polymorphisms has led to the tremendous focus on studying the physiological and pathological role of α-synuclein (Dexter & Jenner, 2013).

Alpha-Synuclein

The discovery of α-synuclein was made over 20 years ago, but its precise function still remains unknown (Jakes et al, 1994; reviewed by Ottolini et al, 2017). The human protein is a 140 amino acid heat-stable, soluble protein with an acidic C-terminal and 6 repeats of KTKEGV on the N-terminus with an internal portion that is required for aggregation. It has a high affinity for lipids and associates with a variety of lipid membranes, including presynaptic vesicles and mitochondria (Galvagnion et al, 2015). Consistent with this binding, α-synuclein is implicated in regulating vesicle trafficking and soluble NSF attachment protein receptor (SNARE) complex assembly, as well as mitochondrial membrane/Complex I binding and inhibition (Ahmad et al, 2007; Fujita et al, 2012; Marques & Outeiro, 2012; Trojanowski & Lee, 2002).

A number of post-translational modifications have been reported on various amino acids in the α-synuclein sequence and are thought to contribute to its aggregation (Barrett & Timothy Greenamyre, 2015). These include phosphorylation of serine at the 129 and 87 amino acid sites, phosphorylation and nitration of tyrosine residues and sulfoxidation of n-terminal methionine. Also, oxidation of methionine prevents fibrillation and promotes formation of oligomers, which may contribute to the mechanism causing increased toxicity of the oligomers (Cole et al, 2005; Hokenson et al, 2004; Zhou et al, 2010a).

As mentioned above, α-synuclein is one of the most abundant proteins contained in Lewy bodies (Leverenz et al, 2007). In fact, in addition to PD, dementia with Lewy bodies and multiple system atrophy are neurodegenerative diseases defined by Lewy body pathology and are collectively termed synucleinopathies (Lim et al, 2016). The precise pathologic structure of α-synuclein that underlies PD remains a point of conjecture, but it has been proposed that soluble oligomeric forms of the protein may be more toxic than the large fibrillar, insoluble deposited forms (Kramer & Schulz-Schaeffer, 2007; Leverenz et al, 2007). On the other hand, deposition of fibrillar α-synuclein may initiate neuroinflammation during clearance of the deposits by glial cells (Beraud et al, 2013).

Various diverse and heterogeneous forms of α-synuclein could cause toxicity (Hashimoto et al, 2004; Lashuel et al, 2013; Luna & Luk, 2015). Oligomers and large aggregates could both be toxic to different types of cells in different conditions. Fibrils found in Lewy Bodies are typically 12–15 nm wide, however short proto-fibrils and spherical oligomers (ranging from 25-150 α-synuclein molecules) both containing β-sheet conformation, exist in Lewy Bodies (Conway et al, 2001; Norris et al, 2005)

Large fibrils have been shown to be toxic. In culture, fibrillar α-synuclein exposure induced 1000-fold greater cell death than the oligomeric forms of α-synuclein (Pieri et al, 2012). Also, α-synuclein fibrils have been shown to be toxic when binding to cell membranes reducing membrane integrity (Pieri et al, 2016; Shrivastava et al, 2015). On the other hand oligomers and short proto-fibrils have been shown to be toxic *in vitro* and *in vivo* altering membrane permeability and increasing of calcium influx, triggering cell

death of dopamine neurons (Campioni et al, 2010; Conway et al, 2000; Winner et al, 2011). Data have shown that oligomers cause toxicity by damaging lysosomal membranes, mitochondrial membranes while increasing oxidative stress (Hsu et al, 2000), or disrupting microtubule transport (Alim et al, 2004) or axonal transport of synaptic proteins leading to a dysfunctional synapse (Scott et al, 2010). Also, oligomers are thought of as intermediates on the pathway from monomer to fibril, however "off-pathway" oligomers have been discovered to be trapped, unable to form fibrils or degrade to monomers (Chen et al, 2015; Lorenzen et al, 2014). It is also possible that concentrations of intermediates increase as fibrils aggregate in cells, which increases the oligomeric-mediated toxicity (Cremades et al, 2012).

Pathophysiology of Parkinson's Disease: Neuroinflammation and Glial Cells

As stated above, neuroinflammation is a key feature of PD. There are two types of cells that play a critical role in regulating neuroinflammation: microglia and astrocytes. Microglia, 10% of all glial cells, normally function in synaptic pruning, scavenging for intruders or cleaning up neuronal cell debris (Sanchez-Guajardo et al, 2013b). However, during the progression of PD, local microglia will respond to α-synuclein aggregation, neuronal cell death, presence of reactive oxygen species and presence of cytokines, such as tumor necrosis factor-alpha (TNFα) and interleukin-1 beta (IL-1β) (Tansey & Goldberg, 2010). The response of the local microglia may include the release of anti-inflammatory as well as pro-inflammatory cytokines, which in turn affect nearby cells such as the astrocytes and neurons (Bruck et al, 2016).

In PD brains, microglia and astrocytes come into contact with α-synuclein (Shrivastava et al, 2016). A number of studies have been carried out to understand α-synuclein-dependent regulation of glial cell functions. For example, neuron-released, oligomeric α-synuclein has been shown to activate microglial cells through Toll-like receptor 2 (TLR2) (Kim et al, 2013). Transgenic mice over-expressing α-synuclein can form aggregates *in vivo*, and when injected with lipopolysaccharide (LPS), there is a synergistic pathologic effect of inflammation, possibly through the LPS inflammatory action on microglia and subsequent TLR2 up-regulation *in vivo* (Laflamme et al, 2001). This demonstrates a prominent role of α-synuclein aggregation and inflammation in pathogenesis of PD (Gao et al, 2008). However, the current literature has not systematically studied the concentration response or time course of inflammation inducing effects of monomeric and aggregated α-synuclein. There is also paucity of data characterizing α-synuclein effects on microglia and investigating whether these cells could act synergistically to enhance neuroinflammation-mediated toxicity.

Astrocytes and Proliferative Reactive Gliosis

Astrocytes, like microglia, have a multitude of roles in the developing nervous system and are becoming increasingly more important as a factor underlying many diseases when these roles are impaired. They can act as neural stem cells within subpopulations of brain regions during development, regulate cerebral blood flow at the vascular interface, store glycogen, transport water, take in extracellular potassium during intense synaptic functions and regulate synapses by the uptake of excess extracellular neurotransmitters (Halassa et al, 2007; Rossi & Volterra, 2009). Astrocytes are the most abundant glial cell

in the adult mammalian brain. Recent analysis of astrogenesis indicates that these cells are primarily generated in the postnatal rodent central nervous system (CNS, Bandeira et al, 2009). The most common contributing sources of astrocyte production are radial glial cells, which transform into astrocyte progenitors cells, and proliferating sub-ventricular zone astrocyte progenitors (Ge et al, 2012; Magavi et al, 2012). Neuron-glial antigen 2 (NG2)-positive glia provide ventral brain regions with a small percentage of astrocytes (Guo et al, 2009; Zhu et al, 2008). Astrocyte progenitor cells contribute small numbers of astrocytes during the first postnatal day (P0-P1), however these cells proliferate 6 to 8 fold by the end of the first postnatal week (P7-P8, Ge et al, 2012). A large portion of astrocytes are produced during these stages, although these cells continue to locally generate the remainder of astrocytes in the adult brain (Ge & Jia, 2016).

Radial glial cells retain their cell bodies in the ventricular zone, where they asymmetrically divide (Yamaguchi et al, 2016). Cell division gives rise to a radial glial cell and a progenitor cell, which will migrate into the outer layers and mature or proliferate further. Basic helix-loop-helix transcription factors play roles in fate determination of the progenitor cells, which express Hes1 during the astrogenesis stages (Imayoshi & Kageyama, 2014). Radial glial cells share many properties with astrocytes including expression of extracellular proteins, namely GLAST (Gotz et al, 2015). GLAST (Glutamate Aspartate Transporter) is expressed on the cell surface of a large majority of early postnatal transforming radial glia and astrocytes in the brain and spinal cord (Chaudhry et al, 1995; Jungblut et al, 2012; Lehre et al, 1995; Shibata et al, 1997;

Zhou et al, 2006), which makes it an excellent candidate marker to utilize when acutely isolating these cells from brain (Jungblut et al, 2012).

In most central nervous system (CNS) diseases or injuries, astrocytes enter a state termed reactive gliosis, in which astrocytes become hypertrophic, stop performing their supportive functions, de-differentiate and in some cases proliferate (de Chevigny et al, 2008; Yu et al, 2006). In moderate to severe cases of gliosis, astrocytes have been shown to secrete molecules such as TNFα and IL-1β, which activate microglia (Medeiros & LaFerla, 2013). The role of astrocytes in PD is not well understood. One hypothesis proposes that astrocytes, as a result of cellular stress, release cytokines, which regulate peripheral immune cells, resulting in a feed-forward mechanism, maintaining neuroinflammation and contributing to PD progression (Sanchez-Guajardo et al, 2013b).

Regardless of specific disease pathologies, reactive glia appear to undergo de-differentiation, leading to a loss of function. If the inflammatory state continues unchecked for long periods of time, the astrocytes (along with other cells) will coalesce to form a permanent barrier referred to as a glial scar. While it is appreciated that the cells undergo de-differentiation it is not understood whether reactive gliosis is representative of a particular stage of development brought about by mediators of inflammation. It is also not clear whether signaling pathways labeled “inflammatory” might also play normal roles in the differentiation of astrocytes (Vazquez-Chona et al, 2011). Many studies have made attempts at this goal by *in vitro* expansion of astrocytes in cellular conditions that may promote artificial cell qualities (Beckervordersandforth et al, 2010; Sirko et al, 2015;

Zamanian et al, 2012; Zhang et al, 2016b) One should use caution when interpreting these results, since these reports may be an incomplete characterization of the state of cells *in vivo*. Furthermore, experiments should be completed using cells from *in vivo* progenitor populations comparing them with mature populations from the brain to better define signaling pathways important in the differentiation of astrocytes. More recent attempts have isolated cells using green fluorescent protein overexpressed in astrocytes, again potentially introducing artificial qualities in the cells (Cahoy et al, 2008).

Within these experiments viable comparisons can be made between progenitor cells and mature astrocytes since these cell types share functions in homeostasis and gliotransmission. However, differences in gene expression would be expected because of major functional differences. The key difference is that differentiated parenchymal astrocytes do not divide in healthy brain, while an astrocyte/radial glial cell acting as a neural progenitor cell divides at a constant yet low frequency (Robel et al, 2011). Emerging technologies for single cell isolation and whole genome sequencing will benefit this research field.

Symptoms of Parkinson's Disease and Parkinsonism

The cardinal motor symptoms of PD are bradykinesia, rigidity, and resting tremor (Figure 4). These symptoms together form what is known as parkinsonism. It is noteworthy that the basal ganglia system requires the loss of 70% of dopamine neurons in the SN before the emergence of the parkinsonism movement disorder (Damier et al, 1999). In earlier stages of the disease (Braak stages 1 and 2), patients predominantly experience symptoms

such as loss of smell and REM sleep disorders that correlates with Lewy pathology in the olfactory nuclei and brain stem, respectively (Halliday & McCann, 2010; Hindle, 2010). Parkinsonism occurs in Braak stages 2 and 3. With further disease progression, patients experience cognitive problems and dementia, consistent with Lewy body pathology in the neocortex (Ding et al, 2015).

Figure 4: Characteristic PD patient
Sketch by Sir William Gowers in 1886 represents a typical PD patient including illustration of a profile and direct facing image view of bradykinesia, asymmetric tremor and rigidity.

Current Treatments of Symptoms of Parkinson's Disease

The currently marketed treatments of PD consist of drugs and procedures that only modify the symptomatic problems of the movement disorder described above, not the underlying pathology. The basis of the treatment is founded on augmenting dopaminergic neurotransmission in the basal ganglia via one of the following mechanisms: boosting dopamine synthesis via a precursor of dopamine, Levodopa (L-DOPA), activation of

dopamine D2 receptors, or inhibition of dopamine metabolizing enzymes, monoamine oxidase B (MAO-B) or catechol-O-methyl transferase (COMT). However, these drugs lose their efficacy or produce intolerable side effects with continued use and disease progression. In severe and refractory cases, deep brain stimulation (DBS) of the basal ganglia nuclei is prescribed to normalize the motor output (Yuan et al, 2010).

Extrapyramidal Basal Ganglia Neuronal Pathways

Dopamine neurons within the SN have a prominent role in regulation of the basal ganglia motor output. When the dopamine neurons in the SN depolarize, they release dopamine into the neostriatal synaptic cleft where it activates the D1 or D2 family of G-protein coupled receptors (GPCR) present on the postsynaptic cells. These postsynaptic cells are termed medium spiny neurons (MSNs) which express the inhibitory neurotransmitter, γ-aminobutyric acid (GABA). Morphological and functional studies have identified two distinct MSN pathways termed the so-called direct and indirect pathways (Gerfen, 1992). The MSNs in the direct pathway selectively express the Gαs-coupled D1 receptor. Activation of D1 receptors by dopamine will stimulate cyclic adenosine monophosphate (cAMP) production by adenylyl cyclase and increase basal ganglia output. The MSNs in the indirect pathway express the Gαi-coupled D2 receptor that inhibits cAMP production (Perreault et al, 2011). The activation of D2 receptors in the indirect pathway inhibits cAMP activity and thereby augments basal ganglia motor output. Thus, dopamine is overall stimulatory for the extrapyramidal motor system. In PD, the loss of SN dopamine neurons leads to disinhibition of the indirect pathway, which results in the decrease in basal ganglia extrapyramidal neuronal output, resulting in bradykinesia. Replacement of

dopamine via L-DOPA or direct activation of the D2 receptor on the indirect pathway provides symptomatic relief in PD patients. On the other hand, D2 receptor antagonists such as antipsychotic medications cause parkinsonism symptoms. As mentioned above, these drugs lose their efficacy over time or produce adverse events. Therefore, there is a continued need to identify additional mechanism and novel therapies that regulate basal ganglia activity.

PDE10 Enzymes and Cellular Pathways

Phosphodiesterase (PDE) enzymes cleave cyclic nucleotides and thereby regulate second messenger signaling casacades. PDE10A, like several other PDEs, cleaves both cAMP and cyclic guanosine monophosphate (cGMP) to AMP and GMP, respectively. PDE10A is of particular relevance to the basal ganglia because it is expressed selectively in the MSNs of the neostriatum in both the D1- and D2-containing neurons (Kleiman et al, 2011).

Studies have identified MP-10 to be a potent PDE10A small molecule inhibitor both *in vitro* and *in vivo*, which increases cAMP/cGMP intracellular concentrations, in turn augmenting D1 agonist and D2 antagonist-mediated effects (Bollen & Prickaerts, 2012; Grauer et al, 2009; Schmidt et al, 2008). PDE10i have been proposed as therapeutics for schizophrenia, since current marketed treatments consist of dopamine D2 receptor blockers (Siuciak, 2008), along with other treatments including weak antagonists of NMDA-type glutamate receptors to offset secondary effects of disinhibition of the subthalamic nucleus and glutamatergic overstimulation of the internal globus pallidus and

SN (Hallett & Standaert, 2004). In order to determine whether PDE10 inhibition may have a liability to induce parkinsonism (Niccolini et al, 2015), it is important to determine relative effects of MP-10 in direct or indirect pathways. Furthermore, MP-10 is a good tool to characterize the basal ganglia circuitry within the context of PD pathophysiology.

CHAPTER 3: MATERIALS AND METHODS

Animal Care and Use

All animal experiments were carried out in accordance with the Declaration of Helsinki and the Guide for the Care and Use of Laboratory Animals by the U.S. National Institute of Health and the EU Directive 86/609/EEC.

Preparation of α-synuclein monomer and fibrils for in vitro assessment

Lyophilized α-synuclein (R-Peptide, Bogart, GA) was resuspended to 1 mg/mL (in 10 mM Tris-HCl, pH 7.4). The amount of endotoxin was found to be <1 endotoxin unit/mg of protein. The unagitated solution was aliquoted and stored at -20^{o} C. To prepare fibrillar α-synuclein, NaN_3 was added at a final concentration of 0.02% and the solution was agitated at 1400 revolutions per minute (RPM) at 37^{o} C for 7 days on an Eppendorf Thermoshaker. Agitated solution was dialyzed against phosphate buffered saline (PBS), pH 7.4 to remove NaN_3 and to enrich for fibrillar α-synuclein using 20K molecular weight cut-off (MWCO) Slide-A-Lyzer dialysis device (Thermo, Rockford, IL). Fibrillar α-synuclein was aliquoted and stored at -20^{o} C. Sister aliquots of the same lot of monomeric and fibrillar α-synuclein was used for all studies described.

Characterization of α-synuclein fibrils by thioflavin-T binding assay

A 10 μL aliquot of agitated and unagitated α-synuclein solutions were mixed separately with 10 μL each of thioflavin-T (120 μM in 100 mM NaPO4, pH 7.4) and directly added

to a black 384 well plate (Thermo Scientific, Rockford, IL) to assess fibril formation by measuring emission at 494 nm.

Characterization of α-synuclein fibrils by Western Blotting

Monomer and fibril concentrations were determined by the Bicinchoninic Acid (BCA) assay (Thermo Scientific, Rockford, IL). Five μg of each solution were denatured at 95^{o}C for 5 minutes and separated by sodium dodecyl sulfate polyacrylamide gel electrophoresis (SDS-PAGE). The proteins were blotted onto polyvinylidene difluoride (PVDF) membrane and blocked with 5% non-fat milk for 16 hours at 4^{o} C. An overnight incubation with 1 μg/mL of anti-α-synuclein (Clone 42, BD Biosciences, San Jose, CA) in 5% non-fat milk was followed by 3 rinses with Tris-buffered saline with 0.05% Tween-20 (TBST). Membranes were incubated with the horseradish peroxidase-conjugated secondary goat anti-mouse antibodies (Cell Signaling, Danvers, MA) for 1 hour at room temperature, then rinsed with TBST and developed for chemiluminescent image acquisition on the ImageQuant LAS 4000 biomolecular imager (GE, Uppsala, Sweden).

Characterization of α-synuclein fibrils by transmission electron microscopy

Agitated protein was prepared for transmission electron microscopy (TEM) evaluation and visualization as previously described (Guo & Lee, 2011). Briefly, 5 μL of undiluted α-synuclein fibrillar preparation was placed on a meshed formvar/carbon coated copper grid for 3 minutes. The protein was rinsed in 50 nM Tris-HCl buffer, pH 7.5, for 5

minutes and negatively stained with 20 drops of 2% aqueous uranyl acetate in 0.5% glacial acetic acid. The specimens were air-dried for 1 hour prior to visualization with a Philips CM-100 TEM at 80 kV. Digital images were collected using Gatan Digital Micrograph software.

BV-2 cell and primary microglia cultures and treatment

BV-2 cells are a transformed microglia cell line (Blasi et al, 1990). BV-2 cells were seeded in a 150 cm^2 flask (Corning, Tewksbury, MA) at 1 x 10^6 cells and cultured in 30 mL of Dulbecco's Modified Eagle's Medium (DMEM; HyClone, Logan, UT) supplemented with 10% fetal bovine serum (FBS; Life Technologies, Grand Island, NY) in a humidified 5% CO_2 incubator at 37^o C for 72 hours. Cells were washed once with Hank's balanced salt solution (HBSS; HyClone, Logan, UT), then dissociated from the flask using TrypLE Express Enzyme (Life Technologies, Grand Island, NY) and resuspended in DMEM (HyClone, Logan, UT) supplemented with 10% FBS (Life Technologies, Grand Island, NY) prior to plating on poly-D-lysine (PDL)-coated plates (Corning, Tewksbury, MA). For RNA analysis by quantitative reverse-transcription-polymerase chain reaction (RT-qPCR), cytokine protein assessment by enzyme-linked immunosorbent assay (ELISA) and imaging studies, BV-2 cells were plated in 96-well plates at 1.5 x 10^4 cells while the primary microglia were plated in 96-well plates at 4 x 10^4. For phagocytosis studies, BV-2 cells were plated at 1 x 10^5 cells/well in 12-well plates. These cell densities reflect experimental optimization through pilot studies. After 24 hours, media was replaced with fresh DMEM (HyClone, Logan, UT) without serum. LPS from *E. coli* (strain 0111:B4, Sigma-Aldrich, St. Louis, MO) was diluted to 100

ng/mL and used as control treatments in indicated experiments. Other treatments and durations are indicated in individual figure legends.

Cytotoxicity Assessment

Following treatment as indicated in figure legends, supernatant media from individual wells were directly tested for presence of lactate dehydrogenase (LDH) using a cytotoxicity detection kit (Roche, Indianapolis, IN). 100 µL of supernatant was added to a clear polystyrene 96 well plate (Corning, Tewksbury, MA) prior to incubation with 100 µL of freshly prepared 1:45 ratio mixture of diaphorase / NAD^+ and iodotetrazolium chloride / sodium lactate (Roche, Indianapolis, IN) for 30 minutes in the dark at room temperature. After incubation, the absorbance of each sample was measured at 490 nm using a SpectroMax M5 Microplate Reader (Molecular Devices, Sunnyvale, CA).

RT-qPCR analysis of BV-2 microglial cells

Total RNA was extracted from BV-2 microglial cells using TRIzol reagent (Life Technologies, Grand Island, NY) followed by reverse transcription using the High Capacity cDNA Archive Kit (Applied Biosystems, Foster City, CA). All cDNAs were assayed for genes of interest using TaqMan Gene Expression Analysis (Applied Biosystems, Foster City, CA) and the Assay-On-Demand primer/probe sets including Il6 (Mm00446190_m1), Tnf (Mm00443258_m1), Nos2 (Mm00440502_m1), Arg1 (Mm00475988_m1), Il10 (Mm01288386_m1), Chil3 (Mm00657889_mH), Mrc1 (Mm01329362_m1), Trem2 (Mm04209424_g1), Tyrobp (Mm00449152_m1), Cd33

(Mm00491152_m1) and Gapdh (Mm99999915_g1). Triplicate samples were subjected to qPCR using ABI 7900HT real-time PCR system (Applied Biosystems, Foster City, CA) with the maximum cycle number of 40. Relative gene of interest mRNA levels were quantitated by determining the cycle number at which amplification detection threshold was achieved followed by normalization to that of the housekeeping gene, glyceraldehyde 3-phosphate dehydrogenase (*Gapdh*).

Immunocytochemistry and image analysis of BV-2 microglial cells

Following treatment of BV-2 microglial cells for 3 and 24 hours, media was replaced with 50 μL of 4% paraformaldehyde (Electron Microscopy Sciences, Hatfield, PA) for 20 minutes. The cells were washed with PBS and permeabilized for 10 minutes with 50 μL of PBST, containing 0.05% Tween 20 (Life Technologies, Grand Island, NY) followed by 3 washes with PBS. Blocking was done with 1% bovine serum albumin (BSA; Life Technologies, Grand Island, NY) diluted in PBS for 24 hours at 4^{o} C. To assess pro-inflammatory phenotype, cells were incubated with a rabbit antibody to ionized calcium binding adaptor molecule 1 (IBA1) at 1 μg/mL in 1% BSA (Wako Chemicals, Richmond, VA) for 24 hours at 4^{o} C. This was followed by incubation with 2 μg/mL of Alexa-fluor 555 labeled goat anti-rabbit IgG secondary antibodies (Life Technologies, Grand Island, NY) for 60 minutes, 3 washes in PBS and addition of 10 μg/mL Hoechst 33342 (Life technologies, Grand Island, NY) for 2 minutes to label cell nuclei. High content images were generated using the Cellomics Arrayscan VTI HCS Reader (Thermo Fisher Scientific, Pittsburgh, PA) and the default software was used to compute mean number of cell bodies, total signal intensity and mean cell body area.

Cytokine level detection in BV-2 microglial cells and primary microglia

Meso Scale Discovery (MSD, Gaithersburg, MD) platform was used for assessment of cytokine levels per the manufacturer's instructions. Briefly, supernatant media from each treatment well were diluted 2 fold with Diluent 41 and 50 µL of each sample was analyzed on the Proinflammatory Panel 1 (mouse) Plate. Plates were shaken at 600 RPM for 2 hours at room temperature. After 3 washes with 150 µL of 1X Wash Buffer, 25 µL of solution containing detection antibodies for 10 different cytokines (Meso Scale Discovery, Gaithersburg, MD) was added to each well followed by shaking at 600 RPM for 2 hours at room temperature. Following 3 washes with 150 µL of 1X Wash Buffer, 150 µL of Read Buffer T was added to each well prior to analyzing with Sector Imager 6000 (Meso Scale Discovery, Gaithersburg, MD). All samples were interpolated using individual standard curves for each of the cytokines and reported at pg/mL.

Phagocytosis detection in BV-2 microglial cells and primary microglia

BV-2 microglial cell lines or primary microglia were treated as specified in the figure legends. 1 mL (for BV-2 cells) or 100 uL (for primary cells) of 0.1 mg/mL pHrodo green conjugated *E. coli* BioParticles (Life Technologies, Grand Island, NY) were added to each sample well in a humidified 5% CO_2 incubator at 37^{o} C for 1 hour. After aspirating the particles, cells were washed with ice cold Live Cell Imaging Solution (Life Technologies, Grand Island, NY) and then completely dissociated from the plate by a 3-minute trypsinization process using TrypLE Express Enzyme (Life Technologies, Grand Island, NY). Each sample was washed individually in 1% BSA (Life Technologies, Grand Island, NY) diluted in PBS. Each sample was analyzed on a Guava easyCyte flow

cytometer (EMD Millipore, Billerica, MA) by collecting 10,000 events per sample. Events were gated based on forward and side scatter plots. Positive thresholds were based on the background level of samples without BioParticles and were used consistently to determine % of cells with positive green fluorescence of each sample. Data are shown as percent of positive cells for each treatment condition normalized to the control signal in samples treated with serum-free media. The data represent average values from multiple independent experiments.

Isolation of GLAST (+) cells

Timed pregnant C57BL/6J mice (Jackson Laboratory, Bar Harbor, ME) were housed at the Indiana University Purdue University Indianapolis Science Animal Resource Center and maintained at a 12 hour light/dark cycle. Whole brains from 4 separate litters with an average of 6 mice per liter for were used for both P0 and P8 isolations. Each litter was considered a single sample and brains from a litter were pooled and dissected in ice cold 1X HBSS. Four separate pooled samples were analyzed by RNA-seq for each developmental stage. Brains were enzymatically dissociated by incubating brain pieces with trypsin using the Neural Tissue Dissociation Kit (Miltenyi Biotec, Auburn CA) and the automated gentleMACS Dissociator (Miltenyi Biotec, Auburn CA) operating on default settings. Briefly, tissue was dissociated for 37 seconds in pre-heated enzyme mix 1 (Miltenyi Biotec, Auburn CA) before incubating at 37° C for 15 minutes with rotation (12 rpm) using the MACSmix Tube Rotator (Miltenyi Biotec, Auburn CA). Following incubation with trypsin, 20 µL of Solution 3 and 10 µL of Solution 4 from the trypsin enzyme mix 2 (Miltenyi Biotec, Auburn CA) were added per P8 brain or per P0 brains.

Tissue was further incubated at 37° C for 10 minutes with rotation (12 rpm) using the MACSmix Tube Rotator, mechanically dissociated for 61 seconds, and then incubated again at 37°C for 10 minutes with rotation (12 rpm) to complete the dissociation. The single cell preparations were applied to a 30 μm cell strainer and resuspended in 500 μL 0.5% Bovine Serum Albumin (BSA) in 1X PBS. Cells were labeled using the Anti-GLAST (ASCA-1) MicroBead Kit and magnetically separated into 1 mL volume through MACS separation columns after washing the column three times with 500 μL of 0.5% BSA in 1X PBS (Miltenyi Biotec, Auburn CA).

Immunofluorescence and image analysis of developing mouse brain sections

Whole brains from embryonic day 16.5 (E16.5), P0, P8 and P14 mice were dissected in ice cold 1X Hank's Balanced Salt Solution (HBSS, Sigma, St. Louis, MO) and fixed in 4% paraformaldehyde in 0.1M phosphate buffer, pH 7.4 overnight. The tissue was cryoprotected in overnight incubations of several graded sucrose solutions (5%, 10%, 15% and 20%) made in 0.1M phosphate buffer, pH 7.4. The tissue was frozen in a 3:1 solution of 20% sucrose/optimal cutting temperature (OCT) and stored at -80° C. Twelve micron thick sections were cut using a Leica CM3050 S cryostat and placed on Superfrost Plus slides (Fisher Scientific, Pittsburgh, PA) treated with Vectabond (Vector Labs, Burlingame, CA), and were stored at -80° C until use. Prior to immunolabeling, sections were warmed to room temperature for 20 minutes, post-fixed with 4% paraformaldehyde for 30 minutes and rinsed in 1X PBS twice for 2 minutes each. To reduce the autofluorescence, sections were treated with 1% sodium borohydride (Acros

Organics, Belgium) in 1X PBS for 2 minutes at room temperature. Tissue was blocked with 10% goat serum in 1X PBS containing 0.25% Triton X-100 (Bio-Rad, Hercules, CA) at room temperature for 1 hour. Sections were incubated with primary antibodies, diluted in 0.025% Triton X-100 in 1X PBS with 2% goat serum, overnight at 4° C (Table 1).

Table 1: Antibodies used for fluorescent immunohistochemistry colocalization studies on different stages of mouse brain sections.

Antibody	Source	Lot#	Dilution
GLAST (EAAT1, ab416)	Abcam (Cambridge, MA)	GR148367-1, GR129023-1	1:250
Vimentin (40E-C)	Developmental Studies Hybridoma Bank (Iowa City, IA)	NA	1:100
NF1A (ab41851)	Abcam (Cambridge, MA)	GR128277-1	1:600
MAP2 (SMI52)	Sternberger Monoclonals (Baltimore, MD)	6	1:1000
MBP (MBP101, ab62631)	Abcam (Cambridge, MA)	GR196620	1:500
Abbreviations: Glutamate Aspartate Transporter, GLAST; Nuclear Factor 1A, NF1A; Microtubule-associated protein 2, MAP2; Myelin Basic Protein, MBP			

Sections were rinsed in 1X PBS twice for 10 minutes each, then incubated with Dylight 488 and 594 conjugated secondary goat antibodies (Jackson Immunoresearch, West Grove, PA) at 1:800 each in 1X PBS for 1 hour at room temperature. Sections were incubated with a 0.2% Hoechst 33342 (Invitrogen, Grand Island, NY) solution in 1X PBS for 5 minutes, rinsed twice with 1X PBS for 10 minutes each, and mounted with Aqua Poly/mount (Polysciences, Inc., Valley Road Warrington). For double-labeling of slides from the same species, one antigen was labeled with TSA™ Plus Fluorescein System

(PerkinElmer, Akron, Ohio) as per manufacturer's instructions while the second antigen was immunolabeled as indicated above.

Olympus Fluoview FV 1000 confocal microscope was used to acquire images of mid-sagittal forebrain, olfactory bulb and cerebellum from E16, P0, P8 and P14 brains. Confocal image files were imported into the FIJI distribution of ImageJ for analysis (Schindelin et al, 2012; Schneider et al, 2012). Analyses of all images were completed using an adapted version of an ImageJ macro that was designed to compute areas of overlap and colocalization (Zinchuk et al, 2007). The degree of overlap was totaled for each image and normalized by scaling the images to the same number of pixels sampled.

FACS analysis of GLAST (+) cells

Subsets of magnetically positive and negative cells were incubated with 1μg/mL of Phycoerythrin (PE) directly labeled anti-GLAST (ASCA-1) or mouse IgG antibodies diluted in 0.5% BSA in 1X PBS at 4° C for 30 min. Cells were washed with 0.5% BSA in 1X PBS and a minimum of 10,000 live cells per sample were analyzed using the FACSCalibur flow cytometer (BD Biosciences, San Jose, CA). The intensity of fluorescent signal of anti-GLAST stained samples were compared to IgG negative controls and percent positive signal was calculated.

RNA extraction and isolation from GLAST (+) cells

RNA was prepared using the PicoPure RNA isolation kit (Applied Biosystems, Foster City, CA). GLAST positive cells were incubated in 100μL of extraction buffer for 30 minutes at 42 ^{o} C. The supernatant was mixed with equal volume of 70% ethanol. The RNA purification column was preconditioned with 250μL of conditioning buffer prior to adding the RNA extract mixture, followed by 3 washing steps and DNase treatment. Eleven microliters of eluted RNA was tested in RNA integrity assays prior to preparation of library for sequencing.

RT-qPCR of genes from GLAST (+) cells

Total RNAs from isolated cells were reverse transcribed using the TaqMan Reverse Transcription Reagents (N8080234, Fisher Scientific, Pittsburgh, PA). cDNAs were assayed for genes of interest using TaqMan Gene Expression Analysis (Applied Biosystems, Foster City, CA) and the Assay-On-Demand primer/probe set (Table 2).

Table 2: qPCR primers used to validate RNA-seq analysis.

Gene symbol (Assay ID)	RefSeq	Exon Boundary	Assay Location	Product size (bp)
Neurod1 (Mm01946604_s1)	NM_010894.2	2	2352	142
Insm1 (Mm02581025_s1)	NM_016889.3	1	2856	79
Dbx2 (Mm01306497_m1)	NM_207533.2	1 – 2	535	59
Dtx1 (Mm00492297_m1)	NM_008052.3	9 – 10	2506	64
Kcnip3 (Mm01339777_m1)	NM_001111331.1 NM_001291005.1 NM_019789.4 NR_110989.1	7 – 8 8 – 9 8 – 9 8 – 9	1035 857 861 1021	77
Olig1 (Mm00497537_s1)	NM_016968.4	1	805	83
Olig2 (Mm01210556_m1)	NM_016967.2	1 – 2	103	99
Msx1 (Mm00440330_m1)	NM_010835.2	1 – 2	724	66
Smad6 (Mm00484738_m1)	NM_008542.3	2 – 3	1912	71
Ptrf (Mm00477266_m1)	NM_008986.2	1 – 2	623	53
Plagl1 (Mm00494251_m1)	NM_009538.2	5 – 6	709	68
Tcea3 (Mm00711952_m1)	NM_011542.2	8 – 9	907	81
Foxc1 (Mm01962704_s1)	NM_008592.2	1	3925	153
Foxc2 (Mm00546194_s1)	NM_013519.2	1	1465	138
Lmx1a (Mm00473947_m1)	NM_033652.5	1 – 2	298	70
Alx4 (Mm00431780_m1)	NM_007442.3	1 – 2	653	54
Hif3a (Mm00469375_m1)	NM_001162950.1 NM_016868.3	12 – 13 12 – 13	1750 1781	64
Fhl2 (Mm00515781_m1)	NM_001289533.1 NM_010212.4	5 – 6 5 – 6	824 973	92

Gene of interest mRNA levels were quantitated by determining the cycle number at which amplification detection threshold was achieved. Real time-PCR reactions were performed in 10 µl reactions. Triplicate samples were subjected to quantitative PCR using QuantStudio 7 Flex Real-Time PCR System with the maximum cycle number of

50. After normalization to the housekeeping gene, *Gapdh*, the relative expression of the gene of interest was reported.

QC and Preparation of library for RNA-seq

Initial isolated RNA concentration was determined using the Qubit 2.0 Fluorometer and RNA High Sensitivity Assay (Life Technologies Corp., Carlsbad, CA). Total RNA integrity was assessed using the Agilent 2100 Bioanalyzer along with the RNA 6000 Pico Kit (Agilent Technologies, Santa Clara, CA). All samples had an RNA Integrity Number (RIN) value greater than or equal to 7.9. A RIN value of 7 or above on a scale of 10 is considered high integrity based on the limit of detection of a fluorescence peak of the 28S rRNA (Schroeder et al, 2006). Libraries were constructed using the TruSeq RNA Sample Preparation Kit v2 set A and protocol companion (Illumina Inc., San Diego, CA). Briefly, poly-A containing mRNA was purified from 60 ng total RNA using poly-T oligo-attached magnetic beads, then heat fragmented at 94° C for 4 minutes. First strand cDNA was synthesized using reverse transcriptase and random hexamers, followed by second strand synthesis. The ends of the double stranded cDNA were polished and 3' adenylated, then ligated with indexing adapters to prepare them for hybridization on the flowcell. The library was then PCR amplified to enrich for properly ligated fragments and purified using AMPure XP beads (Beckman Coulter, Inc.). Final library integrity and size distribution was assessed using the Agilent Bioanalyzer 2100 along with the DNA 7500 Assay (Agilent Technologies, Santa Clara, CA). The Qubit 2.0 Fluorometer along with the High Sensitivity DNA Assay (Life Technologies Corp.) was used to determine final library concentration. Libraries were normalized to 10 nM in buffer EB (Qiagen, Santa

Clarita, CA) and combined together for multiplexing. Sequencing was conducted on one lane of Illumina HiSeq2000 (BGI International) using 100bp paired-end reads. An average of 25 million paired-end reads was obtained per sample.

Bioinformatics and Statistical Analysis of RNA-seq

Reads were analyzed with quality recalibration software (Illumina Inc., San Diego, CA) for each sequence read. A 5-base sliding window was used when assigning quality scores (Q-scores). To eliminate low-quality reads while retaining high-quality regions, a position with an average Q-score of less than 20 was truncated and any read length less than 35 bases was discarded (Breese & Liu, 2013; Juan et al, 2013; Todd et al, 2013). Sequence reads were aligned to the mouse genome (mm9) using TopHat (Trapnell et al, 2009). After aligning the sequence reads to a filtering index, including ribosomal RNAs and other repeat sequences of no interest, three levels of sequence alignment was conducted: genome, known junctions (Waterston et al, 2002) and novel junctions based on enriched regions identified during genomic alignment. Uniquely aligned sequences with no more than two mismatches were allowed. Fragments per kilobase of transcript per million (FPKM) was calculated based on the number of reads aligned to a gene. Differential expression between P0 and P8 cells was determined using EdgeR with continuous dispersion (Robinson et al, 2010). False Discovery Rate (FDR) was calculated according to Benjamini and Hochberg (Benjamini & Hochberg, 1995).

Transcription Factor Network Analysis of RNA-seq data set

A representative list of 500 of the most highly expressed transcripts from P0 or P8 cells based on FPKM were investigated further through network analysis using MetaCore (GeneGo Inc., St. Joseph, MI). The transcription factor network analysis algorithm (version 6.24 build 67895) was applied to identify subsets of genes with coordinate regulation by known transcription factors. Transcription factors were reported based on hypergeometric distribution and ranked according to p-value.

Chromatin Immunoprecipitation from GLAST (+) cells

GLAST positive cells were fixed in freshly prepared 1% formaldehyde solution for 15 minutes, rocking at room temperature. Fixation was stopped with 2.5 M glycine solution for 5 minutes at room temperature. Cells were pelleted and washed once in 10 mL of chilled 0.5% Igepal CA-630 in 1X PBS and resuspended in 10 mL of chilled 0.5% Igepal CA-630 in 1X PBS with 1 mM phenylmethylsulfonyl fluoride (PMSF). Cells were pelleted immediately and supernatant was completely removed before snap-freezing in liquid nitrogen. Chromatin immunoprecipitation (ChIP) was carried out as detailed previously (Labhart et al, 2005). Briefly, chromatin was extracted from frozen samples by adding lysis buffer and processing with a Dounce homogenizer. Lysates were briefly sonicated to shear the DNA. Input control samples were purified from an aliquot of the P0 and P8 chromatin at this stage of processing and quantified using a Nanodrop spectrophotometer (ThermoScientific, Philadelphia PA), while the rest of the samples underwent ChIP. ChIP was performed using an anti-acetylated histone 3 lysine 9

antibody (acH3K9, clone 1B10, Active Motif, Carlsbad, CA). An aliquot of P0 or P8 genomic DNA was precleared with protein G-coupled agarose beads (Invitrogen, Grand Island NY), incubated overnight with anti-acH3K9 antibody, washed, and incubated with protein G–coupled agarose beads. Complexes containing DNA, acetylated histone 3 lysine 9 and antibody were precipitated, washed and eluted from the beads with SDS-containing buffer. DNA/protein complexes were treated with RNAse and proteinase K solution and crosslinks reversed by incubating overnight at 65^0 C. Immunoprecipitated DNA was purified by phenol-chloroform extraction and ethanol precipitated. Immunoprecipitated DNA was prepared for sequencing by PCR amplification. The ends of the sheared DNA samples were polished and 5'-phosphorylated by incubating with a mixture of Klenow fragment, T4 polynucleotide kinase and T4 DNA polymerase followed by addition of a 3'-A to DNA ends using the Klenow fragment, and Illumina adaptors were ligated to the 3' ends. Following addition of adaptors the resulting fragments were size-fractionated on a 2% agarose gel, and fragments between 180-250bp in length were purified and amplified for 18 cycles by PCR. Following quantitation, the libraries were sequenced using the Illumina Hi-Seq Next-Gen sequencing platform (Illumina Inc., San Diego, CA).

Identification of Differentially Modified Gene Regions

The 50-nt sequence reads were mapped to a reference genome (Mouse Genome Sequencing Consortium, 2007) using the Burrows-Wheeler Aligner software package (Li & Durbin, 2009). Illumina's purity filter was used to eliminate duplicate reads and reads

that have 2 or more mismatches from further analysis. The 3' ends of these aligned fragments are extended by 150-300bp in order to identify fragment density. The genome was divided into 32-nt 'bins' and the number of fragments (extended tags) that map to these bins were counted. Regions within the genome that showed a local enrichment of fragments (intervals or active regions) were found using SICER which has been shown to predict large protein binding domains (histone or polymerase binding regions) in histone modification ChIP data (Xu et al, 2014). An interval within 10,000 bp upstream or downstream of a gene region was counted as associated with that gene and identified by chromosome number, and a start and end coordinate. Variation of overlapping intervals between replicates were identified and defined by the most upstream start coordinate and the most downstream end coordinate. The active regions were annotated as upstream, in gene or downstream relative the Transcription Start Site (TSS) and the Transcription Termination Site (TTS) of the associated gene. The numbers of reads that correspond to each active region were counted in P0 and P8 samples. To identify regions of differential enrichment the active regions were analyzed using edgeR v2.14 software package (Robinson et al, 2010). Differentially modified regions were identified using FDR less than 0.01. Active regions corresponding to non-annotated regions in the reference genome were eliminated. This dataset was regrouped based on previously calculated FC values into two groups; active regions with FC values less than or equal to 0.67 that are therefore relatively enriched in the P0 sample, while active regions with FC greater than or equal to 1.5 that are therefore relatively enriched in the P8 sample. The P0-enriched ($FC<1$) and P8-enriched ($FC>1$) active regions were filtered to select for active regions that correspond to the Proximal Promoter Region (PPR) upstream of the 5'-coding region

assigned as -1000 bp to +100 bp relative to the TSS. The resulting active regions located in the PPR were used to perform Gene Ontology and pathway analysis using DAVID (Dennis et al, 2003). The gene lists corresponding to the P0 and P8 active regions located in the PPR were classified into functional groups based on three ontologies as described by the Gene Ontology Database: molecular function, cell component and biological process. Pathway analysis was performed on the same gene lists using the Ingenuity Pathway Analysis software tool (IPA, Ingenuity Systems, http://www.ingenuity.com).

Dosing of animals for PDE10A experiments

All studies were performed on male rodents. Sprague Dawley (SD) rats (Charles River Laboratories, Margate, UK), C57BL/6 mice (Taconic Biosciences, Cambridge City, IN) and Bacterial artificial chromosome (BAC) transgenic Drd1a-tdTomato mice (The Jackson Laboratory, Bar Harbor, ME) were acclimatized for at least 3 days followed by 4 days of saline injection to habituate them to the stress of handling and dosing. Animals were randomly assigned to treatment groups. They were treated either orally (PO) or intraperitoneally (IP) with saline, MP-10 (Selleckchem, Houston, TX), SKF82958 (Sigma Aldrich, St. Louis, MO) or haloperidol (Tocris, Bristol, UK) at doses indicated in figure legends. Doses were selected on the basis of receptor occupancy data and published literature (Lewis et al, 1998; Mukherjee et al, 2001). Animals were euthanized at 3 hours post-dosing by cervical dislocation and brains were flash frozen over isopentane on dry ice followed by storage at -80°C prior to cryosectioning. The 3 hour time point was selected since MP-10 increases cAMP/cGMP levels for 1 to 4 hours after

an acute dose (Schmidt et al, 2008) and c-Fos immunoreactivity peaks between 1 and 3 hours (Dragunow & Faull, 1989; Lensu et al, 2006).

Cryosectioning/Immunohistochemistry of brains for c-Fos analysis

Previously published protocols for c-Fos immunohistochemistry on flash frozen rodent brain were used (Sundquist & Nisenbaum, 2005). Brains were coronally sectioned at 7-μm thickness on a Leica Cryostat CM3050 (Leica, Hiedelburg, Germany) at the following coordinates: Bregma 3.72 mm (rat prefrontal cortex), 1.68 mm (rat striatum), 1.10 mm (mouse striatum), -3.60 mm (rat hippocampus and amygdala) and -4.56 mm (rat ventral hippocampus) according to the atlases of Watson and Paxinos (2004, Figure 5). Cryosections from each brain region were collected at 50 μm intervals on positively charged glass slides and incubated in 4% paraformaldehyde for 20 minutes at room temperature. Slides were then rinsed in TBST and stored at -80° C.

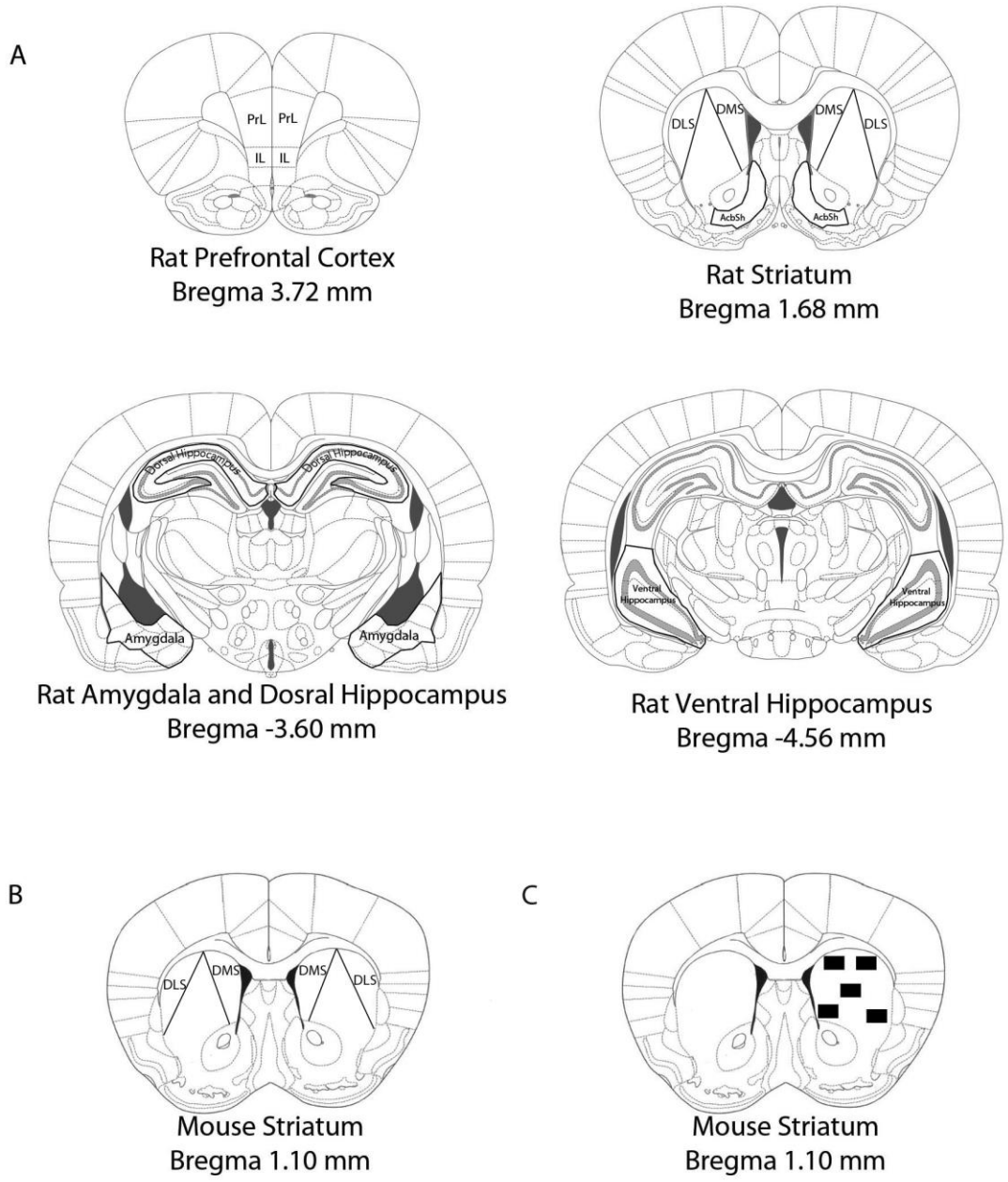

Figure 5: Diagrams from Paxinos and Watson Stereotaxic Atlas of the rat and mouse brain illustrating the brain regions assessed for c-Fos-immunoreactive cells.
A) Diagrams of SD rat brain sections at the level of prefrontal cortex (Bregma 3.72 mm), striatum (Bregma 1.68 mm), amygdala and dorsal hippocampus (Bregma -3.60 mm) and ventral hippocampus (Bregma -4.56 mm) show regions of interest outlined. B-C) Diagrams of a mouse brain section at the level of striatum (Bregma 1.10 mm) shows the DLS and DMS and the five microscopic fields analyzed in BAC transgenic Drd1a-tdTomato mice. PrL, Prelimbic Cortex; IL, Infralimbic Cortex; DLS, Dorsal Lateral Striatum; DMS, Dorsal Medial Striatum; AcbSh, Accumbens Shell.

For c-Fos immunohistochemistry, brain sections were rinsed in TBST buffer, incubated for 10 minutes in Dual Endogenous Enzyme Block (Dako, Carpinteria, CA), rinsed in TBST buffer and blocked with Protein Block (Dako) for 60 minutes using a Dako Autostainer Plus. Slides were incubated for 60 minutes with one of the two primary anti-c-Fos antibodies; either a goat (Santa Cruz, Dallas, TX) or a rabbit antibody (Spring Bioscience, Pleasanton, CA) at 0.8 μg/mL concentration in the antibody diluent with background reducing agents (Dako). Issues with supplies of the antibody from Santa Cruz necessitated the use of the alternate antibody. Both c-Fos antibodies were tested under optimized conditions and shown to produce similar staining patterns with subregions of interest (Figure 6).

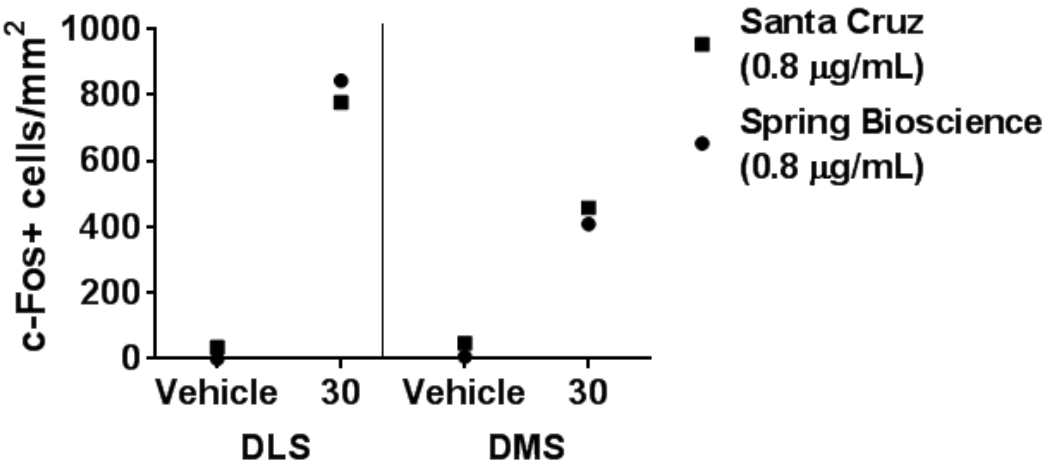

Figure 6: Comparison of Spring Bioscience and Santa Cruz commercially available c-Fos antibodies.
Quantitative analysis of c-Fos immunoreactive cell density in the DLS and DMS of SD rats, three hours after vehicle or MP-10 treatment at 30 mg/kg, PO. Each point represents a subregion of interest within an animal. Note the similar density of positive cells in all four groups of brain sections evaluated.

Slides were then rinsed 3X with TBST followed by addition of biotinylated secondary antibodies; a rabbit anti-goat or goat anti-rabbit IgG (Dako) for 30 minutes and then rinsed 3X with TBST buffer. Next, the slides were incubated with horseradish peroxidase-labelled streptavidin (Dako) for 10 minutes, rinsed 3X with TBST, incubated with 3,3'-Diaminobenzidine (DAB) for 5 minutes, and rinsed with TBST followed by distilled water. Sections were counterstained with hematoxylin for 30 seconds and coverslipped using Cytoseal XYL (Thermo Scientific, Kalamazoo, MI).

For the immunofluorescence studies on BAC transgenic Drd1a-tdTomato mouse, after the incubation with the primary antibody, Alexa-fluor 488 labeled goat anti-rabbit IgG (Life Technologies, Grand Island, NY) was added to the slides for 60 minutes, then rinsed 3X with TBST washing buffer. Sections were counterstained with 10 μg/mL Hoechst 33342 (Life technologies, Grand Island, NY) for 2 minutes and coverslipped using Fluorescent Mounting Media (Dako).

Image Analysis of c-Fos in brain sections

Images of the c-Fos-stained SD rat and C57BL/6 mouse brain sections were acquired at the 20X magnification on an Aperio ScanScope XT (version10.00.00.1805; Aperio, Vista, CA) by an investigator blinded to treatment groups and annotated for storage in the web-based software, Spectrum database (version10.0.1346.1806). Each brain region was outlined bilaterally using a manual inclusion drawing tool in the Aperio image viewer software, ImageScope (version10.0.36.1805). Regions of interest were outlined for each animal. For the MP-10 dose-response study, in addition to the dorsal lateral striatum

(DLS) and dorsal medial striatum (DMS), c-Fos immunoreactivity was analyzed in the prelimbic and infralimbic cortex, nucleus accumbens shell, amygdala and dorsal and ventral hippocampus were analyzed. Cells within each outlined region were counted using an adapted version of Aperio Nuclear Count algorithm using a macro that was designed to count the immunopositive nuclei. The number of positive nuclei per brain region were totaled, normalized by area sampled (mm^2) and averaged to derive a value for each region per animal. Group averages, standard deviations, standard errors of the mean and 95% confidence intervals were computed for statistical analyses.

Images of the c-Fos-stained BAC transgenic Drd1a-tdTomato mouse brain sections were acquired on a Panoramic MIDI fluorescent digital slide scanner (3DHISTECH, Budapest, Hungary). Five 40X images were collected. In addition to the DLS and DMS, central striatal regions were included, so that region selection was not a bias. Images were annotated for storage on the instrument controller using a nomenclature system that blinded both, the treatment groups and regions of interest. Manual analysis of images was performed by counting cells with c-Fos signal (green, Alexa-Fluor 488) and nuclear counterstain (blue, Hoechst 33342) with and without dopamine D1 receptor signal (red, tdTomato). Thus four categories of cells were recorded: (i) c-Fos-expressing (c-Fos+) cells in D1+ neurons (+ red, + green, + blue), (ii) c-Fos+ cells in D1- neurons (- red, + green, + blue), (iii) D1+ neurons without c-Fos (+ red, - green, + blue) and (iv) neurons without D1 or c-Fos (- red, - green, + blue). The raw counts per image of all four categories were normalized to total number of cells. Both D1(-) cells (i.e., presumably D2(+) cells) and D1(+) cells were either categorized as c-Fos(+) or c-Fos(-). Averages for

each treatment group, standard deviations and standard errors of the mean were computed for statistical analyses.

Image Analyses and Statistical Methods of PDE10A studies

Study power was estimated based on effect size in pilot studies, which demonstrated that 5 animals per treatment group would yield 80% power to observe 15% induction of c-Fos. To ensure sufficient power, 6 animals were assigned to each treatment group. Statistical analyses of average c-Fos immunopositive nuclei density was performed by Analysis of Variance (ANOVA). Following significant effects, group-wise comparisons were performed using the Tukey-Kramer test. All tests were conducted at the two-sided 0.05 alpha level and correspondingly all confidence intervals were constructed at 95%. The response variables were evaluated for normality using Kolmogorov-Smirnov's test and evaluated for heterogeneity of variance using Levene's. Results from animals with no measurable c-Fos induction were included in the statistical model and are represented with a value of zero.

In order to illustrate the regional pattern of c-Fos density across treatment groups, a c-Fos dominance index was computed by subtracting the signal in the DMS from that in the DLS for each animal followed by computation of the group average and 95% confidence intervals. Positive values and confidence intervals greater than zero indicate that the signal in the DLS is statistically greater than that in the DMS.

CHAPTER 4: MICROGLIA AND ASTROCYTE PHENOTYPES ARE REGULATED BY FIBRILLAR ALPHA-SYNUCLEIN

Introduction

The precise nature of pathologic forms of α-synuclein is a matter of intense research. Prevailing data suggest that aggregated, but not monomeric α-synuclein, is the toxic species (Dehay et al, 2015). Although Lewy pathology is intracellular, neuronal and glial cells come in contact with α-synuclein aggregates released from dying neurons, by unconventional exocytosis or during the process of phagocytosis of damaged neurons by microglial cells (Lee et al, 2014). Additionally, emerging data indicate that α-synuclein monomers and aggregates may be released from neurons and transported between cells in a prion-like manner, further exposing surrounding neurons and glia to potential toxic effects of α-synuclein (Luna & Luk, 2015).

Imaging, histological and biochemical studies have demonstrated that neuroinflammation, and specifically, microgliosis is a major pathophysiology of PD (Wang et al, 2015) and contributes to the progressive death of dopaminergic neurons (reviewed by Sanchez-Guajardo et al, 2013a). Microglia are the resident immune cells that constantly survey and dynamically respond to their microenvironment to take on a variety of homeostatic functions critical for maintaining the health of the neurons and astroglia (Masuda & Prinz, 2016). These sensing functions are mediated via the expression of a large repertoire of proteins such as cytokine receptors, chemokine receptors, scavenger receptors, pattern recognition receptors, purinergic receptors, ion

channels and neurotransmitter receptors (Kierdorf & Prinz, 2013). These receptors enable microglia to sense extrinsic changes such as pathogens, pH, adenosine triphosphate (ATP), amino acids, neurotransmitters and cytokines in the microenvironment (Kettenmann et al, 2013). When the receptor-ligand interaction occurs, it triggers a cascade of molecular events to alter the activation state and thereby functions of microglia (Shemer et al, 2015). Thus, microglia can exist in a continuum of molecular and morphological phenotypes, which at extremes are termed the classical activation state (M1-like) and alternative activation state (M2-like). In the classical profile, microglia express and release pro-inflammatory and cytotoxic molecules like tumor necrosis factor-alpha (TNF-α), interleukin-6 (IL-6), interferon-gamma (IFNγ) and nitric oxide contributing to amplification of responses during injury or infection. In the alternative activation state, however, microglia are characterized by the release of anti-inflammatory molecules like IL-10 and arginase, which are involved in repair mechanisms. An imbalance in the activation state of microglia favouring the classical activation state is implicated in the neuroinflammatory pathophysiology of PD (Moehle & West, 2015). These data have led to a number of studies to investigate whether α-synuclein alters the activation state of microglia through studies on primary cultures as well as microglial cell line such as the BV-2 cells (Sanchez-Guajardo et al, 2013a).

While microgliosis has been shown to be a major contributor to the pathology of PD, astroglia, the most abundant glial cell type, also has a role in PD pathology (Croisier & Graeber, 2006). In moderate to severe cases of disease, astrocytes enter a state of reactive gliosis and begin to secrete molecules such as TNFα and IL-1β, which are thought to

regulate and further modulate the classical activation state of microglia, maintaining neuroinflammation (Medeiros & LaFerla, 2013; Sanchez-Guajardo et al, 2013a). Several studies have begun examining extracellular α-synuclein-mediated effects of astrocytes (Lee et al, 2010b). These direct effects of α-synuclein have been shown to be mediated through TLR4 receptors, which can induce mitochondrial dysfunction, increase nuclear factor κB activity along with increases in expression of GFAP, pro-inflammatory cytokines, adhesion molecules and MMPs (Braidy et al, 2013; Fellner et al, 2013; Joo et al, 2010; Klegeris et al, 2006; Klegeris et al, 2007; Koob et al, 2010; Lee et al, 2010c; Rannikko et al, 2015; Tousi et al, 2012). In vivo, reactivity of astrocytes is correlated to the distance of the neighboring injury following direct injection of α-synuclein or endogenous α-synuclein inclusions (Ahn et al, 2012; Gan et al, 2012; Gu et al, 2010; Hishikawa et al, 2005; Nakamura et al, 2016; Radford et al, 2015; Sacino et al, 2013; Shrivastava et al, 2016; Tong et al, 2015; Valera et al, 2014; Wakabayashi et al, 2000). Based on the current literature, it is clear that astrocytes play a role in synucleinopathies, however further studies of astrocyte responses to different forms of α-synuclein should be completed.

Unfortunately, the existing literature is confusing and full of contradictory results. Thus monomeric, small molecular weight oligomeric or larger fibrillar α-synuclein have all been shown to either induce or fail to induce the pro-inflammatory, classical activation of microglial and macrophage-like transformed cell lines as well as primary microglia and astrocytes (Sanchez-Guajardo et al, 2015). One reason for the lack of consistency may be that few studies have conducted robust concentration- and time-response studies and

side-by-side comparison of monomeric versus adequately characterized aggregated α-synuclein in a given cell type and experimental conditions. Even those studies that have performed direct comparison of α-synuclein aggregates versus monomeric α-synuclein have reported inconsistent results, which may be due to experimental differences such as concentrations of α-synuclein tested (Beraud et al, 2013; Codolo et al, 2013; Daniele et al, 2015; Fellner et al, 2013; Joo et al, 2010; Klegeris et al, 2006; Koob et al, 2010; Lee et al, 2010a; Park et al, 2008; Rannikko et al, 2015; Russo et al, 2015). Similarly, different groups have reported inconsistent results on the effects of α-synuclein on phagocytic activity (Boza-Serrano et al, 2014; Fellner et al, 2013; Park et al, 2008). Thus, it remains unclear whether monomeric or aggregated α-synuclein induces proinflammatory phenotype in microglia-like cells and its functional effect on phagocytosis.

Characterization of α-synuclein fibrils

Sister aliquots of a single lot of recombinant α-synuclein monomeric and fibrillar preparations were used for all the studies detailed here. To characterize the fibrils prior to testing on cell cultures, we determined protein concentrations and assessed thioflavin-T binding, Western blotting and TEM. As expected, there was no binding of thioflavin-T to monomeric α-synuclein whereas fibrillar α-synuclein showed high level of binding (Figure 7A). SDS-PAGE followed by immunoblotting with an α-synuclein antibody showed low molecular weight bands for the monomer preparation at ~14 and 42 kDa, whereas the fibrillar preparation showed the expected smear of multimeric proteins ranging from 35 to 250 kDa (Figure 4.1B). Analysis of fibrils by TEM revealed straight, elongated and uniform filaments (Figure 4.1C). Taken together, the analyses of the

agitated recombinant α-synuclein indicate the presence of beta-sheet containing, SDS-resistant fibrils.

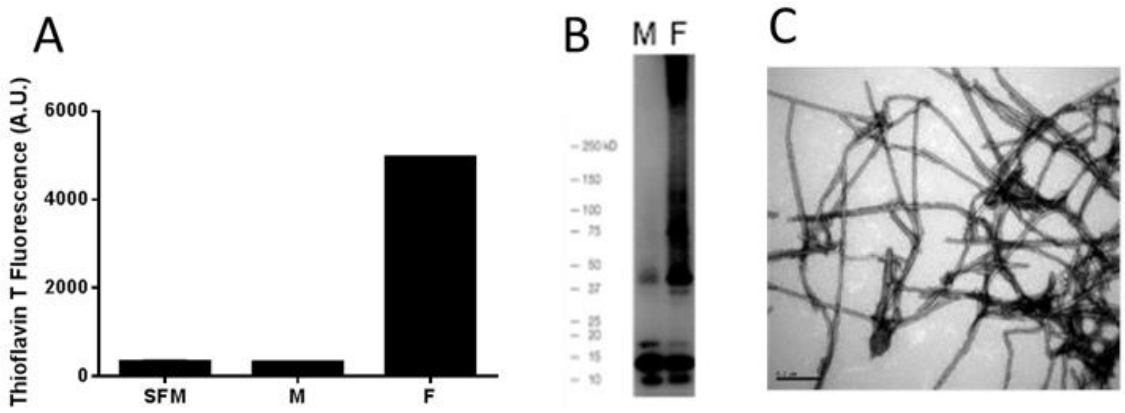

Figure 7: Characterization of α-synuclein fibrils
A) Relative fluorescence units (RFU) of thioflavin-T added to serum-free media (SFM), monomeric α-synuclein (M) or fibrillar α-synuclein (F). Thioflavin-T binding signal of 4957 Arbitrary Units (A.U.) in the fibrillar α-synuclein (F; agitated and dialyzed solution) confirms monomer to fibril conversion of α-synuclein compared to a signal of 311 A.U. at 494 nm of the monomeric (unagitated) α-synuclein (M), comparable to the background of thioflavin-T with serum-free media (SFM). B) Monomeric (M) and fibrillar (F) α-synuclein were assessed by Western blot under reducing conditions. Note the absence of any multimeric forms evident as high molecular weight products in monomeric α-synuclein. Fibrillar α-synuclein separates at high molecular weight, which indicates presence of multimeric fibrillar protein. C) Representative image of TEM analysis of fibrillar α-synuclein. Filaments from fibrillar α-synuclein have lengths of 0.25 to 2.0 μm and a mean width of 14.1 nm. Magnification bar = 0.2 μm.

BV-2 microglial cells show dose-dependent induction in Il6 mRNA levels following treatment with fibrillar, but not monomeric α-synuclein

IL-6 is a pro-inflammatory cytokine that marks the classical activation state of microglia. To understand the dose-response relationship for fibrillar α-synuclein-mediated activation of BV-2 cells, we examined *Il6* mRNA levels at 3 hours following treatment with fibrillar α-synuclein at 0.03, 0.3 or 3 μg/mL or monomeric α-synuclein at 3 μg/mL. Monomeric α-synuclein did not affect *Il6* levels but a dose-dependent response was produced by

fibrillar α-synuclein, with the highest concentration showing a statistically significant effect (Figure 8A). Importantly, the increase in *Il6* was seen in the absence of cytotoxicity, as assessed by LDH release in the media (Figure 8B). The BV-2 cell lysate was used as an analytical positive control and demonstrates the validity of our LDH measurements.

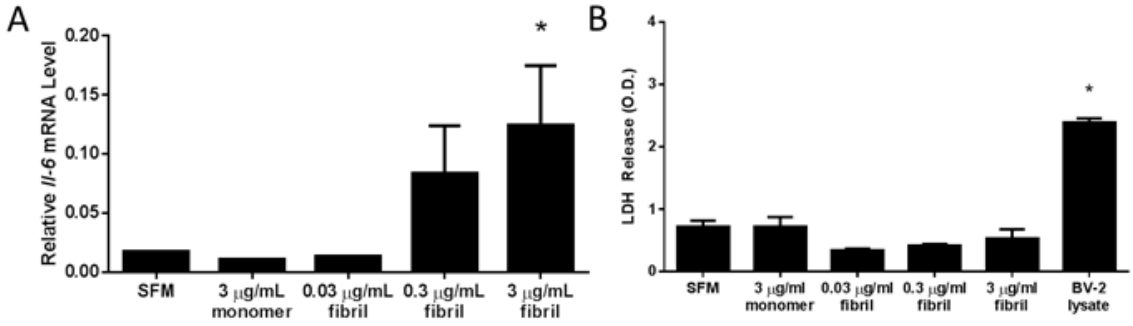

Figure 8: Increasing dose of recombinant α-synuclein fibrils increased Il6 mRNA in vitro without altering microglia cell death after 3 hours.
BV-2 microglia were treated with 3 μg/mL of monomeric α-synuclein or fibrillar α-synuclein at different concentrations (0.03, 0.3 or 3 μg/mL) or serum-free media prior to measuring *Il6* mRNA levels which significantly increased at the highest concentration of fibrillar α-synuclein treatment tested, when compared to serum-free media. * $p<0.05$. B) BV-2 microglia treated with 3 μg/mL of monomeric α-synuclein, fibrillar α-synuclein at different concentrations (0.03, 0.3 or 3 μg/mL) or serum-free media (SFM) did not increase release of lactate dehydrogenase (LDH) into the culture media as measured by optical density (OD) at 490 nm. Total cell lysate of SFM treated BV-2 cells served as a positive control for LDH release. * $p<0.05$, ANOVA followed by student's t.

BV-2 microglial cells are classically activated by fibrillar but not monomeric α-synuclein: histological and morphological markers

Having assessed an active dose of fibrillar α-synuclein, we went on to examine directly BV-2 activation by monitoring the expression of IBA1, a marker of classically activated microglia (Ito et al, 1998). Cultured mouse BV-2 microglial cells were incubated with serum-free media, monomeric α-synuclein (3 μg/mL), fibrillar α-synuclein (3 μg/mL), or

IFNγ (0.1µg/mL) as a positive control for 3 or 24 hours followed by fixation and immunohistochemistry for IBA1. Compared to the serum-free media control, the number of IBA1 expressing BV-2 cells increased time-dependently following treatment with fibrillar α-synuclein and IFNγ but not those treated with monomeric α-synuclein (Figure 9A-D). Quantitative assessment of IBA1 immunofluorescence confirmed these findings (Figure 9E).

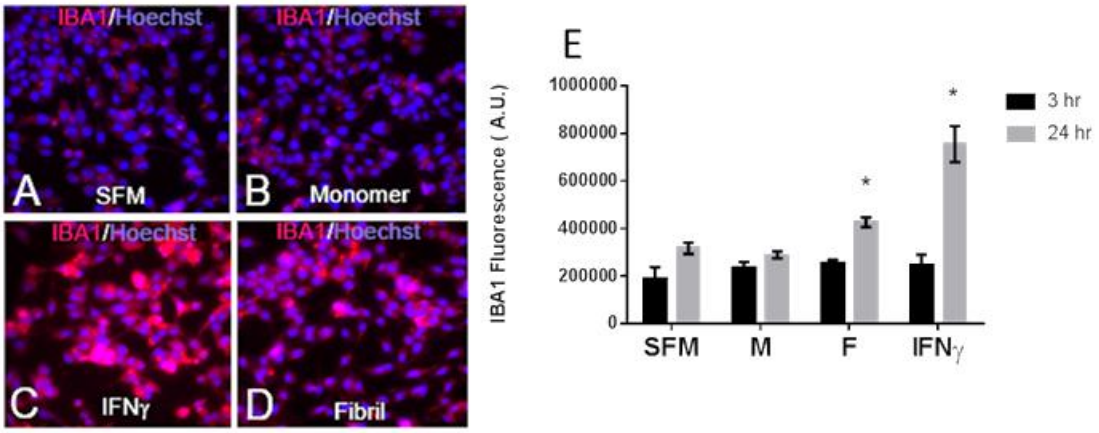

Figure 9: α-Synuclein fibrils and IFNγ activate BV-2 microglia compared to monomeric α-synuclein

A-D) BV-2 microglia treated with serum-free media (SFM, A) 3 µg/mL α-synuclein monomer (B), 0.1 µg/mL interferon γ (IFNγ) (C), or 3 µg/mL α-synuclein fibrils (D) prior to double-labelling with IBA1 and Hoechst stain. Images show IBA1 fluorescence (red) and Hoechst (blue). E) Mean fluorescent intensity of IBA1 in cells treated with serum-free media (SFM), 3 µg/mL monomeric α-synuclein (M), 3 µg/mL fibrillar α-synuclein (F) or 0.1 µg/mL IFNγ for 3 or 24 hours (hr). * $p<0.05$, ANOVA followed by student's t.

Time course of α-synuclein fibril induces increased mRNA levels and release of classical activation markers in BV-2 cells

Classical activation of microglia is accompanied by an increase in the expression of mRNA encoding pro-inflammatory cytokines, *Il6*, *Tnf*, and nitric oxide synthase 2

(*Nos2*). Hence, we assessed the time-course of changes in the mRNA levels of these markers after treating BV-2 cells for 3, 9, or 24 hours with serum-free media, LPS (positive control, 100 ng/mL), monomeric α-synuclein (3 μg/mL), and fibrillar α-synuclein (3 μg/mL). As expected, bacterial LPS-treated cells dramatically increased *Il6, Tnf and Nos2* mRNA levels. Treatment with monomeric α-synuclein failed to induce *Il6, Tnf* or *Nos2* levels at any time point examined. In contrast, aggregated α-synuclein robustly increased the expression of all three mRNAs at all time points examined, but with a time course that was somewhat distinct for each mRNA (Figure 10A-C). Thus *Il6* was significantly and similarly elevated by fibrillar α-synuclein at 3 and 9 hours but began to recover at 24 hours; this pattern was similar to the response produced by LPS. *Tnf* peaked at 3 hours and began to recover at 9 hours following treatment with fibrillar α-synuclein as well as LPS. At 24 hours, the LPS-induced *Tnf* response showed complete recovery but remained significantly high in fibrillar α-synuclein treated cells. Finally, *Nos2* induction appeared to have a biphasic time course in response to both fibrillar α-synuclein and the LPS, with 9 hours showing the least induction followed by a second phase of induction apparent at 24 hours. In order to examine whether the increase in *Il6* and *Tnf* levels is associated with an increase in the release of these inflammatory cytokines, we assessed IL-6 and TNFα protein levels in the media under an extended time-course. A significant increase in secreted IL-6 and TNFα was noted after treatment with both LPS and fibrillar α-synuclein but not monomeric α-synuclein (Figure 10D and E). The peak increases in the protein levels in the media occurred at 9 hours, which were time-shifted compared to the peak increases in the mRNA levels of *Il6* and *Tnf*. By 15 hours, both cytokines appeared to be in the recovery phase but the levels remained

significantly high at 24 hours. It is important to note that none of the treatments affected LDH release (data not shown), indicating that the changes in the cytokine protein levels in the media result from the secretion of the cytokines and not cell death.

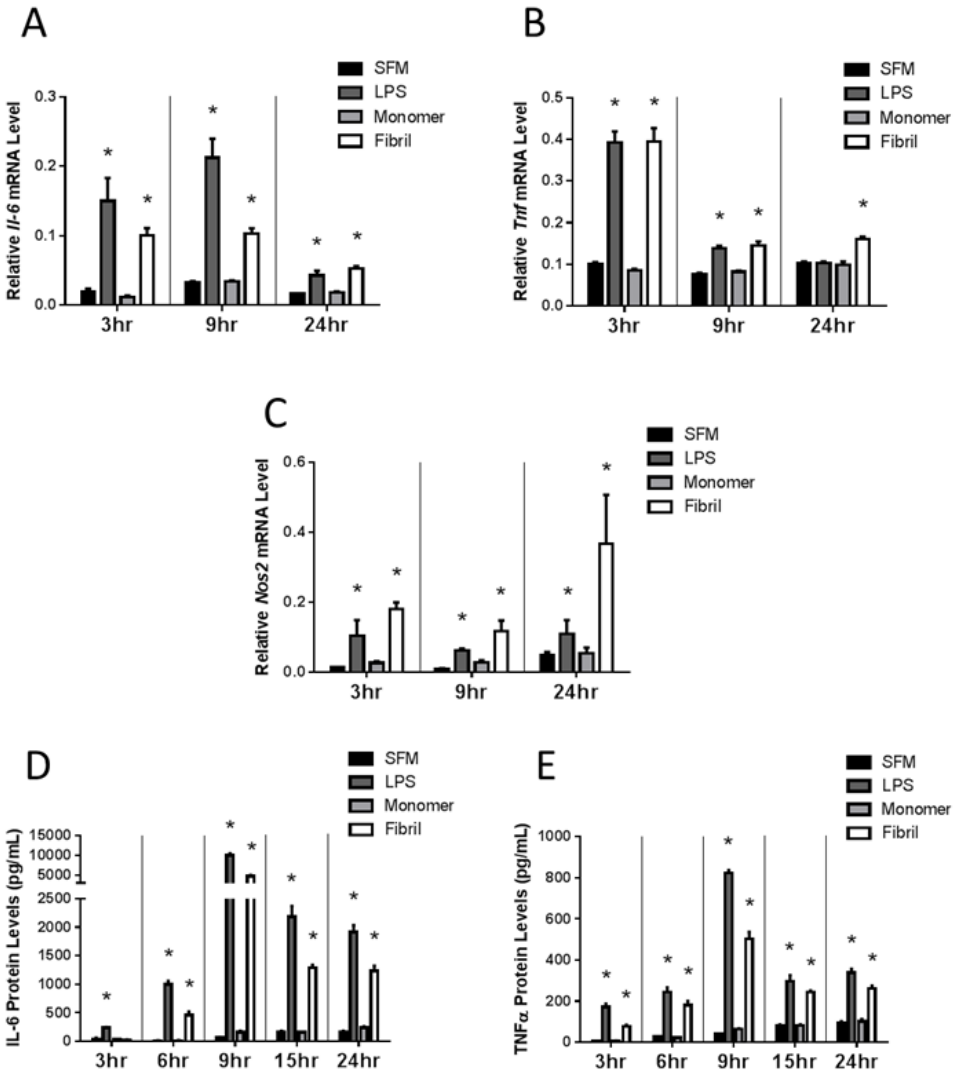

Figure 10: mRNA markers of classical activation and cytokine release increase in the presence of fibrillar α-synuclein compared to monomeric α-synuclein

Relative levels of Il6 (A), Tnf (B) and Nos2 (C) were determined by RT-qPCR at 3, 9, and 24 hours (hr) of treatment with serum-free media (SFM), 0.1 μg/mL LPS, 3 μg/mL α-synuclein monomer or 3 μg/mL α-synuclein fibril. Levels of IL-6 (D) and TNFα were quantified from media by ELISA from BV-2 microglia treated for 3, 6, 9, 15, and 24 hours (hr) with serum-free media (SFM), 0.1 μg/mL, 3 μg/mL α-synuclein monomer or 3 μg/mL α-synuclein fibril. * $p<0.05$, ANOVA followed by student's t.

α -Synuclein fibrils increase TNFα levels in primary microglia

Since BV-2 cells are a transformed cell line, we wanted to confirm that primary microglia are also classically activated by α-synuclein fibrils in a manner similar to what we observed in the BV-2 cells. CD11b-expressing microglia cells were isolated and cultured from early postnatal age as well as 5 month old mice. Primary microglial cultures were treated for 24 hours under serum-free conditions with monomeric α-synuclein, fibrillar α-synuclein or LPS as a positive control and the secretion of the pro-inflammatory cytokine, TNFα, in the media was examined. As seen with BV-2 cells, monomeric α-synuclein failed to alter TNFα secretion whereas α-synuclein fibrils increased TNFα levels in the media by nearly 3-fold (Figure 11A and B). Taken together, these data indicate that BV-2 cells are a viable model to characterize the effects of α-synuclein on activation states of microglia.

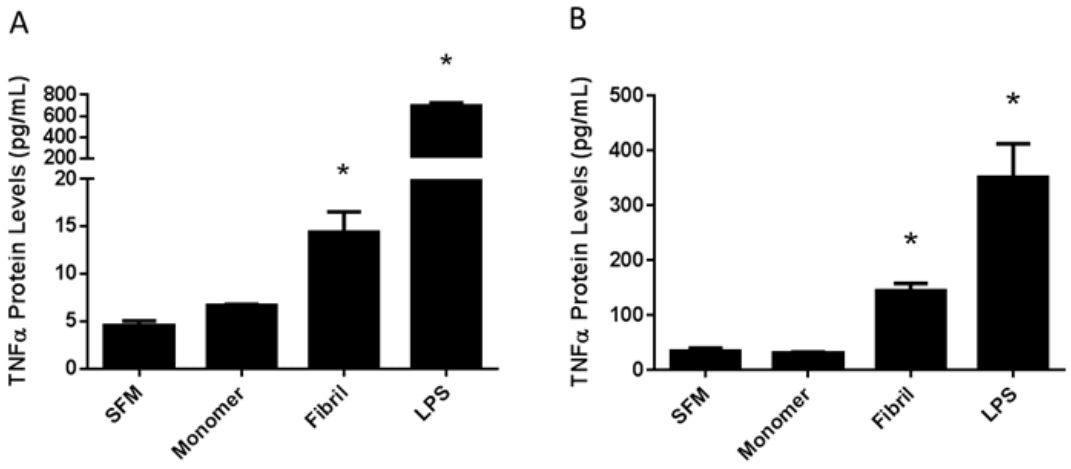

Figure 11: Primary microglia increased TNFα release in the presence of fibrillar α-synuclein

Levels of TNFα released by primary microglia isolated from postnatal day 8 (A) or 5-month old (B) WT mice were quantified from media by ELISA after treatment for 24 hours with serum-free media (SFM), 3μg/mL α-synuclein monomer, 3 μg/mL α-synuclein fibril or 0.1 μg/mL LPS. * $p<0.05$, ANOVA followed by student's t.

α-Synuclein fibrils increase TNFα levels in primary astrocytes

Although a significant increase in IL-6 and TNFα was seen in microglia, it is possible that other glial cells contribute to α-synuclein-mediated pro-inflammatory responses. To understand the α-synuclein responses of astrocytes, another glial cell type with the ability to secrete cytokines and regulate microglia, a pure population of GLAST-expressing mouse astrocytes was treated for 24 hours. These cells increased secretion of TNFα in both LPS and fibril treated cells when compared to monomeric α-synuclein. No increases of TNFα were present with control serum-free media or α-synuclein monomer treatment (Figure 12).

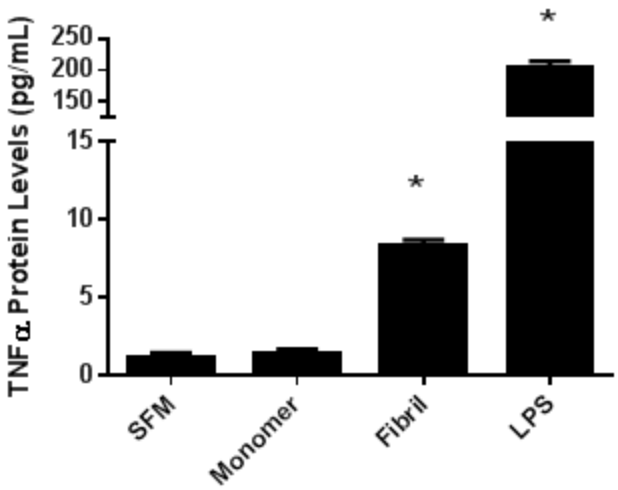

Figure 12: Primary astrocytes increased TNFα release in the presence of fibrillar α-synuclein

Levels of TNFα from primary astrocytes cultured from postnatal day 8 WT mice were quantified from media by ELISA after treatment for 24 hours with serum-free media (SFM), 3μg/mL α-synuclein monomer, 3 μg/mL α-synuclein fibril or 0.1 μg/mL LPS. * $p<0.05$, ANOVA followed by student's t.

α-Synuclein fibrils decrease markers of alternative activation in BV-2 cells

Unlike the pro-inflammatory state of classically activated microglia, the so-called alternative activation state is dominated by anti-inflammatory cytokine expression. In order to determine whether monomeric or fibrillar α-synuclein differentially affect the alternative activation state, we examined their effects of mRNAs for four prototypical alternative state markers, arginase 1 (*Arg1*), interleukin 10 (*Il10*), chitinase 3-like-3 (*Chi3l3*) and mannose receptor C1 (*Mrc1*). Interestingly, α-synuclein fibrils, but not monomers, at 3 μg/mL reduced all four markers, albeit at different time courses. Thus a reduction in *Arg1* was seen as early as 3 hours whereas that in *Il10* and *Chi3l3* was not seen until 24 hours and *Mrc1* was reduced at 9 hours (Figure 13A-D). Another noteworthy observation is that LPS reduced only *Mrc1* mRNA without affecting *Arg1*, *Il10* or *Chi3l3*. Overall, these data indicate that α-synuclein fibrils shift the activation state of BV-2 cells away from the alternative, anti-inflammatory phenotype to a pro-inflammatory phenotype.

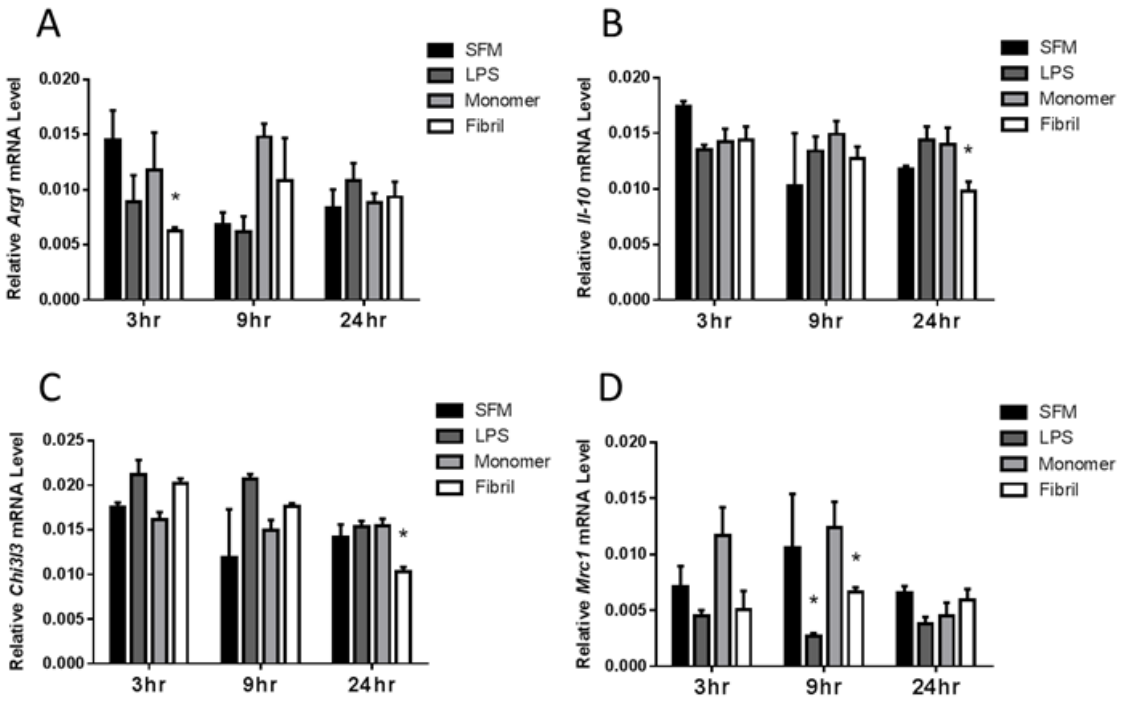

Figure 13: mRNA markers of alternative activations decreased in the presence of fibrillar α-synuclein

The relative levels of arginase 1 (Arg1, A), interleukin 10 (Il10, B), chitinase 3-like-3 (Chi3L3, C) and mannose receptor C1 (Mrc1, D), and were determined by RT-qPCR in BV-2 cells at 3, 9, and 24 hours (hr) following treatment with serum-free media (SFM), 0.1 μg/ml LPS, 3 μg/ml α-synuclein monomer or 3 μg/ml α-synuclein fibril. * $p<0.05$, ANOVA followed by student's t.

Effects of monomer and fibrils of α-synuclein on phagocytosis in BV-2 cells

One major function of microglia is phagocytosis, which is affected by the activation state of these cells. Trem2 is a key receptor expressed exclusively on microglia and myeloid cells that promotes the phagocytic function of microglial cells while reducing pro-inflammatory cytokine expression and inducing anti-inflammatory cytokine expression. Hence, we examined the effects of monomeric and fibrillar α-synuclein on the mRNA encoding *Trem2* and its co-receptor, *Tyrobp*. Treatment of BV-2 cells with fibrillar α-synuclein as well as LPS reduced *Trem2* levels at 9 hours, with the reduction still significantly sustained at 24 hours (Figure 14A). *Tyrobp* levels were also reduced by

fibrillar α-synuclein at 24 hours but the LPS effect did not reach statistical significance (Figure 14B). *Cd33* is another pattern-recognition receptor involved in phagocytosis but its mRNA levels were undetectable in BV-2 cells (data not shown).

In light of the current data on *Trem2* and *Tyrobp* as well as the conflicting literature about the effects of α-synuclein on phagocytosis, we conducted rigorous assessment of monomeric and fibrillar α-synuclein effects on this functional end-point in BV-2 cells. Three independent experiments demonstrated that both monomeric and fibrillar α-synuclein treatment of BV-2 cells for 24 hours increases phagocytosis of *E. coli* bioparticles by ~25% when compared to serum-free media treatment (a representative example is shown in Figure 14C). On the other hand, LPS treatment did not affect phagocytosis despite reducing *Trem2* levels. We used a 30-minute treatment with Cytochalasin D, an actin polymerization inhibitor, as an experimental positive control to demonstrate a decreased phagocytic ability of BV-2 microglia by over 50%. In the absence of bioparticles, very little background fluorescence was observed.

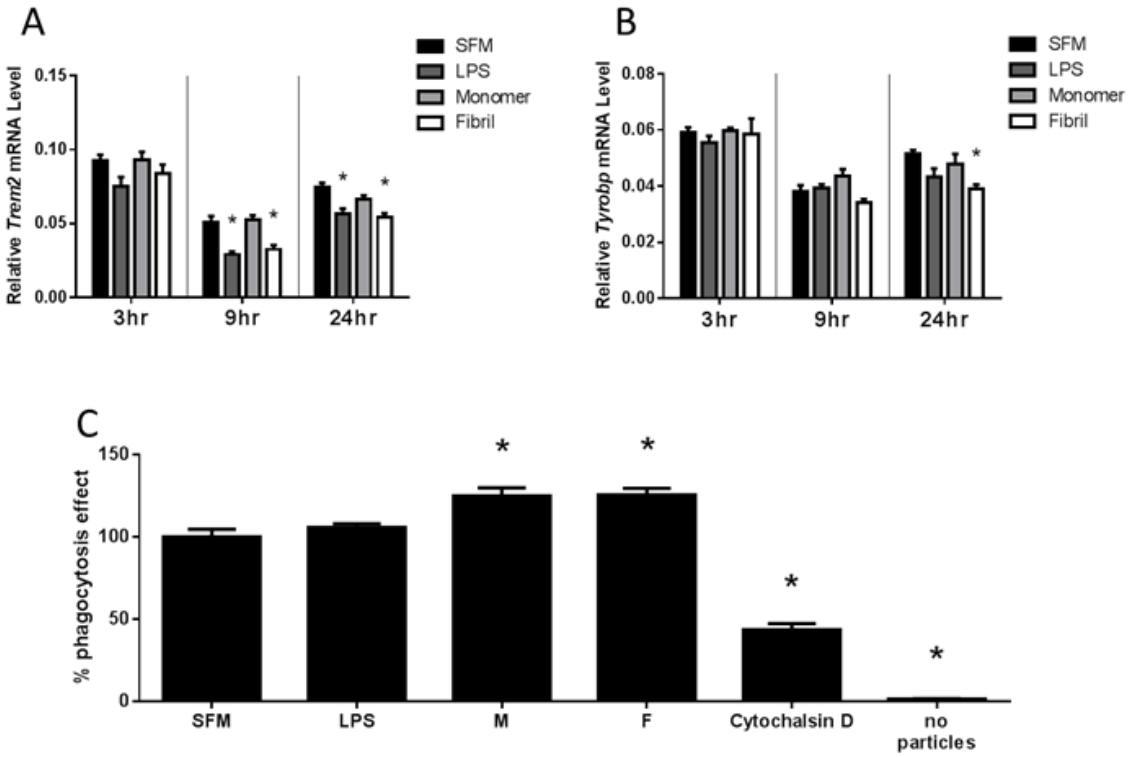

Figure 14: function increased and phagocytosis co-receptors Trem2 and Tyrobp decreased in BV-2 microglia following α-synuclein treatment

Relative Trem2 (A) and Tyrobp (B) mRNA levels in BV-2 microglia following treatment with serum-free media (SFM), 0.1 μg/ml LPS, 3 μg/ml α-synuclein monomer or 3 μg/ml α-synuclein fibril for 3, 9 and 24 hours (hr). C) Percent phagocytosis effect was assessed following 24 hour stimulation with serum-free media (SFM), 0.1 μg/ml LPS, 3 μg/ml α-synuclein monomer (M), 3 μg/ml α-synuclein fibrils (F), 10 μm Cytochalasin D for 30 minutes or no particle negative control in BV-2 cells. * $p<0.05$, ANOVA followed by student's t.

Discussion

The present study sought to systematically compare the effects of α-synuclein monomers and fibrils on the activation states of microglia as well as their phagocytic function. We prepared and characterized α-synuclein high molecular weight fibrils using a method similar to that reported by Beraud *et al*. (Beraud et al, 2013). The fibrillar nature of the aggregated α-synuclein was confirmed by TEM and thioflavin T binding. Furthermore, SDS-PAGE immunoblotting demonstrated the presence of SDS-resistant, high molecular

weight aggregates in the fibrillar preparation but not the monomeric preparation. In order to minimize the effects of lot-to-lot variability in α-synuclein aggregation, we prepared a large batch of aggregated α-synuclein and used sister aliquots for all the studies described here.

Treatment of BV-2 cells, a murine microglial cell line, with different concentrations of fibrillar α-synuclein induced *Il6* mRNA in a concentration-dependent manner, with 3 μg/mL showing robust, reproducible and statistically significant effects in the absence of cytotoxicity. On the other hand, 3 μg/mL of monomeric α-synuclein did not affect *Il6* mRNA expression. This dose of fibrillar α-synuclein also induced hypertrophy of BV-2 cells and expression of IBA1. Taken together, these data indicated that fibrillar α-synuclein induces a pro-inflammatory, M1-like phenotype in BV-2 cells. To characterize and compare the activation state of BV-2 cells exposed to monomeric versus fibrillar α-synuclein, we performed time-course experiments and analyzed alterations in mRNA and protein levels for markers of classical and alternative activation states. These data convincingly demonstrated increases in the mRNA encoding *Il6*, *Tnf* and *Nos2* as well as release of IL-6 and TNFα in the media when BV-2 cells were treated with fibrillar α-synuclein but not monomeric α-synuclein. Importantly, we also demonstrated that primary microglia cultures prepared from either neonatal or 5 month old mice show TNFα release in response to fibrillar α-synuclein but not monomeric α-synuclein and extended our experiments to show similar TNFα response from primary astrocytes. Thus, the classical activation and cytokine release is consistently induced by fibrillar α-synuclein in a transformed cell line as well as primary microglia and astrocytes.

Interestingly, fibrillar α-synuclein reduced the expression of markers of alternative activation, *Arg1, Il10, Chi3l3* and *Mrc1*, whereas monomeric α-synuclein did not induce changes in any M2 marker. In general, the effects of fibrillar α-synuclein on classical activation were similar to those of an endotoxin. On the other hand, LPS treatment had minimal effects on alternative activation markers, agreeing with previous reports of acute treatment of primary microglia with LPS (Tanaka et al, 2015). These data demonstrate that fibrillar α-synuclein shifts microglial cells to the classical activation state and decreases markers of alternative activation, whereas monomeric α-synuclein has no effect at concentrations tested.

The differential effects of fibrillar versus monomeric α-synuclein on markers of classical activation observed in our studies are generally consistent with the report by Beraud *et al*. (Beraud et al, 2013). One notable difference was that the minimally effective concentration we observed for significant induction of the classical activation state in BV-2 cells was 3 μg/mL (~200 nM), which is 4-fold higher than that reported by Beraud *et al*. (Beraud et al, 2013). However, this small discrepancy could be explained by the differences in their method to prepare fibrillar α-synuclein. Following aggregation, Beraud *et al*. (Beraud et al, 2013) used size separation to enrich their preparation for aggregated species >150 kDa in size, which may have increased the potency of their preparation. In fact, a comparison of their data on TNFα release between Beraud *et al*., 2013 and an earlier paper (Beraud et al, 2011) where they did not enrich for larger aggregates indicates that the enriched preparation does have a higher potency as evidenced by greater TNFα release.

It is important to discuss the relevancy of 3 μg/mL (~200 nM) concentration of α-synuclein used in the present studies to PD pathophysiology. Previously, we have assessed α-synuclein release in cultures of a variety of cells, including iPS-derived neurons. These studies consistently show that ~10% of intracellular α-synuclein is released into the media (data not shown). Taken together with estimated concentrations of 2 to 5 μM of total α-synuclein in PD brains (Cremades et al, 2012; Iwai et al, 1995; Westphal & Chandra, 2013), we contend that the concentration of 200 nM used here is within range of expected interstitial fluid levels of α-synuclein. Of course, studies that directly measure interstitial α-synuclein levels in rodent and human brains are needed to definitively establish the pathogenic significance of the α-synuclein concentration tested here.

Our results of selective effects of fibrillar α-synuclein on inducing a pro-inflammatory phenotype in microglial cells appear to be in contradiction with those of others (Beraud et al, 2013; Codolo et al, 2013; Lee et al, 2010a) and a more recent report (Hoenen et al, 2016), which associates wild-type monomeric α-synuclein with weak pro-inflammatory induction. Collectively, these studies report that both monomeric and non-sonicated α-synuclein pre-formed fibrils induced markers of classical activation such as reactive oxygen species, nitric oxide, nuclear translocation of nuclear factor κB, IP-10, TNFα and IL-1β in primary microglia/monocytes or mixed glial culture. However, these studies tested 1 to 10 μM of α-synuclein monomers and fibrils, a range significantly higher than 200 nM of fibrillar α-synuclein tested in the present studies. Whether such high

concentrations of monomeric or aggregated α-synuclein have relevance to PD pathophysiology remains to be seen.

Effects of α-synuclein in primary astrocytes were examined to understand the response of another glial cell type, which can regulate the state of microglia. Astrocytes are able to produce inflammatory cytokines and chemokines that communicate with neighboring microglia. Stimulation of astrocytes by α-synuclein was shown to activate pro-inflammatory cytokine release, which may induce secondary effects such as classical microglia activation, to create a potentially amplified inflammatory response (Lee et al, 2010b). The differential effects of fibrillar versus monomeric α-synuclein are consistent with classical activation of the pro-inflammatory state of microglial cells in present experiments. Few published reports have examined cytokine release following treatment with monomer and fibrillar α-synuclein in astrocytes. Dramatic changes in cytokine expression following neuron-secreted α-synuclein exposure over 24 hours were previously reported (Lee et al, 2010c). Also, IL-1-induced CXCL10 protein expression and secretion was potentiated by co-exposure with aggregated α-synuclein (Tousi et al, 2012). However, these results along with the current findings conflict with other literature reports. Monomeric α-synuclein treatment has been shown to increase MMP9, a pro-inflammatory mediator, compared to aggregated treatment (Joo et al, 2010). Also, TLR4, GFAP, IL-6, and ICAM1 have all shown to be increased in astrocytes when treated with the monomeric α-synuclein (Klegeris et al, 2006; Koob et al, 2010; Rannikko et al, 2015). The main discrepancy of these experiments is that the tested concentrations are

again much higher than in present studies and presumed physiologically relevant concentrations.

To investigate the functional implications of altered activation state, we studied phagocytic capacity of α-synuclein treated BV-2 cells 24 hours after treatment with monomeric or fibrillar α-synuclein. This time point was selected for functional assessment since we observed a sustained change in a number of M1-associated molecular and morphological markers. These studies showed that both monomeric and fibrillar α-synuclein similarly enhanced phagocytosis in BV-2 cells. These data are consistent with other reports (Boza-Serrano et al, 2014; Fellner et al, 2013). Fellner *et al*. included primary microglia and observed that 3 μM of soluble monomers as well as fibrillar α-synuclein increased phagocytosis. Note that they assessed phagocytosis at 2 hours of treatment, a significantly earlier time point, which may have required a higher concentration to observe an effect of α-synuclein. Boza-Serrano *et al*. also demonstrated an increase in phagocytosis by BV-2 cells, but again at a higher concentration of 20 μM of fibrillar α-synuclein and following a shorter treatment duration of 12 hours (Boza-Serrano et al, 2014). There is one literature report that shows results that contradict ours as well as the literature discussed above. Thus Park *et al*. reported an increase in phagocytosis by BV-2 cells following 24 hour treatment with 5 μM monomeric α-synuclein but a decrease by 1 μM fibrillar α-synuclein (Park et al, 2008). The reasons underlying the apparent discrepancy remain unclear but indicate the importance of conducting systematic concentration- and time-response studies to select optimal experimental conditions.

In order to evaluate a possible mechanism associated with phagocytic effects of α-synuclein discussed above, we focused on the TREM2 pathway. TREM2 and its adapter protein, TYROBP, are highly expressed in microglia (Colonna & Wang, 2016), where they are thought to regulate phagocytic function and inflammation (Painter et al, 2015; Thrash et al, 2009). Although not consistently replicated, TREM2, and specifically the R47H variant, has been implicated in the etiology of PD through genetic association (Mengel et al, 2016; Rayaprolu et al, 2013). We assessed the effects of α-synuclein on mRNA levels of *Trem2* and *Tyrobp*. Contrary to our expectations founded on the observed increases in phagocytosis discussed above, fibrillar α-synuclein reduced the levels of *Trem2* and *Tyrobp* whereas monomeric α-synuclein was without effect.

Previous studies (Beraud et al, 2011; Fellner et al, 2013; Rannikko et al, 2015; Stefanova et al, 2011; Su et al, 2009; Su et al, 2008) have implicated several microglial receptors in the uptake of α-synuclein. Thus deletion of toll-like receptor 4 (*Tlr4*), a signaling pattern recognition receptor, or *Cd36*, a scavenger receptor important for endocytosis, dampens α-synuclein mediated effects. Beraud *et al*. were unable to show significant decreases in several *Tlr* genes or *Cd36* following α-synuclein treatment in BV-2 cells (Beraud et al, 2011). Together, these data should prompt further interrogation of phagocytic receptors, including TREM2, and their capacity for phagocytosis following cellular interaction with α-synuclein. In the current study using the same cell line, we were unable to detect significant mRNA levels of *Cd33*, an innate immunity integrin-associated transmembrane protein implicated in neurodegeneration by genome-wide association studies. Further studies using a cell line or primary microglia with different genetic makeup should be

completed to understand the impact of CD33 on α-synuclein mediated uptake. Regardless of the mechanism, the increase in phagocytosis by both monomeric and aggregated α-synuclein indicates that microglia may be involved in clearance of extracellular α-synuclein. However, an inflammatory milieu may be induced only by α-synuclein aggregates, which may contribute to the progressive loss of dopamine neurons (reviewed by Sanchez-Guajardo et al, 2013a).

In summary, through systematic dose-response and time-course studies and a combination of molecular and morphological markers, we have convincingly demonstrated that fibrillar α-synuclein but not monomeric α-synuclein, induces pro-inflammatory, classical activation of BV-2 cells while reducing the alternative activation state. The selective increase in pro-inflammatory cytokines by fibrillar α-synuclein was observed also in primary mouse microglia, further strengthening the translational implications of the data from BV-2 cell cultures. In contrast to the molecular phenotypes, the phagocytic function of BV-2 cells was increased similarly by monomeric and fibrillar α-synuclein. This dichotomy between molecular phenotypes and phagocytic function of microglia exemplify the complexity in the relationship between molecular activation state markers and functions of microglia. Overall, the direct comparative analysis of the effects of α-synuclein monomers and fibrils shown here addresses several inconsistencies in the literature and support previous studies indicating that α-synuclein aggregation, but not monomeric α-synuclein, triggers an inflammatory milieu that may contribute to the chronic pathophysiology of Parkinson's disease and other synucleinopathies.

Conclusions

Overall the data shown here lead us to conclude that, fibrillar α-synuclein, but not monomeric α-synuclein, shifts the activation state of microglia towards the classical proinflammatory state. This response could contribute to the chronic neuroinflammatory pathophysiology and progressive neurodegeneration seen in PD brains. On the other hand, the phagocytic function of microglia is induced similarly by monomeric and fibrillar α-synuclein (Figure 15).

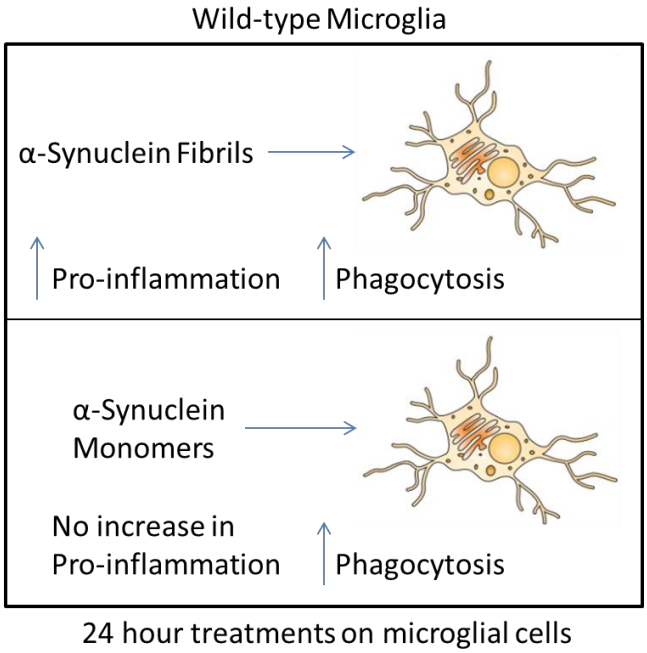

Figure 15: Diagram of working hypothesis of α-synuclein-mediated regulation of microglia

CHAPTER 5: COMPARITIVE ANALYSIS OF MURINE RADIAL GLIA AND ASTROCYTE TRANSCRIPTOMES

Introduction

One aspect of the previous chapter examines the response of primary astrocytes in the presence of fibrillar α-synuclein, a pro-inflammatory stimulus. Astrocytes were shown to produce TNFα, an inflammatory cytokine, following this treatment. The release of this cytokine has been shown to induce a cycle of reactivity in astrocytes and induce many different functions related to reactive astrogliosis (Montgomery & Bowers, 2012). In some cases of neurodegenerative diseases or CNS injuries when TNFα is present, astrocytes de-differentiate, begin to proliferate and continue to release cytokines, which maintains reactive astrogliosis while forming a glial scar and may contribute to disease progression (Carrero et al, 2012). Although it is clear that interaction with released TNFα is involved in the trigger of astrocyte de-differentiation into a progenitor cell prior to proliferation, the mechanisms involved in the process of proliferation are far from defined. To begin to understand this process, it is important to determine the significant factors that are expressed during astrogenesis. One model used to study proliferating astrocytes is developmentally recapitulated during early postnatal stages within the brain (Molofsky et al, 2012). It is unlikely that complete overlap of factors found in developing astrocytes is found during reactive astrogliosis; however studying proliferation of astrocytes during the healthy state may be informative toward understanding a possible comparative factor involved during reactive astrogliosis and proliferation.

Many open questions still remain regarding the differentiation of radial glial cells and astrocytes and the roles they play in the developing central nervous system (Molofsky & Deneen, 2015). A comparative analysis of developing murine astrocytes and the cells from which the earliest astrocytes arise, postnatal radial glial cells, would be of interest in order to determine pathways and factors necessary for astrocytes to begin differentiation.

Many studies have made attempts to investigate either radial glia or astrocyte precursor cells; however, these studies have been complicated by various issues, including methodologies that could possibly introduce artificial qualities within the cells (Beckervordersandforth et al, 2010; Cahoy et al, 2008; Johnson et al, 2015; Pollen et al, 2015; Sirko et al, 2015; Thomsen et al, 2016; Zamanian et al, 2012; Zhang et al, 2014b), the use of shallow sequencing methods (Pollen et al, 2014), amplification of cells *in vitro* prior to mRNA isolation and sequencing (Beckervordersandforth et al, 2010; Sirko et al, 2015; Zamanian et al, 2012), the use of impure populations of cells (Ayoub et al, 2011) or the use of novel non-validated markers (Zhang et al, 2016b). More importantly, a systematic comparative analysis of developing murine astrocytes to the radial glia from which they arise has not been performed.

During the span of proliferative postnatal gliogenic events, many permissive signaling pathways are expressed (Molofsky et al, 2013). Transcription factors that have been implicated in astrocyte differentiation, include Nuclear Factor I-A (NFIA, Deneen et al, 2006), NFE2L1 and ID3 (Molofsky et al, 2013) and SOX9 (Stolt et al, 2003). Pathways with multiple upregulated transcription factors during gliogenesis include BMP signaling

factors like SMAD1/5/8 (Scholze et al, 2014), Notch signaling factors like RBP/J, ID and HES1 (Nagao et al, 2007; Taylor et al, 2007; Zhou et al, 2010b), JAK/STAT related factors including CyclinD1, CBF-1 and STAT3 (Ge et al, 2002; Ma et al, 2015) and MEK signaling factors like ERM and ERK1/2 (Li et al, 2012). On the other hand, LHX2 and nuclear receptor co-repressor (N-CoR) have been implicated as suppressors of astrocyte differentiation (Hermanson et al, 2002; Subramanian et al, 2011). Epigenetic regulation and DNA methylation also has a negative effect on astrocyte differentiation regulated by DNA methyltransferase I (Fan et al, 2005).

In the current study, systematic comparisons of the transcriptome of a large population of whole brain radial glial cells and astrocyte precursors have been analyzed based on gene expression. This study focuses on the characterization of acutely isolated and purified GLAST (+) cells at P0 and P8. GLAST positivity and co-expression of cell type-specific markers confirm the population and expression patterns of the cells of interest. Differential expression and pathway analyses identified novel factors as well as known genes that play a role in radial glia and astrocyte cell functions. Also, transcription factor analysis revealed clusters of differentially expressed and regulated genes within these cells. Overall, this dataset will help to better understand the mechanisms of factors involved in radial glia and astrocyte precursors, using technical conditions with little known bias from the *in vivo* state of these cells.

GLAST-expressing astrocytes are generated postnatally in murine brain

In order to perform a comparative analysis of transcriptomes from radial glia and astrocyte precursor cells, a classification of the stages at which these cells exist in the mouse brain was needed. Moreover, it was imperative to characterize the expression of a protein that spans the cell membrane to be utilized for the isolation of these brain cells. To identify stages and confirm that GLAST, a transporter glycoprotein, was expressed in radial glial cells and astrocyte precursors, sections through developing and postnatal murine brains were co-labeled using immunofluorescence. Markers of radial glial cells and proliferating subventricular zone (SVZ) cells (VIMENTIN), neurons (microtubule associated protein-2; MAP2), oligodendrocytes (myelin basic protein; MBP), and astrocytes (nuclear factor 1A; NF1A) were compared at 4 stages in the cortex; 1) E16.5, a stage at which the large majority of cells will become neurons and low levels of astrocytes/oligodendrocytes are being produced, 2) P0, a low level of neurons and oligodendrocytes are generated, radial glial cells are decreasing, and proliferating astrocyte precursors are generated (Ge et al, 2012), 3) P8, mid-astrogenesis, and 4) P14, astrogenesis is nearly complete (Skoff & Knapp, 1991). Co-expression analyses of GLAST in mid-sagittal cortical sections revealed substantial co-localization of VIMENTIN at E16.5 (Figure 16A) and P0 (Figure 16E), and co-localization of NF1A at P8 (Figure 16J) and P14 (Figure 16N). Other markers did not show high levels of co-localization. The degree of overlap per region in different stages was quantified and correlation coefficients (r) were calculated using confocal images. These calculations confirm co-localization of GLAST/VIMENTIN in E16.5 and P0 as well as

GLAST/NF1A in P8 and P14 cortex, while other stages and markers show low levels of co-localization (Figure 16Q).

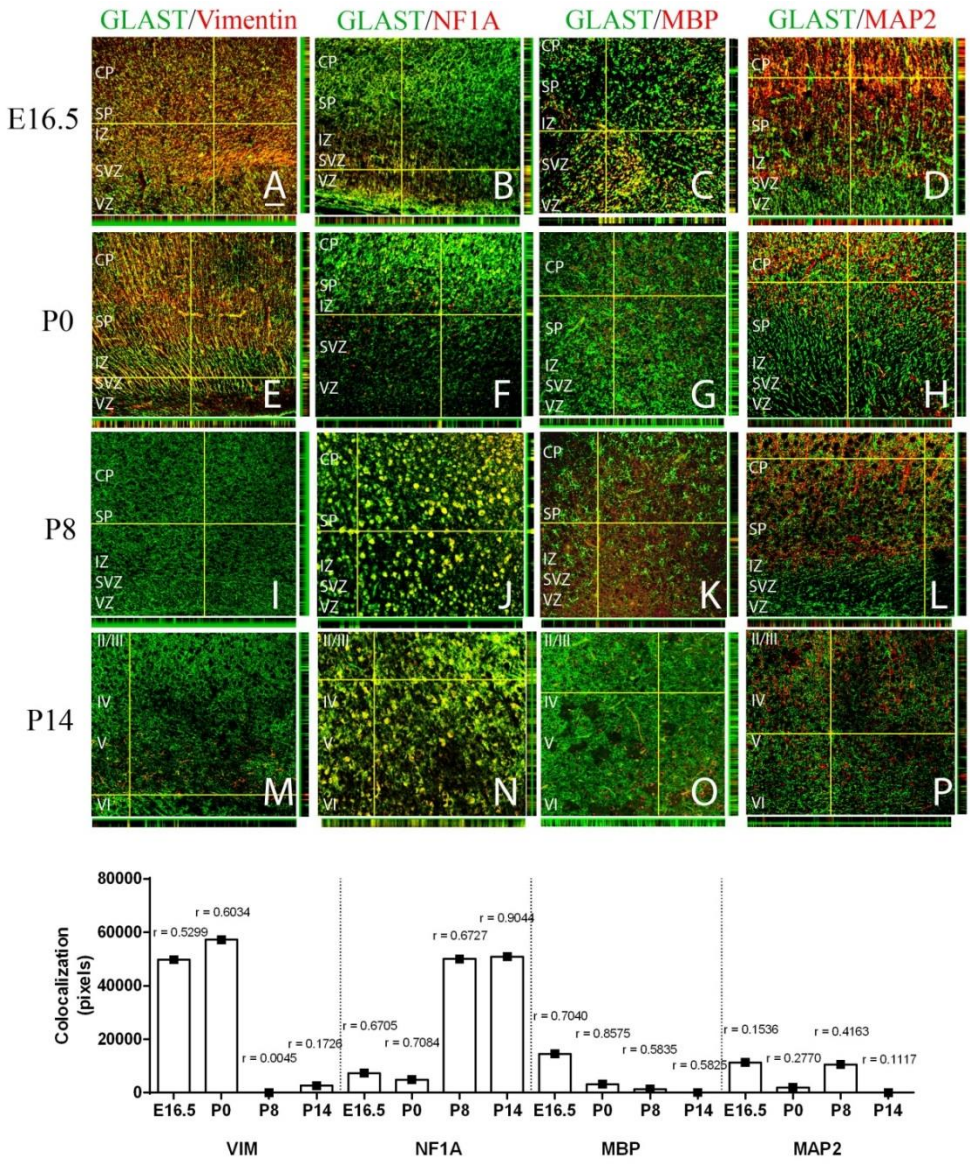

Figure 16: Immunohistochemical analysis of GLAST and cell specific markers in developing murine cortex

Confocal images of sections double-labeled with GLAST (green) and cell type specific markers (red) at E16.5 (A-D), P0 (E-H), P8 (I-L) and P14 (M-P) in the frontal cortex of the developing murine brain during astrogenesis. A, E, I and M) Double-label for GLAST and VIMENTIN (radial glial marker). At E16 and P0 radial glial cells were present and

spanning the width of the cortex. Radial glial cells were replaced by a progenitor population in the subventricular zone at P8 and P14 (I, M). B, F, J and N) GLAST and NF1A (early astrocyte marker) double-label showed little colocalization at E16.5 and P0 and increased colocalization at P8 and P14. C, D, G, H, K, L O, and P) Low levels of GLAST and MBP (oligodendrocyte marker) or GLAST and MAP2 (neuronal marker) were detected. Q) Quantitative colocalization (number of pixels) of each stage and cell type specific labeling with GLAST confirmed the high levels of colocalization of VIMENTIN at E16.5 and P0 and that of NF1A at P8 and P14. CP – Cortical Plate, SP – Subplate, IZ – Intermediate Zone, SVZ – Subventricular Zone, VZ – Ventricular Zone, VIM- VIMENTIN, NF1A- Nuclear Factor 1A, MBP-myelin basic protein, MAP2-microtubule associated protein 2. Magnification bar in A = 50 μm.

GLAST expression during astrogenesis was subsequently labeled in the developing cerebellum and olfactory bulb at the same stages (Figures 17 and 18). Co-localization of GLAST with radial glial and astrocyte precursors confirms peak production of GLAST expressing astrocytes at P8 (Figure 17). The peak co-localization of GLAST and NF1A was detected at P14 within the olfactory bulb (Figure 18). Since the bulk area analyzed displayed the most VIMENTIN/GLAST co-label at P0 and the most GLAST/NF1A co-label at P8, P0 and P8 stages were chosen for further analysis.

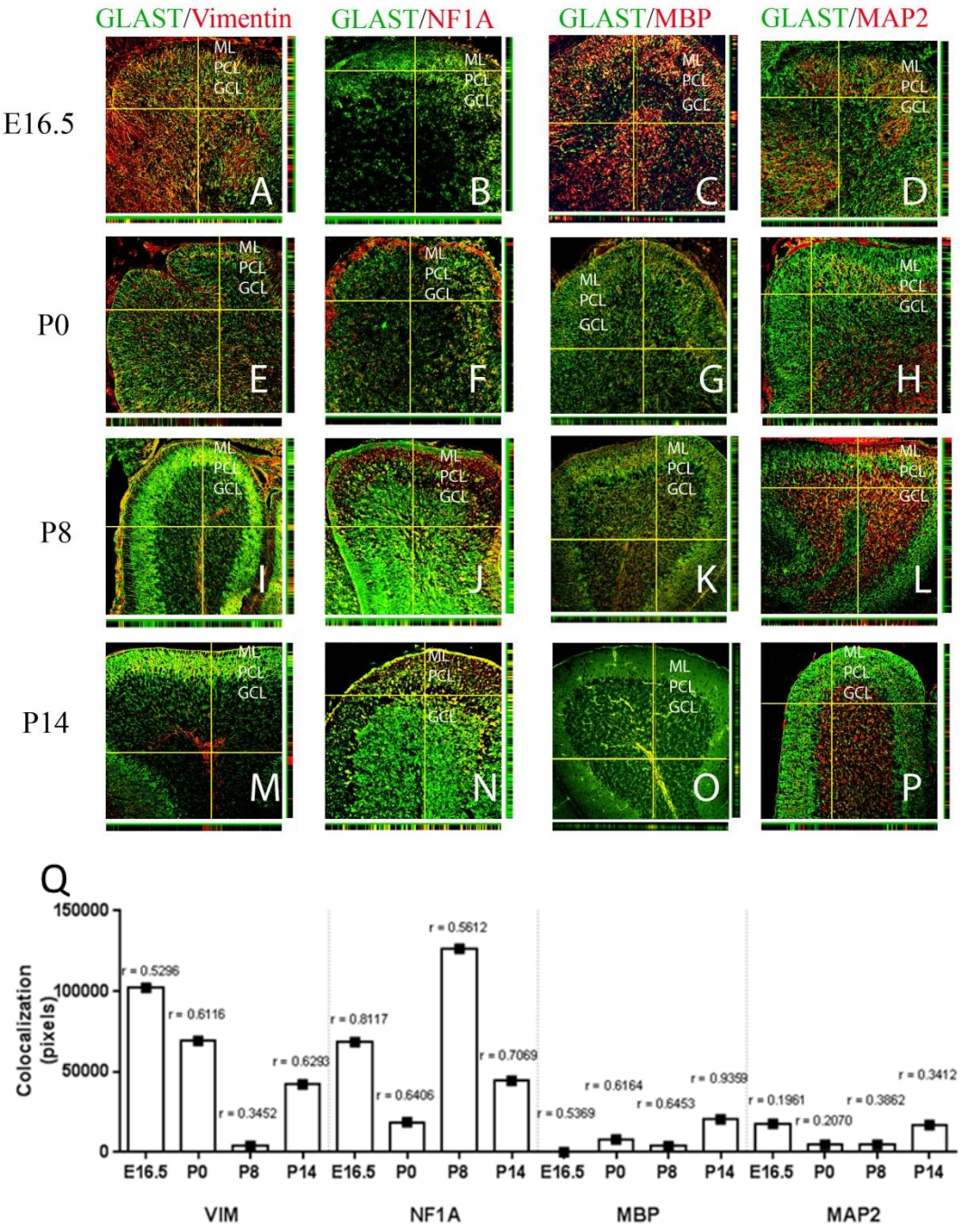

Figure 17: Cerebellum IHC of GLAST and cell specific markers in developing mouse cerebellum.

Confocal images of double-label immunofluorescence with GLAST (green) and cell type specific markers (red) at E16.5 (A-D), P0 (E-H), P8 (I-L) and P14 (M-P) in the cerebellum of the developing murine brain during astrogenesis. A, E, I and M) Double-labeling of GLAST and VIMENTIN (radial glial marker) indicated colocalization at E16.5 and P0 and less colocalization at P8 and P14. B, F, J and N) GLAST and NF1A

(early astrocyte marker) labeling showed weak colocalization at E16.5 and increased colocalization at P8 and P14. C, G, K and O) MBP (oligodendrocyte marker) and; D, H, L and P) MAP2 (neuronal marker) labeling both indicate very low level colocalization with GLAST. Q) Quantitative colocalization (number of pixels) of each stage and cell type specific labeling with GLAST confirmed the high levels of colocalization of VIMENTIN at 16.5 and P0 and that of NF1A at P8 and P15. ML – Molecular Layer, PCL – Purkinje Cell Layer, GCL – Granular Cell Layer, NF1A- Nuclear Factor 1A, MBP- myelin basic protein, MAP2- microtubule associated protein 2 Magnification bar in A= 50 μm.

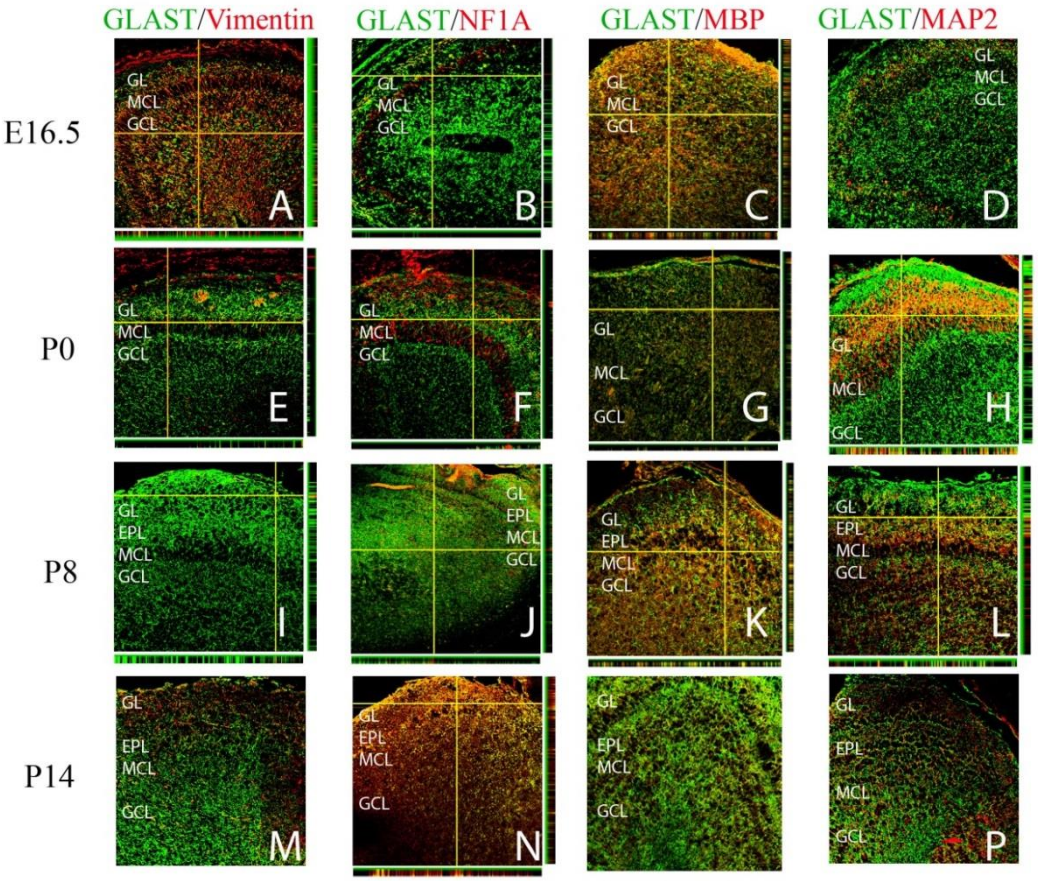

Figure 18: Olfactory IHC of GLAST and cell specific markers in developing mouse olfactory bulb.

Figure 18 continued

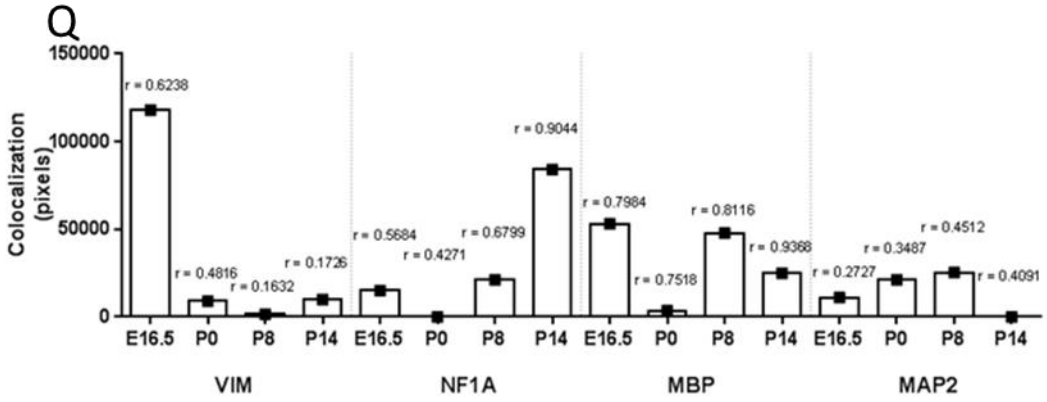

Confocal images of double-label immunofluorescence with GLAST (green) and cell type specific markers (red) at E16.5 (A-D), P0 (E-H), P8 (I-L) and P14 (M-P) in the olfactory bulb of the developing murine brain during astrogenesis. A, E, I and M) Double-labeling of GLAST with VIMENTIN (radial glial marker) indicated colocalization early at E16.5; however, low levels of colocalization are seen at P0, P8 and P14. B, F, J and N) GLAST and NF1A (early astrocyte marker) labeling showed little colocalization at E16.5, P0, P8 and increased colocalization was detected at P14. C, G, K and O) MBP (oligodendrocyte marker) colocalized with GLAST at E16.5; however, colocalization was detected thereafter. D, H, L and P) Low levels colocalization of GLAST with MAP2 (neuronal marker) was seen. Q) Quantitative colocalization (number of pixels) of each stage and cell type specific labeling with GLAST confirmed the high levels of colocalization of VIMENTIN at E16.5 and P0 and that of NF1A at P8 and P14. GL – Glomerular Layer, EPL- External Plexiform Layer, MCL – Mitral Cell Layer, GCL – Granule Cell Layer, NF1A- Nuclear Factor 1A, MBP-myelin basic protein, MAP2- microtubule associated protein 2. Magnification bar in A = 50 μm

GLAST(+) radial glia and astrocytes isolated from P0 and P8 brains

To determine if radial glia and astrocyte populations could be isolated from enzymatically dissociated P0 and P8 brains, a GLAST antibody (ASCA-1 clone; extracellular epitope) coupled to magnetic beads was used to isolate cells from whole mouse brain (depicted in Figure 19A). Using flow cytometry, the positively isolated fraction showed a 94% purity of GLAST (+) cells (Figure 19B), whereas 18% of the cells in the negative fraction were GLAST (+). Purified GLAST (+) cells at P0 and P8 (n=4 for each stage) were further analyzed by RNA sequencing to determine the radial glial and

astrocyte transcriptome immediately following isolation procedures as shown in a flow diagram (Figure 19C). Prior to RNA sequencing and differential gene analysis, high quality of RNA material (Figure 20) and library constructs (Figure 21) were confirmed.

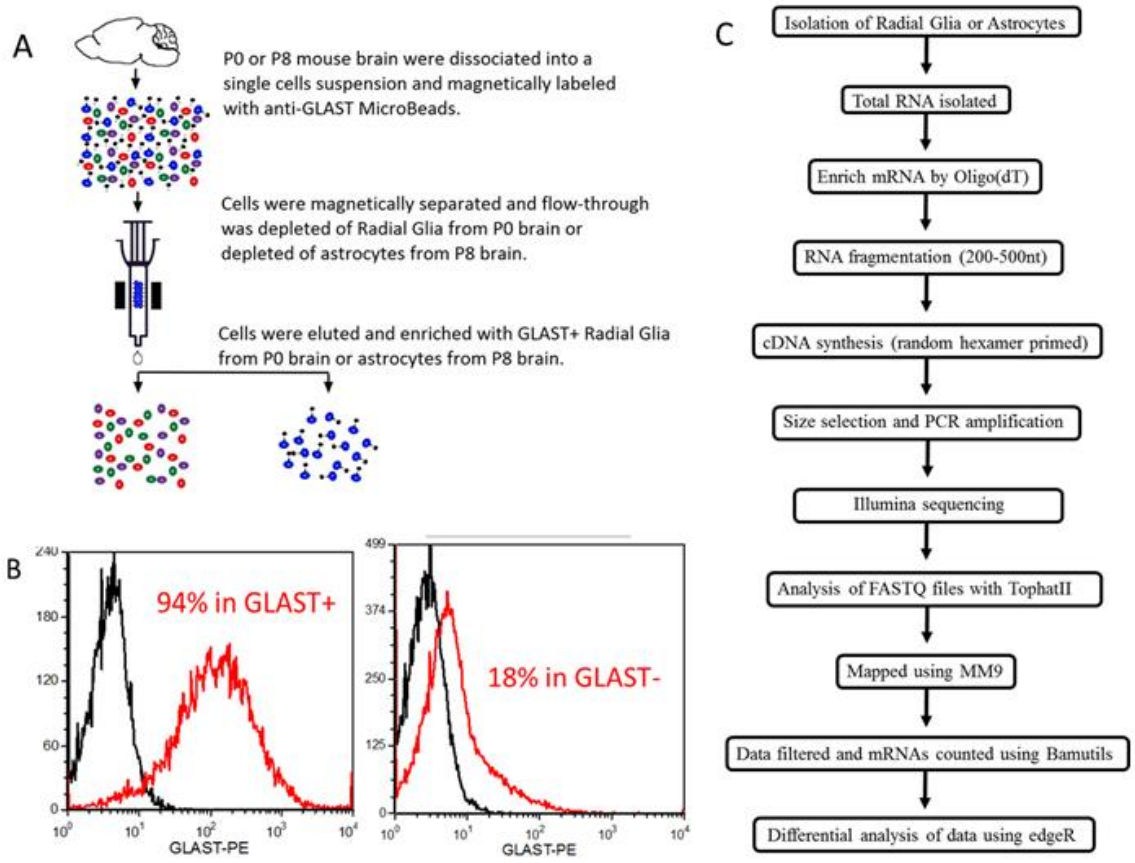

Figure 19: Isolation methods and diagrammatic representation of data analysis. A) A diagram of isolation procedures using neonatal (P0) or postnatal (P8) brains from C57BL/6J mice. A diagrammatic representation of brain dissociation into single cell suspension using anti-GLAST microBeads following magnetic separation and elution of radial glia from P0 brain or astrocyte precursors from P8 brain. B) Flow cytometry histograms representing an analysis of positively separated GLAST+ cells showing 94% positivity (red line) compared to the IgG control stained cells (black line) and negative elution showing 18% positivity (red line) compared to the IgG control stained cells (black line). C) Flow chart indicating the steps of RNA processing and analysis beginning with isolated cells and ending with the statistical analysis of transcripts identified by RNA-seq.

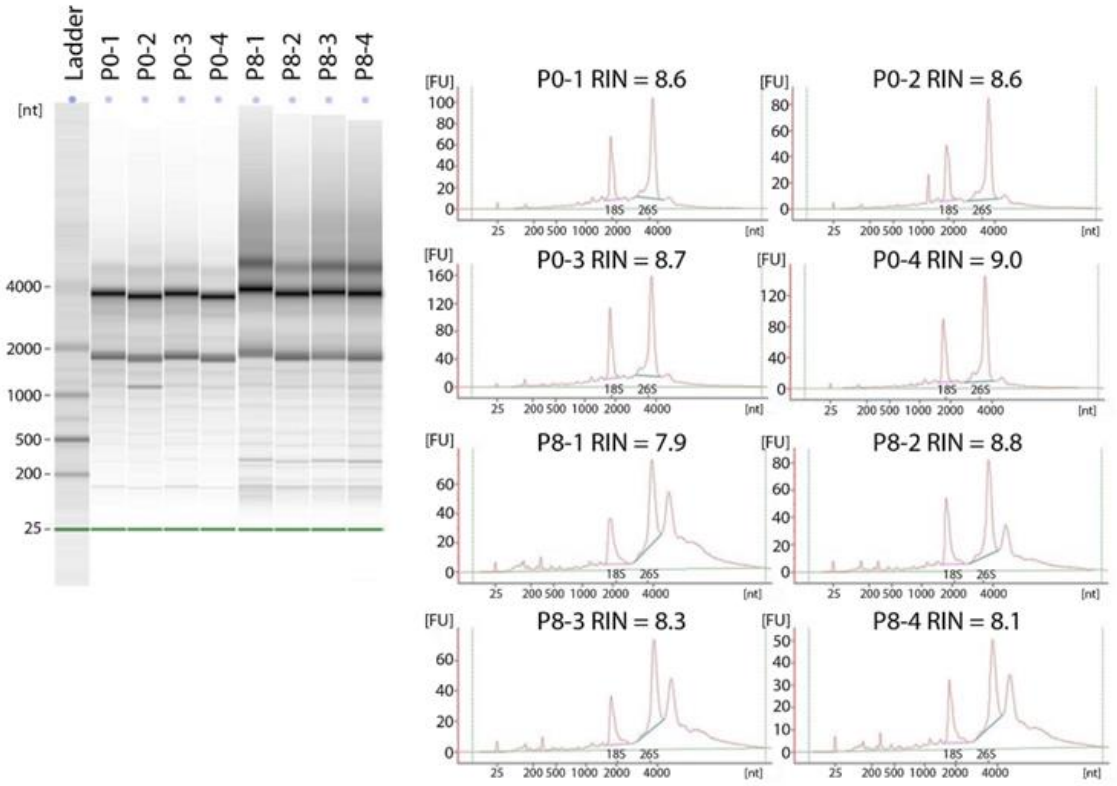

Figure 20: Quality assessment of RNA purity.
Quality assessment from isolated RNA from 4 separate preparations of GLAST positive cells from each stage (P0 and P8) measured on an Agilent Bioanalyzer 2100. RNA integrity numbers (RIN) calculated by measuring 18S and 26S rRNA for each sample shown on a gel image along a Ladder of 25, 200, 500, 1000, 2000 and 4000 nucleotides (nt). Bioanalyzer output measured by fluorescent units (FU) is plotted showing peaks of 18S and 26S, which are used to determine RIN values. All 8 samples were detected at or above 7.9 and represented above each individual sample plot.

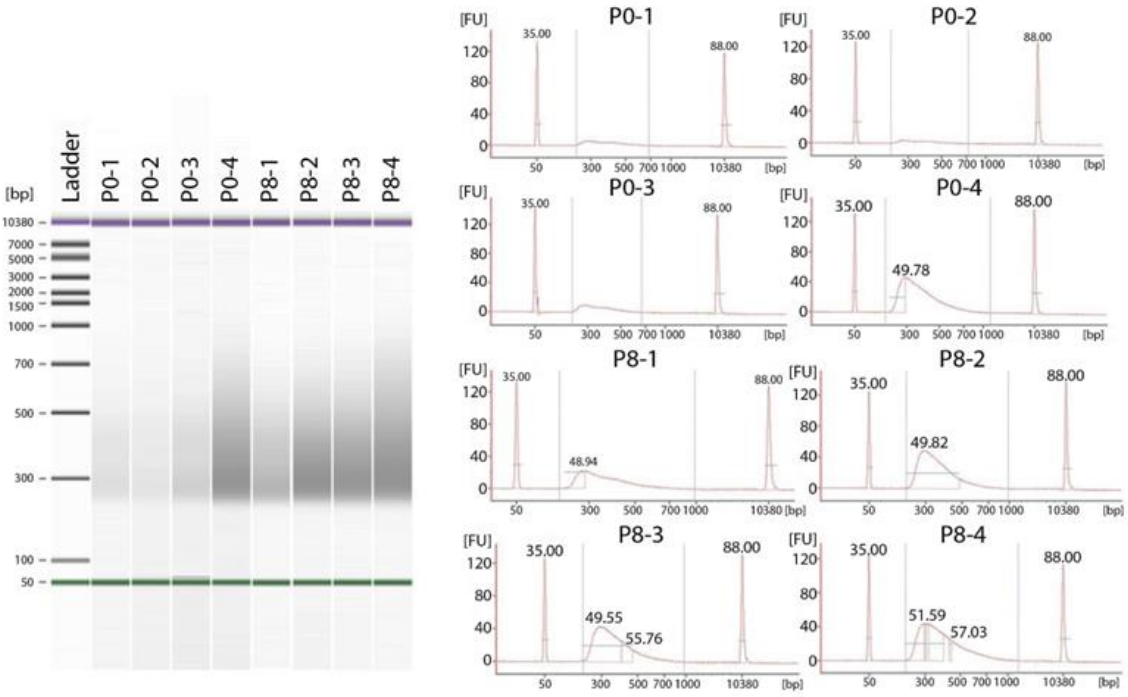

Figure 21: Quality assessment of DNA library.
Quality is based on integrity, size distribution and concentrations of the final library construct for each sample by Agilent Bioanalyzer 2100 and shown on a gel image for all 8 samples along a Ladder of base pairs (bp). DNA quality output measured by FU is plotted for each sample library based on the intensity of gel images.

Read mapping and cell type marker assessment of RNA sequence

In order to compare the transcriptomes of P0 radial glia and P8 astrocyte precursor cells, RNA isolated from GLAST (+) cells was processed as explained above in Figure 19C and used in high throughput RNA profiling analysis. After sequencing, approximately 25 million clean paired-end reads per sample were generated and subsequently mapped with the annotated mouse genome, mm9, and filtered to remove low quality reads (Figure 22A). Total filtered reads were also separated by chromosomal region, revealing the high junctional alignment along with coding and untranslated 3’ regions (Figure 22B).

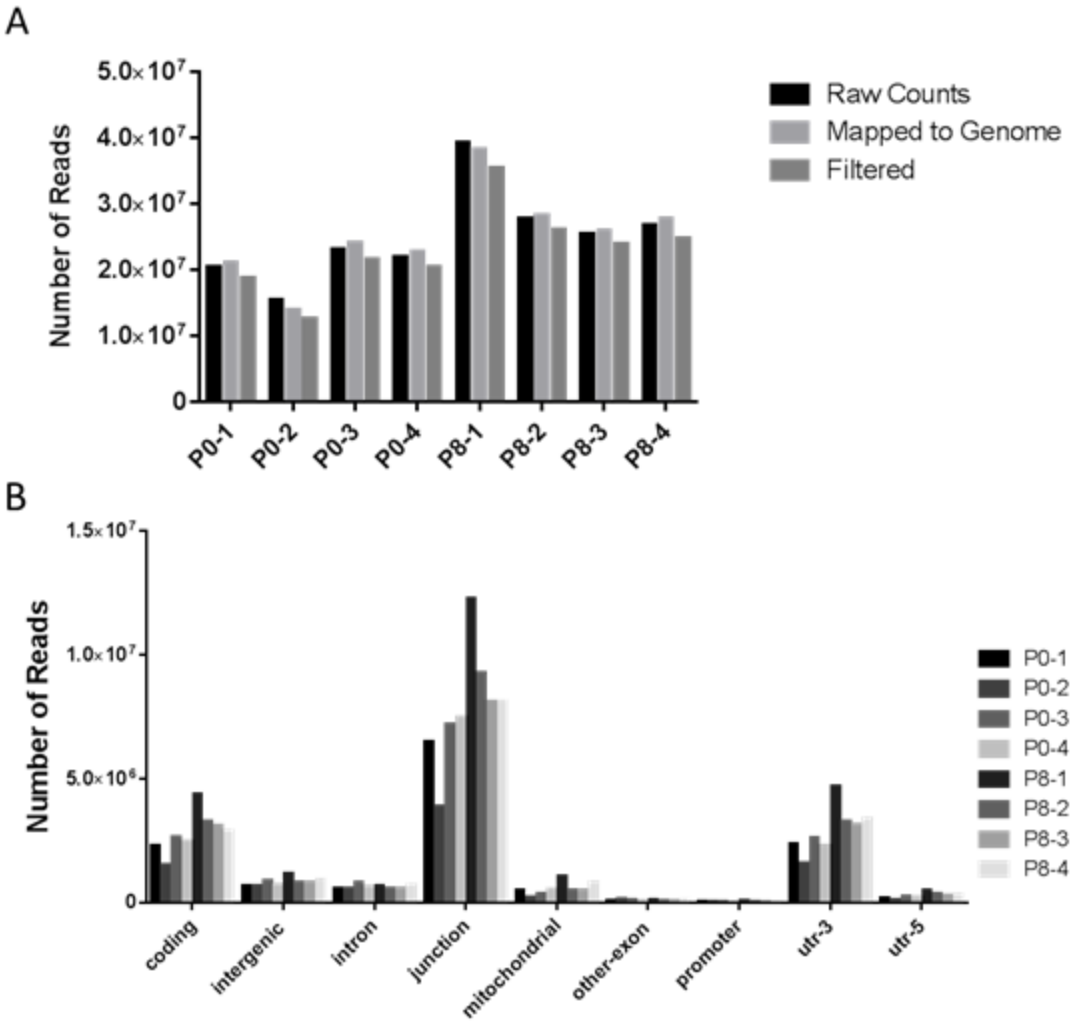

Figure 22: Number of sequencing reads mapped by region.
A) Number of sequencing reads plotted on a log scale for all 8 samples. Sequencing reads were plotted for each sample including raw counts and after mapping to the mm9 genome and finally after filtering the reads for final alignment. B) Number of aligned sequencing reads were plotted on a log scale for each sample based on genomic region. Genomic regions plotted include coding, intergenic, intron, junction, mitochondrial, other-exon, promoter, untranslated 3' (utr-3) and untranslated 5' (utr-5).

Table 3: Mapped reads aligned by chromosome with reported counts and percentages within each sample.

	P0-1		P0-2		P0-3		P0-4		P8-1		P8-2		P8-3		P8-4	
Reference counts	Count	%	Count	%	Count	%	Count	%	Count	%	Count	%	Count	%	Count	%
chr1	1,229,816	7%	761,969	6%	1,228,230	6%	1,147,561	6%	2,119,161	6%	1,523,575	6%	1,411,636	6%	1,487,218	6%
chr2	1,531,444	8%	931,202	7%	1,605,670	7%	1,505,831	7%	2,659,488	7%	1,936,389	7%	1,763,671	7%	1,826,878	7%
chr3	756,972	4%	534,926	4%	859,975	4%	789,798	4%	1,484,618	4%	1,154,546	4%	1,029,262	4%	1,062,556	4%
chr4	1,038,504	6%	727,289	6%	1,261,616	6%	1,126,959	6%	1,982,670	6%	1,495,942	6%	1,407,998	6%	1,359,191	5%
chr5	988,411	5%	695,160	5%	1,190,126	6%	1,085,892	5%	2,185,826	6%	1,643,596	6%	1,524,248	6%	1,536,961	6%
chr6	899,262	5%	614,060	5%	1,004,203	5%	930,050	5%	1,936,438	5%	1,470,550	6%	1,350,399	6%	1,382,772	6%
chr7	1,456,736	8%	900,949	7%	1,612,463	7%	1,540,968	8%	2,746,043	8%	2,023,530	8%	1,772,006	7%	1,835,279	7%
chr8	917,533	5%	647,905	5%	1,123,810	5%	1,000,039	5%	1,984,559	6%	1,450,136	6%	1,333,553	6%	1,361,387	5%
chr9	1,171,326	6%	787,492	6%	1,264,756	6%	1,208,410	6%	2,002,080	6%	1,514,087	6%	1,384,951	6%	1,421,758	6%
chr10	990,213	5%	630,633	5%	1,107,141	5%	1,034,786	5%	1,717,141	5%	1,268,504	5%	1,175,333	5%	1,183,009	5%
chr11	1,579,141	8%	1,052,785	8%	1,826,463	8%	1,693,290	8%	2,941,886	8%	2,157,539	8%	2,021,916	8%	2,018,140	8%
chr12	554,230	3%	405,514	3%	710,895	3%	628,737	3%	1,107,513	3%	815,137	3%	768,803	3%	778,872	3%
chr13	480,767	3%	340,446	3%	610,793	3%	533,168	3%	1,000,256	3%	754,350	3%	681,248	3%	688,741	3%
chr14	631,399	3%	429,371	3%	741,178	3%	697,685	3%	1,230,056	3%	932,499	4%	825,612	3%	853,997	3%
chr15	796,665	4%	538,867	4%	931,036	4%	850,362	4%	1,561,323	4%	1,175,834	5%	1,078,730	5%	1,075,501	4%
chr16	552,493	3%	390,083	3%	643,539	3%	564,072	3%	879,939	2%	656,620	3%	625,041	3%	630,357	3%
chr17	766,331	4%	699,363	6%	922,051	4%	834,490	4%	1,483,298	4%	1,127,163	4%	1,059,787	4%	1,066,930	4%
chr18	833,476	4%	534,451	4%	1,175,584	5%	1,490,496	7%	993,719	3%	701,462	3%	670,156	3%	730,493	3%
chr19	638,821	3%	456,566	4%	736,845	3%	667,679	3%	1,424,236	4%	1,012,548	4%	898,397	4%	981,015	4%
chrM	491,557	3%	233,167	2%	362,047	2%	532,973	3%	1,077,259	3%	500,444	2%	511,629	2%	808,456	3%
chrX	542,226	3%	392,065	3%	623,556	3%	594,678	3%	1,002,126	3%	736,183	3%	667,269	3%	735,803	3%
chrY	4,202	0.02%	1,467	0.01%	3,026	0.01%	3,339	0.02%	3,207	0.01%	1,415	0.01%	1,593	0.01%	781	0.00%
%= Count/Number of Filtered Reads; chr = Chromosome																

Separation of aligned reads per chromosome indicates similar distributions of reads across samples based on the percentage of reads per chromosomes (Table 3).

Additional confirmation of the cell isolation and RNA sequencing was completed by the selection of 45 known cell type-specific markers of various cells within the brain, including markers for radial glial cells, astrocytes, oligodendrocytes, neurons, and microglial cells. Calculation of FPKM for these markers in P0 and P8 samples demonstrates that mRNA isolated from P0 GLAST (+) cells was consistent with markers associated with radial glial cells, while mRNA isolated from P8 GLAST (+) cells was consistent with markers associated with astrocytes (Figure 23). Transcriptomes from P0 and P8 GLAST (+) cells displayed low levels of known markers associated with oligodendrocytes, neurons and microglia.

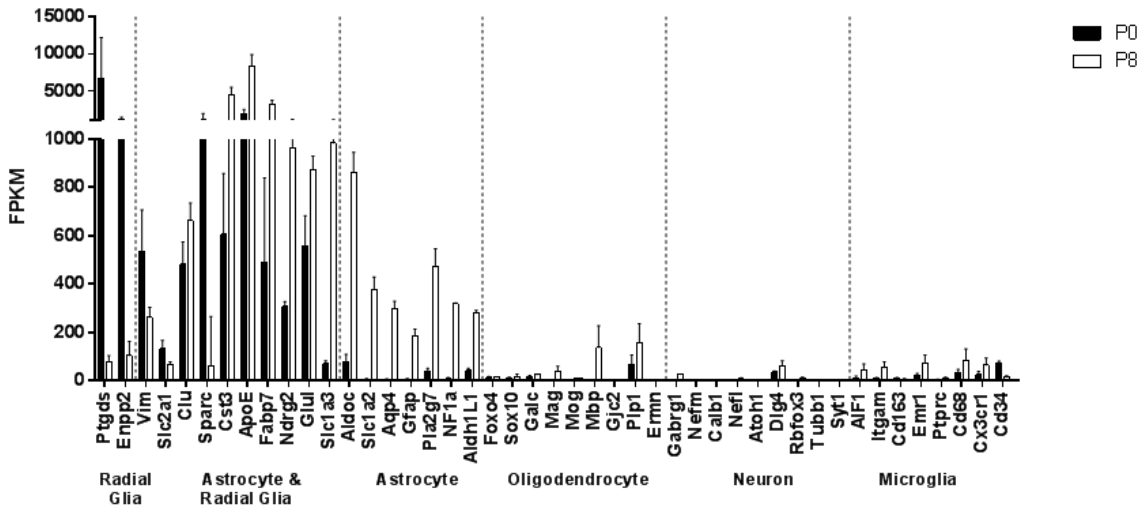

Figure 23: GLAST+ cell transcripts from P0 and P8 mouse brain were consistent with radial glial and astrocyte expression.
Average FPKM and standard deviation were plotted on a split y-axis at 1000 for 45 different cell markers in P0 and P8 cells. These markers are divided into cell specific

markers, with 2 radial glial-specific markers, 10 astrocyte and radial glial markers, 7 astrocyte-specific markers, 9 oligodendrocyte markers, 9 neuronal markers and 8 microglial markers.

Differential gene expression and gene ontology

To extend the investigation of common and unique characteristics between P0 radial glia and P8 astrocyte precursors, further RNA sequencing differential analyses were performed to compare their transcriptomic profiles. Differential expression analysis at the gene level following FPKM calculation was carried out using the EdgeR software package and reported by graphing p-value and fold change on a volcano plot (Figure 24A). With a false discovery rate of less the 0.05 and an average FPKM greater than 1.0, a total of 6,278 transcripts were found to be differentially expressed. Of those genes that were differentially expressed, 3,334 were upregulated in astrocyte precursors compared to 2,944 in radial glial cells.

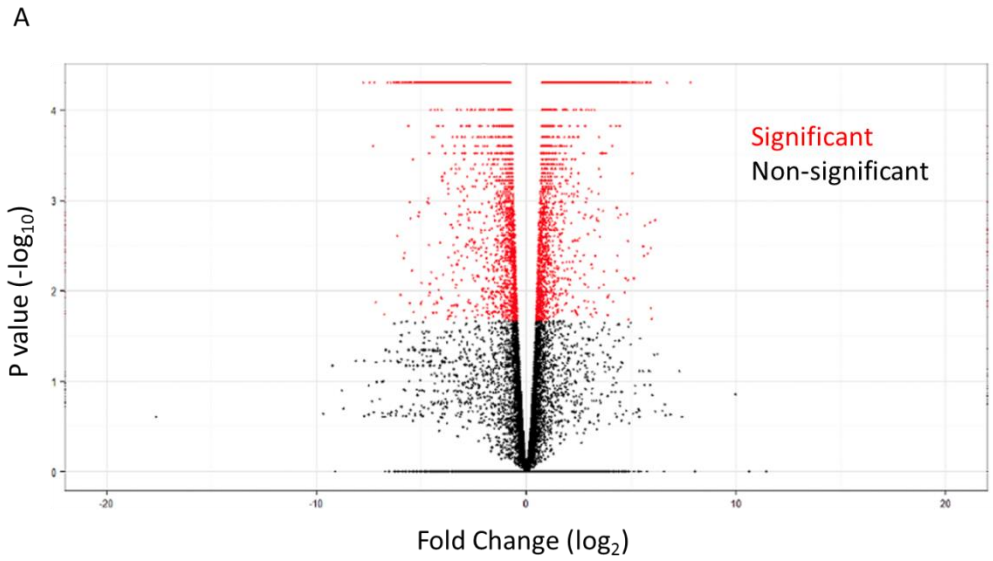

Figure 24: Differential gene expression and gene ontology analyses.

Figure 24 continued

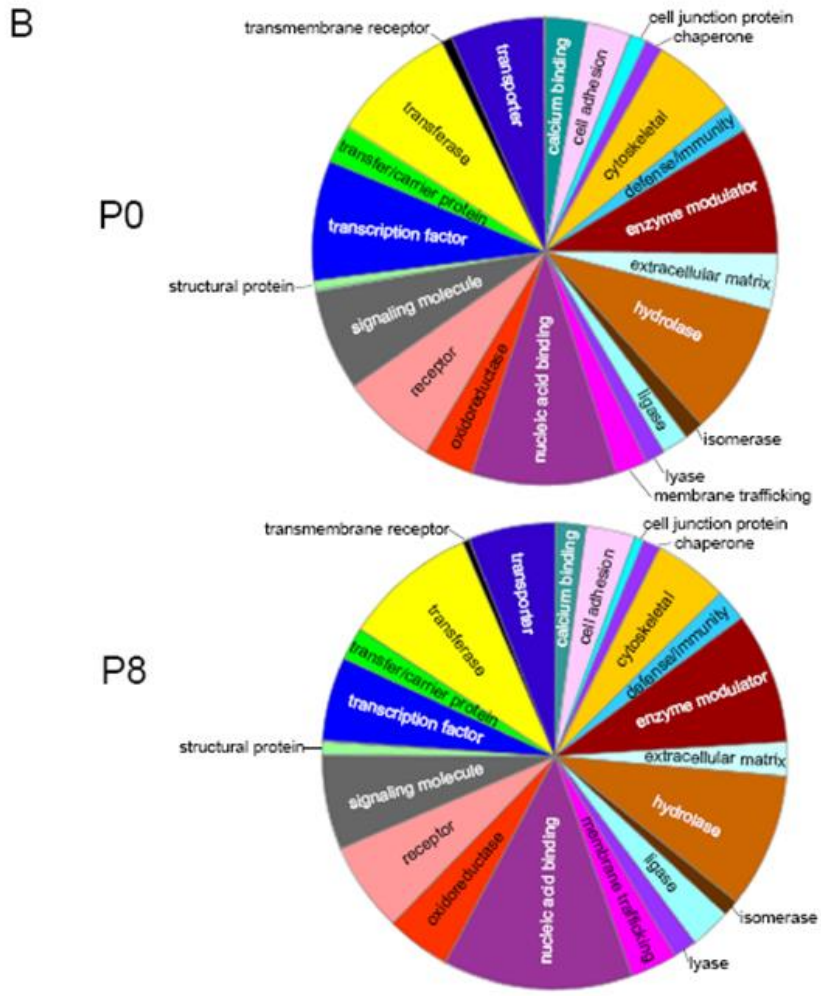

A) Sequenced genes are plotted by negative log of the p-value and natural log of the fold change. Fold change of the genes are calculated using a ratio of the P8 value versus the P0 value. Genes with p-values less than 0.05 are significant and points are colored red. Genes with p-values greater than 0.05 are black. B) The list of significantly expressed genes were analyzed using the Panther gene ontology classification system. A summary of the classification for each of the genes enriched in P0 or P8 are shown by pie charts.

The top 20 differentially expressed genes from radial glial cells and astrocyte precursors are listed in Table 4 and 5 respectively. Transcripts include those that are known to be expressed in radial glia, such as E-cadherin and carbonic anhydrase, in addition to other genes novel to radial glia, and/or genes with unknown functions (Table 4; Cammer & Zhang, 1992; Xu et al, 2011). The top 20 differentially expressed genes from astrocyte

precursors include transporters, channels, junctional proteins and intermediate filaments known to be expressed in astrocyte precursors, however, other membrane proteins and receptors with novel functions are also highly expressed (Table 5). A full list of genes can be found under the GEO accession number GSE83498.

Table 4: Top 20 differentially expressed transcripts from GLAST(+) radial glial cells.

Gene ID	Entrez Gene Name	logFC	Function of Product
Wfikkn2	WAP, follistatin/kazal, immunoglobulin, kunitz and netrin domain containing 2	-7.20565	Protease inhibitor
Cdh1	cadherin 1, type 1, E-cadherin (epithelial)	-6.53492	Ca2+-dependent cell adhesion molecule
Ptgds	prostaglandin D2 synthase 21kDa (brain)	-6.45147	glutathione-independent prostaglandin D synthase
Slc4a5	solute carrier family 4 (sodium bicarbonate cotransporter), member 5	-6.37708	Sodium bicarbonate co-transporter
Kcne2	potassium voltage-gated channel, Isk-related family, member 2	-6.17309	voltage-gated potassium channel
Mir675	microRNA 675	-6.08159	microRNA
H19	H19, imprinted maternally expressed transcript (non-protein coding)	-6.05752	long non-coding RNA; tumor supressor
Clic6	chloride intracellular channel 6	-6.03696	unknown
Krt18	keratin 18	-6.01277	Type I intermediate filament
Penk	Proenkephalin	-5.98531	Preproprotein for opioids Met-enkephalin and Leu-enkephalin
Scube3	signal peptide, CUB domain, EGF-like 3	-5.9155	secreted glycoprotein and TGF-β receptor ligand
Slc13a4	solute carrier family 13 (sodium/sulfate symporter), member 4	-5.90863	Sodium/sulfate symporter
Aqp1	aquaporin 1 (Colton blood group)	-5.90762	Water transporter
Car12	carbonic anhydrase XII	-5.90094	zinc metalloproteinase; catalyzes hydration of CO2
Plvap	plasmalemma vesicle associated protein	-5.86561	unknown
Lox	lysyl oxidase	-5.80289	Copper-dependent amine oxidase
Nov	nephroblastoma overexpressed	-5.67279	Extracellular matrix-associated signaling growth factor
Sult1a1	sulfotransferase family 1A, phenol-preferring, member 1	-5.60341	Sulfotransferase enzyme
Gpc3	glypican 3	-5.58516	Cell surface heparin sulfate proteoglycan
Prr32	Proline rich 32	-5.50988	unknown

Table 5: Top 20 differentially expressed transcripts from GLAST(+) astrocyte precursors.

Gene ID	Entrez Gene Name	logFC	Function of Product
Gpr37l1	G protein-coupled receptor 37 like 1	7.687901	G-protein coupled receptor
Slc1a2	solute carrier family 1 (glial high affinity glutamate transporter), member 2	6.162791	Glutamate transporter
Aqp4	aquaporin 4	5.797053	Water channel activity
Mbp	myelin basic protein	5.512077	Structural constituent of myelin sheath
Baalc	brain and acute leukemia, cytoplasmic	5.495443	Neural and hematopoietic proliferation, Mesodermal lineage
Kcnj10	potassium inwardly-rectifying channel, subfamily J, member 10	5.173263	Inward rectifier potassium channel
Gfap	glial fibrillary acidic protein	5.129057	Intermediate filament cytoskeleton
Slc6a11	solute carrier family 6 (neurotransmitter transporter), member 11	5.06563	GABA:sodium symporter
Slc25a18	solute carrier family 25 (glutamate carrier), member 18	5.059534	Glutamate transporter
Cxcl14	chemokine (C-X-C motif) ligand 14	5.02691	Chemokine activity
Hspa1b	heat shock 70kDa protein 1A	5.014375	Protein chaperone
Gabbr2	gamma-aminobutyric acid (GABA) B receptor, 2	5.000194	G-protein coupled GABA receptor
Thy1	Thy-1 cell surface antigen	4.987354	GPI anchor binding
Acsbg1	acyl-CoA synthetase bubblegum family member 1	4.941877	Fatty acid metabolism
Tmem229a	transmembrane protein 229A	4.926987	Membrane protein
Gpc5	glypican 5	4.923884	HSPG co-receptor
Ppp2r2c	protein phosphatase 2, regulatory subunit B, gamma	4.89862	Serine/Threonine phosphatase
Grm3	glutamate receptor, metabotropic 3	4.897113	G-protein coupled metabotropic glutamate receptor
Mlc1	megalencephalic leukoencephalopathy with subcortical cysts 1	4.838703	Cell-cell junction
Cldn10	claudin 10	4.704806	Tight junction protein

To determine if any of the differential transcript levels in radial glia or astrocyte precursors could be grouped into particular molecular pathways, the data was analyzed using the, Ingenuity Pathway Analysis tool (IPA; Ingenuity Systems,

http://www.ingenuity.com; Tables 6 and 7). A cut-off of 2-fold or greater change in mRNA level was applied, leaving 1,438 radial glial genes and 1,100 astrocyte precursor genes that were included in the analysis. IPA analysis revealed the presence of well-known growth factor, axonal guidance, pluripotency, stem cell and glioblastoma signaling pathways in proliferating astrocytes along with neurotransmitter/hormone metabolism in the P0 radial glial cells (Table 6). Other notable pathways that are important in radial glial cells include inflammatory-related pathways, like endocytosis signaling, eicosanoid signaling, and inhibition of matrix metalloproteases, IL-1 signaling and LXR/RXR activation. Pathway analysis of astrocyte precursor genes reveals regulation of neurotransmitter and G-protein coupled receptor signaling, long term synaptic plasticity, cholesterol and fatty acid biosynthesis along with vascular homeostasis (Table 7). In addition, astrocyte precursor pathways also include neuroinflammatory-related pathways such as neuropathic pain signaling, CREB signaling and Amyotrophic Lateral Sclerosis signaling.

Table 6: Ingenuity pathway analysis of genes from radial glial cells

Canonical Pathway	*P*-value	Ratio (Actual vs. Expected)	Hits (gene symbol)
Hepatic Fibrosis / Hepatic Stellate Cell Activation	6.31E-13	2.13E-01	*COL8A2,FN1,CTGF,LEPR,COL4A3,COL9A3,COL8A1,COL10A1,COL4A2,COL15A1,PGF, COL1A2,COL5A1,COL6A1,FIGF,LBP,TNFRSF11B,MYH1,COL4A1,COL6A2,Agtr1b,MYH7, MMP2,COL20A1,IL1R1,MET,COL1A1,IGF2,COL13A1,COL6A3,IGFBP3,TGFB3,COL4A4,KDR, COL25A1,COL9A2,A2M,AGTR1,COL3A1*
Basal Cell Carcinoma Signaling	4.37E-07	2.36E-01	*SHH,BMP15,BMP4,BMP3,WNT9A,WNT2B,WNT16,WNT6,BMP5,WNT8B,FZD4,FZD5,BMP7,BMP6, WNT11,WNT5B,FZD7*
Axonal Guidance Signaling	3.98E-06	1.13E-01	*SLIT3,ENPEP,SHH,PAPPA2,BMP15,BMP4,NTF4,BMP3,WNT16,WNT6,NGF,WNT8B, ADAMTS2,PGF,SHC1,PLCD3,ITGA3,SEMA3D,RHOD,MMP8,EFNA5,FIGF,SEMA3B,SEMA3F,RTN 4R,ACE,WNT5B,GDF7,PAPPA,NRP2,ADAMTS1,ARHGEF15,EPHA1,WNT9A,WNT2B, MMP2,SLIT2,BMP5,MET,SEMA3A,FZD4,ADAM12,BMP7,FZD5,PRKCH,SEMA3C,BMP6, WNT11,FZD7*
Human Embryonic Stem Cell Pluripotency	6.92E-06	1.64E-01	*BMP15,BMP4,NTF4,BMP3,WNT9A,WNT2B,SMAD6,WNT16,WNT6,NGF,FOXD3,WNT8B,BMP5, FZD4,SPHK1,TGFB3,FZD5,BMP7,BMP6,WNT5B,WNT11,FZD7*
Role of NANOG in Mammalian Embryonic Stem Cell Pluripotency	1.55E-05	1.71E-01	*BMP15,BMP4,BMP3,WNT9A,WNT2B,WNT16,WNT6,FOXD3,BMP5,WNT8B,SHC1,FZD4,GATA6, FZD5,BMP7,BMP6,WNT5B,WNT11,FZD7*
Regulation of the Epithelial-Mesenchymal Transition Pathway	1.74E-05	1.41E-01	*LOX,SNAI2,TWIST1,WNT16,PARD6B,WNT6,WNT8B,FOXC2,NOTCH2,FGF18,FGF7,WNT5B, TWIST2,ESRP2,WNT9A,WNT2B,SNAI1,MMP2,MET,CDH1,FZD4,TGFB3,FZD5,WNT11,CLDN3, FZD7*
Nicotine Degradation III	4.07E-05	2.22E-01	*CYP2F1,UGT1A6,CYP4B1,Ugt1a7c,UGT1A3,GYLTL1B,UGT1A4,UGT1A1,UGT1A7(includes others),CYP1B1,Aox3,CYP2S1*
Nicotine Degradation II	4.57E-05	2.06E-01	*FMO2,UGT1A6,UGT1A3,UGT1A4,UGT1A1,CYP1B1,CYP2F1,CYP4B1,Ugt1a7c,GYLTL1B,UGT1A7 (includes others),CYP2S1,Aox3*
PCP pathway	4.57E-05	2.06E-01	*RSPO3,FZD4,SDC1,WNT9A,VANGL1,WNT2B,WNT16,FZD5,WNT6,WNT8B,WNT11,WNT5B,FZD7*
Melatonin Degradation I	7.24E-05	2.11E-01	*CYP2F1,UGT1A6,CYP4B1,Ugt1a7c,Sult1a1,UGT1A3,GYLTL1B,UGT1A4,UGT1A1,UGT1A7 (includes others),CYP1B1,CYP2S1*
Superpathway of Melatonin Degradation	1.70E-04	1.94E-01	*CYP2F1,UGT1A6,CYP4B1,Ugt1a7c,Sult1a1,UGT1A3,GYLTL1B,UGT1A4,UGT1A1,UGT1A7 (includes others),CYP1B1,CYP2S1*
Factors Promoting Cardiogenesis in Vertebrates	2.09E-04	1.63E-01	*BMP15,NOX4,FZD4,BMP4,BMP3,TGFBR3,TGFB3,BMP7,FZD5,PRKCH,MYH7,BMP6,BMP5, WNT11,FZD7*
Role of Osteoblasts, Osteoclasts and Chondrocytes in Rheumatoid Arthritis	3.24E-04	1.19E-01	*BMP15,BMP4,FRZB,BMP3,WNT16,WNT6,SP7,WNT8B,ITGA3,MMP8,WNT5B,TNFRSF11B, CTSK,WNT9A,WNT2B,SMAD6,IL1R1,GSN,BMP5,COL1A1,FZD4,BMP7,FZD5,BMP6,WNT11,FZD7*
Serotonin Degradation	3.63E-04	1.79E-01	*UGT1A6,ALDH1A3,Ugt1a7c,ALDH1A2,ADH1C,Sult1a1,UGT1A3,GYLTL1B,UGT1A4,ALDH3A1, UGT1A1,UGT1A7 (includes others)*
Caveolar-mediated Endocytosis Signaling	6.31E-04	1.69E-01	*CD55,ITGA2B,ITGA3 HLA-A,FLNC,ITGA11,ITGA8,INS,ITGB4,ITGA10,ITGB6,PTRF*
Thyroid Hormone Metabolism II (via Conjugation and/or Degradation)	6.46E-04	2.29E-01	*UGT1A6,Ugt1a7c,Sult1a1,UGT1A3,GYLTL1B,UGT1A4,UGT1A1,UGT1A7(includes others)*
Eicosanoid Signaling	9.12E-04	1.72E-01	*PTGIS,PTGFR,DPEP1,PTGDR,PTGER3,PLA2R1,PLA2G5,ALOX12,PTGDS,GGT1,PLA2G2C*
Inhibition of Matrix Metalloproteases	1.38E-03	2.05E-01	*HSPG2,SDC1,ADAM12,MMP8,RECK,THBS2,MMP2,A2M*
Sperm Motility	1.41E-03	1.32E-01	*SLC16A10,PDE4C,ZAN,SLC12A2,PLA2R1,NPPC,ITPR1,PDE1A,FRK,PLA2G2C,Cngb1,PLCD3ITP R3,PLA2G5,PRKCH,MST1R*
Calcium Transport I	1.66E-03	4E-01	*ATP2B3,ATP2C2,ATP2B2,ATP2A1*
LPS/IL-1 Mediated Inhibition of RXR Function	1.86E-03	1.09E-01	*GSTA3,ABCG8,ABCB1,GSTM1,ABCG5,SULT1C2,FMO2,NR1H4,CPT1B,IL1R1,HMGCS2, CHST15,GSTT2/GSTT2B,ALDH1A3,ALDH1A2,PPARGC1B,FABP4,NR5A2,HS6ST2,HS3ST1, LBP,ALDH3A1,ACSL1,TNFRSF11B*
Oxidative Ethanol Degradation III	3.55E-03	2.63E-01	*ACSS3,ALDH1A3,ALDH1A2,ALDH3A1,ACSL1*
Wnt/β-catenin Signaling	3.63E-03	1.12E-01	*FRZB,TGFBR3,WNT9A,WNT2B,WNT16,WNT6,WNT8B,RARG,CDH1,FZD4,CDH5,CDH3,RARBTG FB3, NR5A2,FZD5,WNT5B,WNT11,FZD7*
LXR/RXR Activation	3.72E-03	1.24E-01	*ABCG8,ABCG5,TTR,HPX,APOB,NR1H4,UGT1A3,IL1R1,A1BG,PON1,S100A8,LBP,RBP4, TNFRSF11B, APOD*
Glioblastoma Multiforme Signaling	3.98E-03	1.16E-01	*WNT9A,WNT2B,WNT16,WNT6,ITPR1,WNT8B,PLCD3,SHC1,IGF2,FZD4,RHOD,ITPR3,RHOU,FZD 5, WNT5B,WNT11,FZD7*

Table 7: Ingenuity pathway analysis of genes from astrocyte precursors

Canonical Pathway	*P*-value	Ratio (Actual vs. Expected)	Hits (gene symbol)
GABA Receptor Signaling	2.51E-17	3.73E-01	*SLC32A1,KCNN3,GABRA5,ADCY2,GABRA4,GABBR1,GABRB2,GABBR2,SLC6A11,GABRG3,KCNN1,GAD2,GABRB3,GABRG2,KCNQ2,GABRG1,GPR37,GAD1,MRAS,GABRB1,SLC6A1,KCNQ3,ADCY8,GABRA2,ALDH5A1*
Glutamate Receptor Signaling	5.01E-17	4.04E-01	*GRIN1,GRIN2B,GRM2,HOMER2,SLC1A4,GRM3,SLC17A6,GRM1,GRID1,GRID2,GRIA1,SLC1A3,GRIA2,SLC1A1,GRM4,GRIA4,GNG7,GRM5,GRM7,SLC17A7,GRIN2C, SLC1A2,GRIK2*
Synaptic Long Term Depression	5.13E-10	1.83E-01	*GRM2,GRM3,GRIA1,GRID2,GRID1,PLCH2,PLA2G7,GRIA4,PLA2G4E,LCAT,MRAS,RYR1,PPP2R2C,PNPLA3,Gucy1b2,ABHD3,GRM1,GRIA2,PLA2G3,GRM4,CRHR1,GRM5,GRM7,PPP2R2B,GNAO1, GUCY2F*
Neuropathic Pain Signaling In Dorsal Horn Neurons	1.05E-08	2E-01	*GRIN1,GRIN2B,KCNN3,GRM2,GRM3,GRM1,GRIA1,GRIA2,GRM4,PLCH2,GRIA4,GRM5,GRM7,KCNN1,KCNQ2,CAMK2A,GPR37,GRIN2C,KCNQ3,CAMK2B*
CREB Signaling in Neurons	1.20E-07	1.46E-01	*GNG4,GRIN1,GRIN2B,ADCY2,GRM2,GRM1,GRM3,GRID1,GRIA1,GRID2,GRIA2,GRM4,PLCH2,GRIA4,GNG7,GRM7,GRM5,CAMK2A,GRIN2C,GNAO1,MRAS,GRIK2,ADCY8,GNG12,CAMK2B*
Gαi Signaling	2.51E-07	1.67E-01	*GNG4,GPR17,ADCY2,GRM2,GRM3,CNR1,RGS7,GABBR1,GRM4,GNG7,GRM7,GABBR2,P2RY13,RGS10,MRAS,S1PR1,P2RY12,ADORA1,ADCY8,GNG12*
Oleate Biosynthesis II (Animals)	4.07E-07	5.38E-01	*SCD,FADS6,Scd2,FADS2,PTPRT,Scd4,FADS1*
Synaptic Long Term Potentiation	9.77E-07	1.6E-01	*GRIN1,PPP1R14C,GRIN2B,GRM2,GRM3,GRM1,GRIA1,GRIA2,GRM4,PLCH2,GRIA4,GRM5,GRM7,PPP1R3D,CAMK2A,GRIN2C,MRAS,ADCY8,CAMK2B*
Superpathway of Cholesterol Biosynthesis	1.86E-06	3.21E-01	*MVD,NSDHL,DHCR7,IDI1,LSS,HMGCR,TM7SF2,SC5D,CYP51A1*
G-Protein Coupled Receptor Signaling	2.88E-06	1.13E-01	*ENPP6,GPR17,GRM2,GRM3,Htr5b,HRH1,ADRB1,CAMK2A,RGS10,MRAS,ADORA1,ADCY8,CAMK2B,ADCY2,GRM1,CNR1,RGS7,GABBR1,GRM4,CRHR1,PDE1C,ADRA1D,GRM5,GRM7,GABBR2,P2RY13,GNAO1,S1PR1,P2RY12*
Amyotrophic Lateral Sclerosis Signaling	5.13E-06	1.63E-01	*GRIN2B,GRIN1,CACNA1S,NEFL,GRID1,GRID2,GRIA1,GRIA2,NEFH,GRIA4,PAK1,HECW1,GRIN2C,SLC1A2,GRIK2,CAPN3*
Cholesterol Biosynthesis I	9.12E-06	4.62E-01	*NSDHL,DHCR7,LSS,TM7SF2,SC5D,CYP51A1*
Cholesterol Biosynthesis II (via 24,25-dihydrolanosterol)	9.12E-06	4.62E-01	*NSDHL,DHCR7,LSS,TM7SF2,SC5D,CYP51A1*
Cholesterol Biosynthesis III (via Desmosterol)	9.12E-06	4.62E-01	*NSDHL,DHCR7,LSS,TM7SF2,SC5D,CYP51A1*
cAMP-mediated signaling	3.47E-05	1.1E-01	*ENPP6,GPR17,GRM2,ADCY2,GRM3,CNR1,RGS7,GABBR1,Htr5b,GRM4,CRHR1,PDE1C,GRM7,P2RY13,GABBR2,ADRB1,CAMK2A,GNAO1,RGS10,S1PR1,P2RY12,ADORA1,ADCY8,CAMK2B*
Cellular Effects of Sildenafil (Viagra)	4.79E-05	1.32E-01	*CACNA1S,KCNN3,ADCY2,CACNG4,PLCH2,PDE1C,CACNG2,CACNG3,KCNN1,KCNQ2,GPR37,CACNG5,GUCY2F,KCNQ3,ADCY8,CACNG8,Gucy1b2*
Dopamine-DARPP32 Feedback in cAMP Signaling	2.51E-04	1.12E-01	*GRIN1,PPP1R14C,GRIN2B,CACNA1S,ADCY2,KCNJ16,KCNJ3,PLCH2,PPP1R3D,GRIN2C,KCNJ10,PPP2R2B,KCNJ9,PPP2R2C,KCNJ6,ADCY8,CALY,Gucy1b2*
Chondroitin Sulfate Biosynthesis	6.76E-04	1.61E-01	*NDST3,CHST1,SULT4A1,CHST7,HS3ST2,B3GAT1,CHST10,HS3ST4,HS3ST5*
Cardiac β-adrenergic Signaling	7.24E-04	1.13E-01	*GNG4,ENPP6,PPP1R14C,CACNA1S,ADCY2,SLC8A2,GNG7,PDE1C,PPP1R3D,ADRB1,PPP2R2B,MRAS,PPP2R2C,ADCY8,GNG12*
Dermatan Sulfate Biosynthesis (Late Stages)	7.76E-04	1.74E-01	*NDST3,CHST1,SULT4A1,CHST7,HS3ST2,CHST10,HS3ST4,HS3ST5*
Glutamate Degradation III (via 4-aminobutyrate)	7.76E-04	6E-01	*GAD2,GAD1,ALDH5A1*
Heparan Sulfate Biosynthesis	1.00E-03	1.53E-01	*NDST3,CHST1,SULT4A1,CHST7,HS3ST2,B3GAT1,CHST10,HS3ST4,HS3ST5*
Dermatan Sulfate Biosynthesis	1.00E-03	1.53E-01	*NDST3,CHST1,SULT4A1,CHST7,HS3ST2,B3GAT1,CHST10,HS3ST4,HS3ST5*
Chondroitin Sulfate Biosynthesis (Late Stages)	1.05E-03	1.67E-01	*NDST3,CHST1,SULT4A1,CHST7,HS3ST2,CHST10,HS3ST4,HS3ST5*
Endothelin-1 Signaling	1.48E-03	9.88E-02	*ADCY2,EDNRB,ABHD3,SHC3,PLA2G3,PLCH2,PLA2G7,PLA2G4E,LCAT,ECE2,SHC2,GNAO1,GUCY2F,MRAS,PNPLA3,ADCY8,Gucy1b2*

Functional classification of differentially expressed genes into ontologies was completed using the Panther classification system (pantherdb.org; Figure 24B). This analysis indicated that the two categories showing the largest changes between radial glial and astrocyte precursor cells were nucleic acid binding (13.2% increase from P0 to P8), and transcription factors (5.8% decrease from P0 to P8). Other gene ontology categories that showed a 1.0% or more change include; extracellular matrix proteins that were increased in P0 radial glia in comparison to P8 astrocyte precursors and oxidoreductases and ligases that were increased at P8 in comparison to P0.

Transcription Factor Analysis

Since the transcription factor ontology had the greatest dynamic changes between P0 and P8 in addition to the greatest abundance of differentially expressed genes (Figure 24), a more comprehensive analysis on those categories was completed. Transcription factors were placed into 7 classes; 1) High mobility group (HMG) box, 2) bHLH, 3) basic leucine zipper (bzip), 4) helix-turn-helix, 5) nuclear hormone receptor, 6) zinc finger, and 7) transcription cofactors. Of the 124 transcription factors classified from the radial glia transcriptome, a large majority of the transcripts fell into 2 categories; zinc finger transcription factors and transcription cofactors, including *Evi1*, Teashirt homologue 2 (*Tshz2*), *Jade1*, and lysine-specific demethylases 5A and 5B (*Kdm5a; Kdm5b*) (See Table 8 for a full list of differentially expressed transcription factors in radial glia). The co-activators found in radial glia included nuclear receptor co-activator 2 (*Ncoa2*), CREB binding protein (*Crebbp*), histone acetyl transferase p300 (*p300*), YES associated protein 1 (*Yap1*), and Wilms' tumour protein 1 interacting protein (*Wtip*). In contrast to radial

glial cells, message isolated from astrocyte precursors showed a distinct decrease in zinc finger transcription factors and co-factors, however increased expression of mRNA encoding HMG box, bHLH, and helix-turn-helix transcription factors (Table 9). Consistent with past studies, many of the HMG box messages that were found in astrocyte precursors were part of the Sry-related HMG box factors (*Sox*), including *Sox1, 2, 3, 4, 5, 6, 8, 11,* and *21* (Gomez-Lopez et al, 2011; Nakajima-Koyama et al, 2015; Obayashi et al, 2009; Reiprich & Wegner, 2015; Schlierf et al, 2007). Messages encoding bHLH transcription factors included achaete-scute homolog 1 (*Ascl1*), transcription factor E2-alpha (*Tcf3*), oligodendrocyte transcription factor 1 and 2 (*Olig1 and 2*), while helix-turn helix mRNAs included empty spiracles homeobox 2 (*Emx2*), paired homeobox 6 (*Pax6*), prospero homeobox 1 (*Prox1*), and Iroquois homeobox 2 (*Irx2*).

Table 8: Differentially expressed transcripts identified as transcriptional regulators in radial glia

Class/Gene ID	Entrez Gene Name	logFC	P value
HMG box			
Sp100	Nuclear autoantigen Sp-100	-0.99	0.004614
Ccdc108	Coiled-coil domain-containing protein 108	-2.44	1.17E-10
Hmg20a	High mobility group protein 20A	-0.53	0.00966
bHLH			
Mxd4	Max dimerization protein 4	-0.91	1.28E-05
Atoh8	Protein atonal homolog 8	-2.93	6.59E-19
Cttn	Src substrate cortactin	-0.91	1.79E-05
Arnt	Aryl hydrocarbon receptor nuclear translocator	-0.90	1.16E-05
Npas2	Neuronal PAS domain-containing protein 2	-0.94	0.002003
Mitf	Microphthalmia-associated transcription factor	-2.49	6.17E-18
bLeucine Zipper			
Creb3	Cyclic AMP-responsive element-binding protein 3	-0.55	0.015422
Creb3l1	Cyclic AMP-responsive element-binding protein 3-like protein 1	-1.24	6.09E-09
Creb3l2	Cyclic AMP-responsive element-binding protein 3-like protein 2	-1.38	2.21E-09
Helix-turn-helix			
Prrx2	Paired mesoderm homeobox protein 2	-2.75	5.94E-14
Msx1	Homeobox protein MSX-1	-4.40	5.9E-52
Otx2	Homeobox protein OTX2	-4.31	1.84E-40
Phtf1	Putative homeodomain transcription factor 1	-0.87	6.24E-05
Six5	Homeobox protein SIX5	-1.07	6.76E-05
Crip3	Cysteine-rich protein 3	-1.25	0.009958
Lmo4	LIM domain transcription factor LMO4	-1.83	4.59E-12
Hormone Receptor			
Rarg	Retinoic acid receptor gamma	-2.35	4.08E-22
Nr1h2	Oxysterols receptor LXR-beta	-0.51	0.016377
Nr2f2	COUP transcription factor 2	-2.32	1.69E-23
Rxra	Retinoic acid receptor RXR-alpha	-1.96	6.05E-17
Nr4a2	Nuclear receptor subfamily 4 group A member 2	-1.49	2.59E-07
Rarb	Retinoic acid receptor beta	-2.74	2.93E-17
Rara	Retinoic acid receptor alpha	-1.71	1.15E-12
Tec	Nuclear receptor subfamily 4 group A member 3	-0.74	0.007083

Table 8 continued

Class/Gene ID	Entrez Gene Name	logFC	P value
Zinc Finger			
Zfp212	Protein Zfp212	-0.79	0.00252
Zfp579	Zinc finger protein 579	-0.76	0.00346
E430018J23Rik	Protein E430018J23Rik	-1.06	0.004926
Zfp651	Protein Zfp651	-0.95	7.84E-06
Mecom	MDS1 and EVI1 complex locus protein EVI1	-0.89	0.012715
Zfp777	Protein Zfp777	-0.55	0.045948
Zfp280d	Zinc finger protein 280D	-0.60	0.013007
Tshz2	Teashirt homolog 2	-0.93	0.000434
Zfp385a	Zinc finger protein 385A	-0.58	0.009839
Sp1	Transcription factor Sp1	-1.30	5.74E-07
Zbtb38	CtBP-interacting BTB zinc finger protein	-0.68	0.034976
Zfp266	Protein Zfp266	-0.72	0.002237
Ing5	Inhibitor of growth protein 5	-0.68	0.014661
Prdm16	PR domain zinc finger protein 16	-1.73	8.75E-11
Zbtb4	Protein Zbtb4	-0.69	0.00084
Phf17	Protein Jade-1	-1.16	6.69E-07
Brd1	Protein Brd1	-0.62	0.004236
Prdm4	PR domain zinc finger protein 4	-0.90	0.000171
Zbtb7c	Zinc finger and BTB domain-containing protein 7C	-2.01	4.56E-10
Kdm5a	Lysine-specific demethylase 5A	-0.67	0.001476
Zbtb39	Protein Zbtb39	-0.57	0.021398
Kdm5b	Lysine-specific demethylase 5B	-0.39	0.046901
Zfp949	Protein Zfp949	-1.13	0.000463
Zfp9	Protein Zfp9	-0.71	0.037165
Zfp784	Zinc finger protein 784	-1.18	0.000386
Zbtb46	Zinc finger and BTB domain-containing protein 46	-0.74	0.015682
Zfp536	Zinc finger protein 536	-0.78	0.014055
Zbtb44	Zinc finger and BTB domain-containing protein 44	-1.03	2.29E-05
Zbtb34	Protein Zbtb34	-1.39	2.39E-08
Peg3	Paternally-expressed gene 3 protein	-2.21	9.42E-18

Table 8 continued

Class/Gene ID	Entrez Gene Name	logFC	P value
Transcriptional cofactors			
Limd1	LIM domain-containing protein 1	-1.20	6.75E-09
Rnh1	Ribonuclease inhibitor	-0.50	0.033506
Arid5b	AT-rich interactive domain-containing protein 5B	-2.17	4.88E-16
Taz	Tafazzin	-0.44	0.045102
Ncoa2	Nuclear receptor coactivator 2	-0.64	0.001513
Wwtr1	WW domain-containing transcription regulator protein 1	-0.54	0.009331
Rbm43	RNA-binding protein 43	-1.24	0.000127
Crebbp	CREB-binding protein	-0.59	0.004683
Phf12	PHD finger protein 12	-0.57	0.005158
Btbd6	BTB/POZ domain-containing protein 6	-0.49	0.029912
Dcp1a	mRNA-decapping enzyme 1A	-0.84	0.000552
Ep300	Histone acetyltransferase p300	-0.70	0.000967
Per2	Period circadian protein homolog 2	-0.74	0.006361
Yap1	Transcriptional coactivator YAP1	-1.32	3.8E-10
Rybp	RING1 and YY1-binding protein	-0.79	0.00028
Fblim1	Filamin-binding LIM protein 1	-1.24	3.96E-05
Ell	RNA polymerase II elongation factor ELL	-0.61	0.011724
Tada2b	MCG49644	-0.61	0.010226
Mysm1	Histone H2A deubiquitinase MYSM1	-0.58	0.012896
Trim35	Tripartite motif-containing protein 35	-0.61	0.00357
Ddi2	Protein DDI1 homolog 2	-0.48	0.032342
Wtip	Wilms tumor protein 1-interacting protein	-1.04	6.95E-05
Cited2	Cbp/p300-interacting transactivator 2	-0.77	0.001717
Spop	Speckle-type POZ protein	-0.53	0.007263
Arid4b	AT-rich interactive domain-containing protein 4B	-0.48	0.019285
Ldb1	LIM domain-binding protein 1	-0.55	0.018336
Per1	Period circadian protein homolog 1	-1.45	1.19E-07
Nod1	Nucleotide-binding oligomerization domain-containing protein 1	-0.86	0.002206
Tle4	Transducin-like enhancer protein 4	-0.42	0.047362

Table 9: Differentially expressed transcripts identified as transcriptional regulators in astrocyte precursors

Class/Gene ID	Entrez Gene Name	logFC	P value
HMG box			
SSrp1	FACT complex subunit SSRP1	0.52	0.017637
Sox2	Transcription factor SOX-2	2.82	1.21E-21
Sox21	Transcription factor SOX-21	2.82	1.21E-21
Sox3	Transcription factor SOX-3	1.95	1.28E-06
Sox6	Transcription factor SOX-6	2.42	6.12E-15
Tox2	Protein Tox2	1.02	0.002122
Sox4	Transcription factor SOX-4	0.97	8.37E-06
Tox3	TOX high mobility group box family member 3	1.51	2.6E-07
Sox11	Transcription factor SOX-11	1.62	2.74E-08
Sox1	Transcription factor SOX-1	1.97	1.54E-10
Hmgb3	High mobility group protein B3	0.70	0.001861
Hmgb2	High mobility group protein B2	0.64	0.005825
Sox5	Transcription factor SOX-5	0.75	0.003167
Sox8	Transcription factor SOX-8	2.13	1.77E-17
bHLH			
Ascl1	Achaete-scute homolog 1	2.17	9.03E-10
Srebf2	Sterol regulatory element-binding protein 2	1.30	2.32E-09
Hcls1	Hematopoietic lineage cell-specific protein	1.60	3.23E-08
Tcf3	Transcription factor E2-alpha	0.47	0.037583
Lyl1	Protein lyl-1	1.06	0.000227
Olig2	Oligodendrocyte transcription factor 2	3.42	4.49E-27
Arnt2	Aryl hydrocarbon receptor nuclear translocator 2	0.96	1.83E-05
Tcf4	Transcription factor 4	0.94	2.9E-05
Olig1	Oligodendrocyte transcription factor 1	4.54	1.44E-52
Npas3	Neuronal PAS domain-containing protein 3	2.27	9.58E-18
Mycn	N-myc proto-oncogene protein	1.81	6.92E-06
Mycl1	Protein L-Myc	0.97	0.003203

Table 9 continued

Class/Gene ID	Entrez Gene Name	logFC	P value
bLeucine Zipper			
Atf4	Cyclic AMP-dependent transcription factor ATF-4	0.61	0.00449
Helix-turn-helix			
Otx1	Homeobox protein OTX1	0.75	0.048972
Satb1	DNA-binding protein SATB1	1.08	3.45E-05
Emx2	Homeobox protein EMX2	1.95	1.12E-07
Zfhx2	Protein Zfhx2	0.78	0.018059
Pax6	Paired box protein Pax-6	2.97	4.39E-19
Irx2	Iroquois-class homeodomain protein IRX-2	1.85	1.46E-05
Arx	Homeobox protein ARX	1.59	5.98E-05
Lmo1	Rhombotin-1	2.50	1.23E-11
Prox1	Prospero homeobox protein 1	1.51	8.87E-07
Lhx2	LIM/homeobox protein Lhx2	2.78	1.12E-18
Zhx3	Zinc fingers and homeoboxes protein 3	0.78	0.000789
Hormone Receptor			
Nr2e1	Nuclear receptor subfamily 2 group E member 1	2.80	1.06E-23
Nr3c1	Glucocorticoid receptor	0.64	0.008349
Rxrg	Retinoic acid receptor RXR-gamma	1.45	1.33E-05
Thra	Thyroid hormone receptor alpha	0.83	0.000307
Nr2f1	COUP transcription factor 1	0.98	4.77E-06
Nr1d1	Nuclear receptor subfamily 1 group D member 1	0.68	0.000821
Zinc Finger			
Ikzf1	DNA-binding protein Ikaros	1.25	0.000741
Hr	Lysine-specific demethylase hairless	1.81	3.9E-08
Zfp280c	Zinc finger protein 280C	0.79	0.000723
Zfpm2	Zinc finger protein ZFPM2	1.94	8.11E-10
Zbtb41	Zinc finger and BTB domain-containing protein 41	0.48	0.0432
Zfp40	Protein Zfp40	0.74	0.01024
Bcl6	B-cell lymphoma 6 protein homolog	0.95	0.000948
Zeb1	Zinc finger E-box-binding homeobox 1	0.89	0.0001
Pogk	Pogo transposable element with KRAB domain	0.52	0.019269
Dpf1	Zinc finger protein neuro-d4	1.88	1.68E-06
Sall3	Sal-like protein 3	2.34	2.99E-14
Zfp142	MCG133876, isoform CRA_a	0.82	0.001265
Hivep2	Transcription factor HIVEP2	0.76	0.008583
Zfp532	Zinc finger protein 532	0.54	0.023905
Sall2	Sal-like protein 2	1.74	2.51E-15
Zfp238	Zinc finger and BTB domain-containing protein 18	1.37	1.22E-08
Trps1	Zinc finger transcription factor Trps1	0.69	0.003573
Zfp423	Zinc finger protein 423	0.60	0.00754
Zfp219	Protein Zfp219	0.90	8.4E-06
Zfp521	Zinc finger protein 521	0.65	0.004126
Zeb2	Zinc finger E-box-binding homeobox 2	0.92	2.73E-05
Zhx3	Zinc fingers and homeoboxes protein 3	0.78	0.000789
Sall1	Sal-like protein 1	1.83	4.43E-08
Zfp277	Protein Zfp277	1.12	1.67E-06
Zfp62	Zinc finger protein 62	0.59	0.009096
Gm14295	Novel KRAB box and zinc finger, C2H2 type domain containing protein	2.01	6.19E-14
Nacc2	Nucleus accumbens-associated protein 2	2.00	8.6E-17

Table 9 continued

Class/Gene ID	Entrez Gene Name	logFC	P value
Transcriptional cofactors			
Lrrc16a	Leucine-rich repeat-containing protein 16A	1.81	1.95E-15
Ell2	RNA polymerase II elongation factor ELL2	0.91	0.006741
Arid5a	AT-rich interactive domain-containing protein 5A	0.88	0.00202
Grip1	glutamate receptor interacting protein 1	1.07	1.16E-05
Phf21b	PHD finger protein 21B	2.17	1.25E-14
Abtb2	Ankyrin repeat and BTB/POZ domain-containing protein 2	2.58	1.76E-29
Ccnk	Cyclin-K	0.65	0.003636
Pqbp1	Polyglutamine-binding protein 1	0.59	0.00755
Mpnd	MPN domain-containing protein	0.71	0.000522
Khdrbs3	KH domain-containing, RNA-binding, signal transduction-associated protein 3	1.77	1.19E-11
Psip1	PC4 and SFRS1-interacting protein	0.43	0.048187
Yaf2	YY1-associated factor 2	0.88	5.44E-05
Ctbp1	C-terminal-binding protein 1	0.51	0.017951
Fam58b	Cyclin-related protein FAM58B	0.59	0.044727
Lrrc16b	Leucine-rich repeat-containing protein 16B	1.64	5.9E-10
Nlrp3	NACHT, LRR and PYD domains-containing protein 3	1.03	0.005454
Edf1	Endothelial differentiation-related factor 1	0.48	0.049259
Cited1	Cbp/p300-interacting transactivator 1	1.46	0.001031
Ccnh	Cyclin-H	0.84	0.000227
Btbd1	BTB/POZ domain-containing protein 1	0.77	0.000311
Ppargc1a	Peroxisome proliferator-activated receptor gamma coactivator 1-alpha	0.80	0.001402
Med12l	Mediator of RNA polymerase II transcription subunit 12-like protein	1.18	3.89E-06

To validate expression patterns of transcription factors in the RNA-seq, RT-qPCR was used to validate the differential expression of 18 highly expressed transcriptional regulators (Figure 25B). Both techniques agreed with the directionality and differential expression of all 18 genes. When comparing mRNA levels between the two techniques, RNA sequencing detects a greater level for most of these factors. This finding was expected since the RNA sequencing methods used here were completed with paired-end sequencing to increase sensitivity and specificity of deep-sequencing techniques (Fang & Cui, 2011).

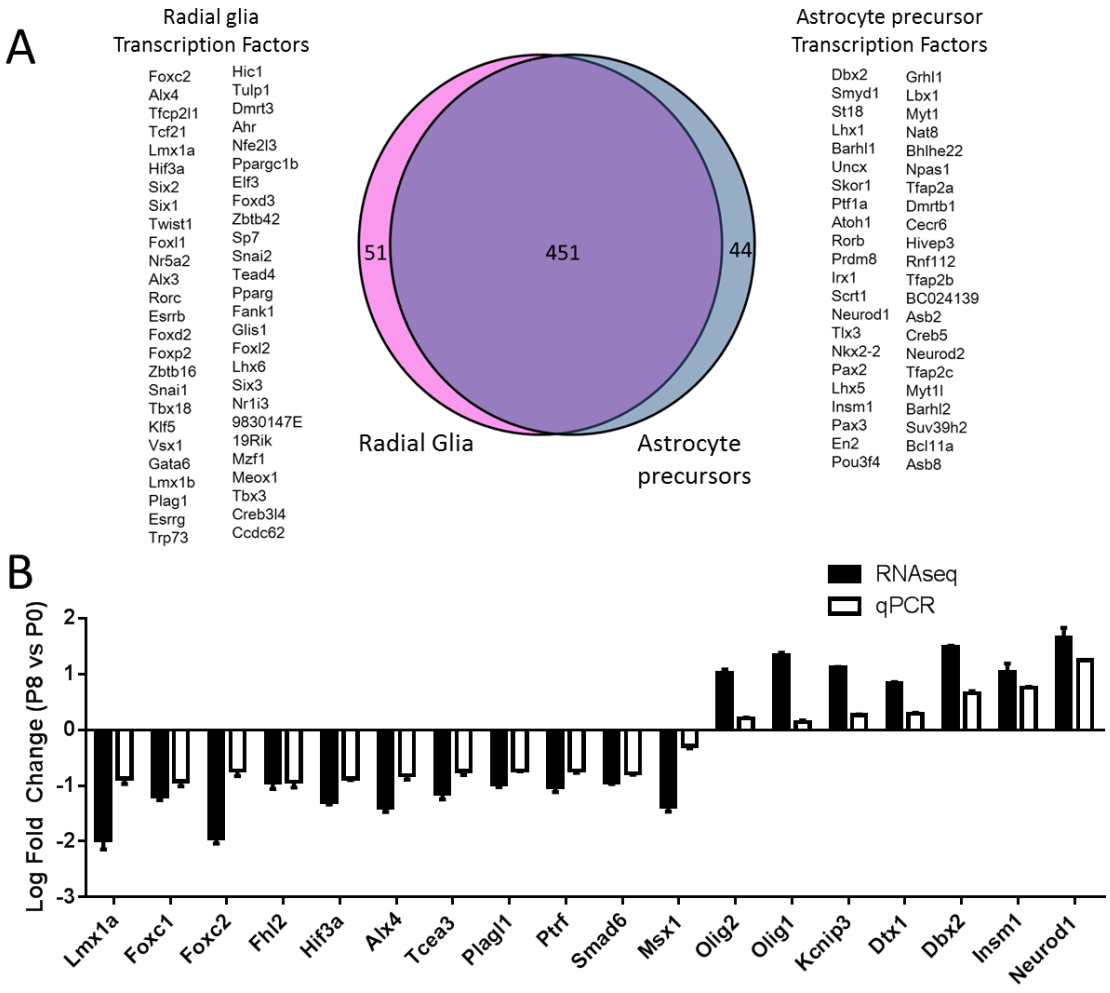

Figure 25: Analysis of transcription factors within GLAST+ radial glia and astrocyte precursors.

A) 502 and 495 significant genes were identified using gene ontology as transcription regulators in P0 and P8 gene sets, respectively. Using the venn diagram software creator Venny, a comparative analysis of transcriptional regulators in P0 and P8 data sets shows 451 regulators that were found in both data sets, 51 transcriptional regulators that are represented in the P0 dataset only (left-hand list), and 44 (right-hand list) regulators that are represented in the P8 dataset only. B) RT-qPCR validation of selected transcription factor genes using independent biological samples. The natural log fold change of mRNA levels of P8 over P0 samples using RNAseq and qPCR analysis. Both analyses were completed and plotted for 18 selected genes. 7 selected genes show a positive fold change for P8 cell mRNA levels when compared to P0 for both analyses. 11 selected genes show a negative fold change for P8 cell mRNA levels when compared to P0 for both analyses.

To identify signals that may regulate a cohort of the transcription factors, a MetaCore transcription factor analysis was completed using the radial glial and astrocyte precursor

datasets. This functionality builds networks of enriched transcription factors and the genes they have been shown to regulate. The top 500 differentially enriched mRNAs from radial glia or astrocyte precursors were included in the analysis and the top 25 significant transcription factors are reported for each cell type (Tables 10 and 11). Of these 25 factors, 10 were identified as unique to radial glia, and 9 were unique to astrocyte precursors (unique factors are highlighted in yellow). These unique transcription factors identified in Table 10 and 11 can be classified as regulators of one or more of the following ontologies; 1) cell proliferation, 2) inflammation (pro- and anti-inflammation), 3) lipid biosynthesis or metabolism.

Table 10: Potential regulatory factors in radial glial cells.

Transcription Factor	Actual Interactions	Connectivity Ratio	z-score	P-value
SP1	144	3.573	17.19	2.969E-43
c-Myc	159	2.559	13.22	2.765E-30
GCR-alpha	80	2.702	9.645	3.879E-16
c-Jun	59	2.904	8.86	2.06E-13
ESR1 (nuclear)	76	2.443	8.397	4.316E-13
PPAR-gamma	33	4.188	9.132	4.183E-12
SP3	43	3.32	8.56	6.305E-12
p53	71	2.383	7.865	8.959E-12
HNF4-alpha	41	3.141	7.93	1.113E-10
C/EBPbeta	45	2.874	7.623	2.437E-10
Androgen receptor	58	2.384	7.073	8.595E-10
Oct-3/4	67	2.129	6.61	4.072E-09
NANOG	47	2.542	6.834	5.198E-09
USF1	23	4.155	7.558	9.054E-09
FOXE1	8	16.35	10.88	1.081E-08
EGR1	34	3.022	6.942	1.195E-08
RelA (p65 NF-kB subunit)	50	2.32	6.334	3.212E-08
C/EBPalpha	29	3.12	6.604	7.257E-08
BAPX1	12	7.17	8.099	8.765E-08
RFX6	10	9.032	8.571	1.054E-07
TCF7L2 (TCF4)	28	3.107	6.461	0.000000133
NFIC	10	8.63	8.33	1.675E-07
SRF	29	2.837	6.006	0.000000537
AP-2A	22	3.404	6.228	6.416E-07
E2F1	44	2.174	5.452	0.000001298

Table 11: Potential regulatory factors in astrocyte precursors.

Transcription Factor	Actual Interactions	Connectivity Ratio	z-score	P-value
c-Myc	149	2.42	11.99	1.173E-25
SP1	98	2.454	9.671	6.497E-17
p53	66	2.236	6.994	7.556E-10
GCR-alpha	65	2.215	6.856	1.491E-09
ESR1 (nuclear)	67	2.174	6.796	1.756E-09
SREBP1 (nuclear)	19	5.396	8.383	2.4E-09
PPAR-gamma	28	3.586	7.374	6.172E-09
SREBP2 (nuclear)	13	7.72	8.847	0.00000001
LXR-alpha	15	5.999	8.026	2.718E-08
Oct-3/4	64	2.053	6.133	3.709E-08
PU.1	29	2.983	6.32	1.887E-07
c-Jun	45	2.235	5.722	4.574E-07
EGR1	30	2.691	5.778	0.000001039
RelA (p65 NF-kB subunit)	45	2.107	5.288	0.000002252
SP3	32	2.493	5.485	0.000002342
HNF4-alpha	32	2.474	5.434	0.000002766
PPAR-alpha	17	3.702	5.89	0.000003896
SRF	27	2.666	5.42	0.000004282
CREB1	174	1.348	4.589	0.000005483
C/EBPalpha	25	2.714	5.315	0.000007077
C/EBPbeta	35	2.256	5.085	0.000007317
SOX10	8	7.647	6.894	0.000007762
LXR-beta	8	7.647	6.894	0.000007762
SP2	8	7.465	6.786	0.000009376
NRF2	16	3.625	5.609	0.000009752

Although some unique signals were found in the MetaCore analysis, there were also commonalities (outlined in grey, Tables 10. and 11). Since the analyses of the datasets highlighted differential mRNA levels, it was somewhat surprising to see so many factors common to both radial glial cells and astrocyte precursors. To understand the potential genes these factors were regulating in the two cell types, a network analysis of two common transcription factors, EGR1 and RELA, was completed (Figure 26). Figure 26

clearly shows that although EGR1 and RELA may play a role in both cell types, they regulate two completely different cohorts of genes in radial glia and astrocyte precursors.

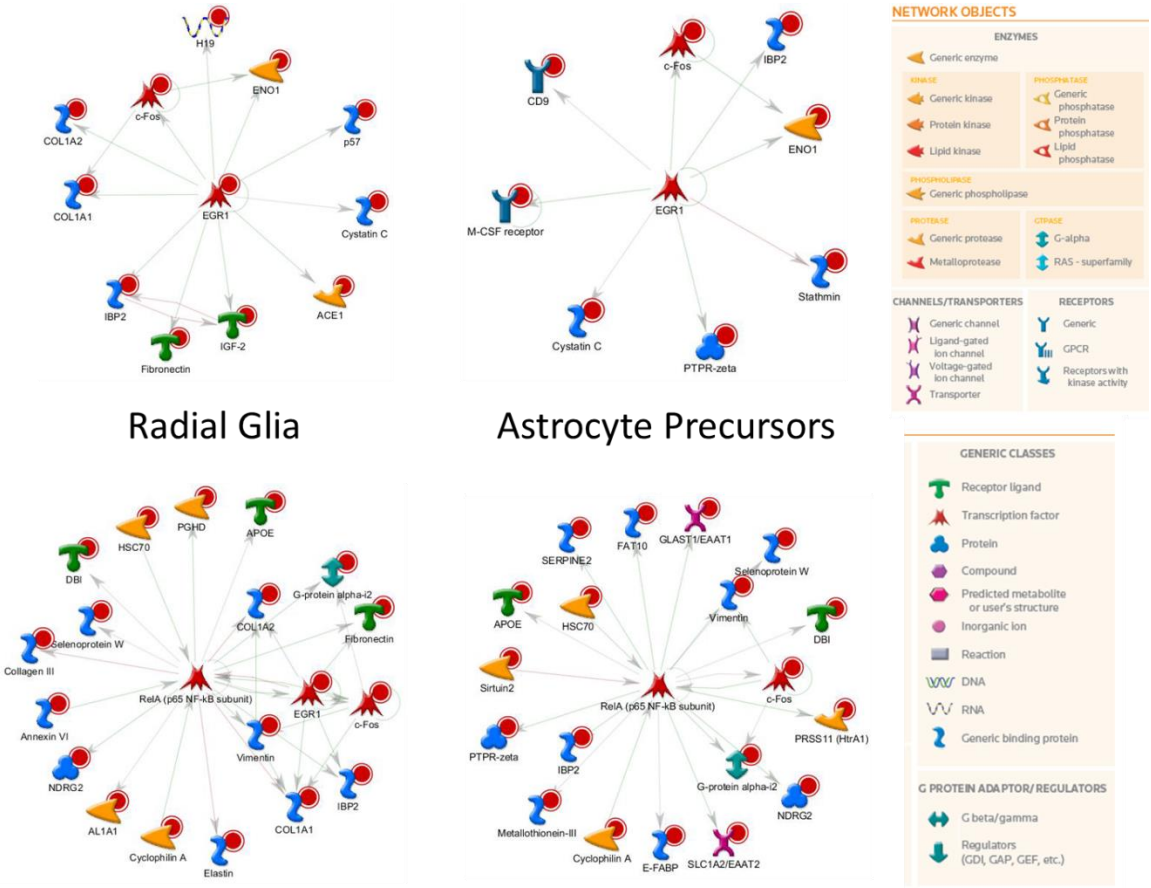

Figure 26: Metacore transcription factor regulation analysis for GLAST+ radial glia and astrocyte precursor datasets.
EGR1 and RELA (p65 of NF-kB subunit) networks for both P0 and P8 GLAST+ cells including selected genes from pathway interaction analysis. Up-regulated genes in both P0 or P8 datasets are marked with red circles. Note the differences in networked interactions in both transcription factors between the two cell populations.

Interactions with different combinations of protein partners may be one way that the same transcription factor can regulate the expression of different genes in different cell types. To test this, MetaCore was used to build a network map of factors present in the radial glial and astrocyte precursor datasets that regulate transcription and interact with

RELA. Figure 27 confirmed the presence of distinct binding partners that could interact with RELA in radial glia and astrocyte precursors.

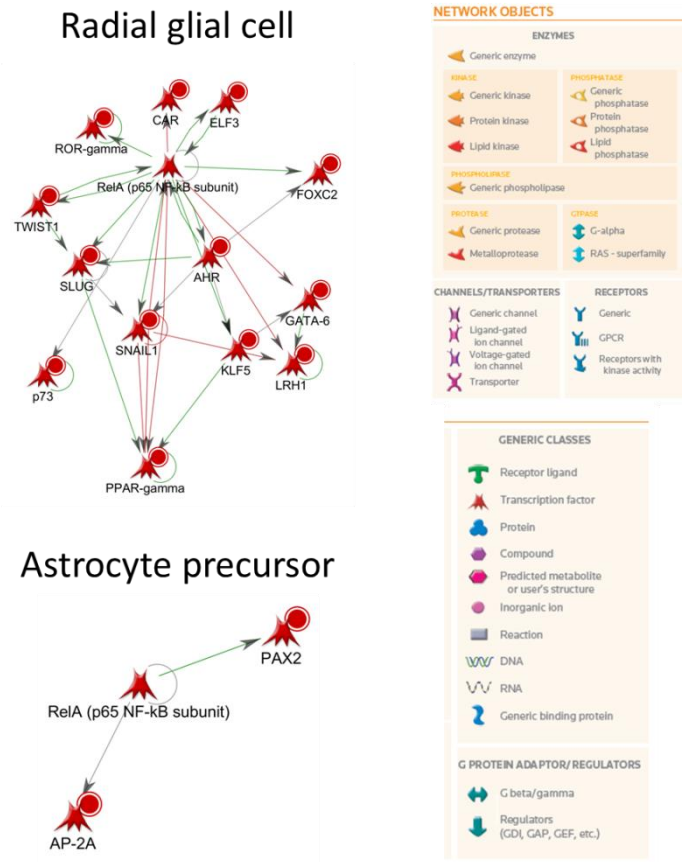

Figure 27: Metacore direct network interactions for RELA in radial glia and astrocyte precursors.
Different potential binding partners for RELA are shown by connecting arrows with representative network objects found in radial glial cells (top) and astrocyte precursors (bottom).

Discussion

The present study compares the transcriptome of GLAST (+) brain cells isolated from radial glial cells at P0 and astrocyte precursors at P8. The appropriate stages to isolate each cell type was determined using double-label immunofluorescence using GLAST and

radial glial or astrocyte precursor markers in the cerebral cortex, olfactory bulb and cerebellum. Confirmation that radial glial cells and astrocytes were indeed isolated at P0 and P8 respectively was determined by comparing FPKM in each dataset for different gene markers of radial glia, astrocyte, neurons, oligodendrocytes and microglia. We chose to use an antibody approach to purify astrocytes from whole brain cells expressing the extracellular epitope for the transmembrane glycoprotein, GLAST. GLAST is an abundant glutamate transporter and is predominantly expressed by astrocytes in the developing and neonatal mammalian CNS (Jungblut et al, 2012). Also radial glia, a cell within the astrocyte lineage, play important roles in development and are known to express GLAST (Shibata et al, 1997). During postnatal astrogenesis, secondary radial glia only persist in a few regions, such as Bergmann glia in the cerebellum, Müller glia in the retina, and radial glia in the dentate gyrus of the adult hippocampus, while mature astrocytes and precursors are present during P8 (Brunne et al, 2013). The cell populations and resulting datasets are well-founded and interpretation made about factors involved in astrocyte development using these data for comparison of astrogenesis is valid, however cell selection using this method may have an unknown bias toward individual cells with increased GLAST expression or increased sensitivity/responsiveness to glutamate or aspartate. Furthermore, high-throughput RNA sequencing methods were carefully conducted. Differential and pathway analyses were performed using EdgeR and IPA, exposing known genes and pathways within our cell populations of interest, along with novel genes with unknown relevance within astrocyte development. Interestingly, an unproportioned number of genes are known to be involved in transcriptional regulation. As mentioned above, proliferative gliogenesis involves many permissive signaling

pathways. Transcription factors, along with epigenetic regulation, are essential to the gene expression changes seen during these signaling events. Using bioinformatic techniques, our data has indicated combinatorial transcriptional cofactors could be involved in astrocyte proliferation and differentiation.

Current data show differential expression within gene categories important for coordinating the intercellular movement of ions or water between astrocytes, which is an important function of astrocytes as they develop and form radiating processes (Simard & Nedergaard, 2004). Astrocytes have important functions for transporting glutamate, dopamine, glucose and many other important molecules in the CNS (Sery et al, 2015). The specific genes of the transporters group have functional relevance to these properties such as Slc4a5, Kcne2 and Clic6S13a4 transporters and Aqp1 water channel within the P0 cells. In P8 cells, neurotransmitter transporters include Slc1a2, Slc6a11 and Slc25a18 along with Aqp4 water channel. Genes included in the canonical pathways within IPA analyses indicate that extracellular molecules, like growth factors such as BMPs and Wnts and collagens are important in the P0 cells. Specifically, BMP signaling is important for differentiation signals within proliferating astrocytes (Scholze et al, 2014; Sehgal et al, 2009).Genes included in canonical pathways for P8 cells include many neurotransmitter receptors, transporters and other channels which are important for astrocyte function. As an example, mRNA encoding GABA and glutamate receptors are represented in the IPA analysis, which is expected since these proteins have important roles in the astrocytes (Jo et al, 2014).

Analyses of possible upstream transcriptional regulatory factors in radial glia or astrocyte precursors belong in three functional categories. In the radial glial cells, factors necessary for pluripotency were found. Nanog is well-known for its expression in embryonic stem cells, where it blocks the differentiation process (Saunders et al, 2013).Both radial glial cells and astrocyte precursors are actively dividing cells; the radial glial cells produce neurons, astrocytes, and oligodendrocytes in a context and time-dependent manner, while astrocyte precursors produce more astrocytes (Ge et al, 2012). Therefore, it is no surprise that both radial glial and astrocyte precursors contain factors important in controlling proliferation, including the androgen receptor, Nanog, TCF7L2, AP2α, E2F1, SREBP1, SREBP2 and Sox10 (Bengoechea-Alonso & Ericsson, 2016; Hashimoto et al, 2016; Helin, 1998; Ishimoto et al, 2010; Melnikova et al, 2010). Negative regulators of proliferation were also found, including CREB1 and PPARα (Cimini & Ceru, 2008; Perry et al, 2004).The list of regulatory factors in radial glial cells appeared to contain proteins that were positive regulators of proliferation, while the list of factors from astrocyte precursors contained both positive and negative regulators of proliferation.

A second functional category that became apparent in the investigation of proteins that regulate expression of transcription factors found in radial glial cell and astrocyte precursors was that of lipid biosynthesis. For instance, the androgen receptor enhances the expression of cholesterolgenic enzymes by regulating SREBP2 activation, USF1 is critical for lipid and glucose metabolism, LXRα is involved in sterol metabolism and PPARα, CREB1, and SOX10 are all involved in regulating expression of proteins involved in sterol biosynthesis (Hashimoto et al, 2016; Kim et al, 2010; Lemberger et al,

2008; Naukkarinen et al, 2005). Finally, NRF2 plays a dual role, increasing synthesis and catabolism of cholesterol in liver (Chambel et al, 2015; Wu et al, 2012). Lipid biosynthesis and metabolism is critical for all living cells. Whereas the body maintains cholesterol homeostasis through a lipoprotein shuttle in which lipids made in the liver are transported to other organs and tissues via the bloodstream, the blood-brain barrier prohibits this process; hence the brain is responsible for its own lipid biosynthesis (Pfrieger & Ungerer, 2011). Although cholesterol synthesis takes place in both neurons and glial cells in the developing nervous system, it is confined primarily to the glial cells in the mature nervous system (Goritz et al, 2002). In the developing nervous system, cholesterol and its carrier protein, apolipoprotein E, are released from astrocytes and play a critical role in synaptogenesis (Goritz et al, 2005; Mauch et al, 2001).

The final functional category identified were factors that play a critical role in inflammatory signaling. For instance, the androgen receptor has been shown to regulate both macrophage infiltration as well as expression of pro-inflammatory factors, PPARα and LXRs appear to work in conjunction with glucocorticoid receptors using a number of mechanisms to regulate inflammatory responses in macrophages and lymphocytes, SREBPs are known to increase IL-1β expression and activate inflammasome activity, and a number of factors we identified in our datasets (Nanog, BAPX1, NFIC,CREB1 and NRF2) have been identified as anti-inflammatory (Cyster et al, 2014; Duan et al, 2013; Glass & Ogawa, 2006; Lai et al, 2012; Pardo et al, 2016). Inflammatory mediators normally associated with disease processes may also play roles in the normal development of the nervous system. A good example of a factor that plays multiple roles

in nervous system development and inflammation is the cytokine superfamily, IL-6. The IL-6 superfamily includes IL-6, cardiotrophin 1 (CT-1), oncostatin M (OSM), IL27, and leukemia inhibitory factor (LIF) and is marked by the use of a common receptor, gp130, in the signaling process (Dixon et al, 2010). This class of cytokines is also referred to as a neuropoietic cytokine precisely because it has many of the pleiotropic effects of a neurotrophin but signals through cytokine receptors rather than the receptor tyrosine kinases typically associated with neurotrophins (Stolp, 2013). The IL-6 family has been implicated in glial fate switching, differentiation of all three major cell types in the developing nervous system, neurite outgrowth, synaptogenesis and maintenance of synapses, and survival (Adachi et al, 2005; Barnabe-Heider et al, 2005; Gadient & Otten, 1997; Gregg & Weiss, 2005; Islam et al, 2009; Nakashima et al, 1999; Oh et al, 2010; Pickering & O'Connor, 2007; Stolp, 2013; Sun & He, 2010). The possibility that some of the pathways and molecules we have identified in our datasets as also utilized in inflammatory mediation is therefore not far-fetched.

Astrocytes have a multitude of roles in the developing nervous system and are becoming increasingly more important as a factor underlying many diseases when these roles are impaired. They can act as neural stem cells within subpopulations of brain regions during development, regulate cerebral blood flow at the vascular interface, store glycogen, transport water, take in extracellular potassium during intense synaptic functions and regulate synapses by the uptake of excess extracellular neurotransmitters (Halassa et al, 2007; Rossi & Volterra, 2009). Although extensively studied, traditional astrocyte analysis has not described how subtypes of astrocytes function differently during

development or the multiple origins and the heterogeneity that underlie glial development until recently (Tabata, 2015). This gap has been mainly due to lack of tools to isolate wild-type astrocytes for systematic studies. Although the present experiments shed light into this knowledge gap, future work will be needed to better understand expression changes among the diversity of different groups of astrocytes during differentiation. Also, the postnatal days and duration between astrogenesis chosen here were grounded on previous studies to understand diversity and functionality of different cells within the whole brain, however regional differences of rate of proliferation and timing of invading progenitors of astrocytes within the brain may differ between neural circuits (Khakh & Sofroniew, 2015).

CHAPTER 6: COMPARITIVE ANALYSIS OF MURINE RADIAL GLIA AND ASTROCYTE HISTONE ACETYLATION

Introduction

Previously we set out to determine potential factors and pathways that maybe necessary to the differentiation of astrocyte precursors from postnatal radial glia. A comparative analysis of the transcriptome of murine radial glial cells isolated at P0 and astrocyte precursors isolated at P8 indicated an enrichment of transcripts associated with proliferation, inflammatory pathways and lipid biosynthesis or metabolism. Although these cellular functions and the collective expression patterns correspond to characteristics found during the development of astrocytes, regulatory elements that control the expression of DNA at these stages are not well defined. One of these regulatory elements, acetylation, alters the basicity of histone proteins and disassociation to DNA, which epigenetically controls gene expression (Allfrey et al, 1964; Hebbes et al, 1988). Also, methylation can regulate constricted associations of histone proteins and DNA (Zhang & Reinberg, 2001). This epigenetic regulation of nucleosomes can be a dynamic and complex process with many different acetylation sites within the histone octamer, containing histones H2A, H2B, H3, and H4, which is wrapped by 146 base pairs of DNA in an open (euchromatin) or closed (heterochromatin) chromatin structure (Kouzarides, 2007). Acetylation of histones is mutually influenced by methylation, for example, hypoacetylated chromatin is methylated on histone H4, whereas chromatin with increased histone H4 acetylation contain more methylated histone H3 (Annunziato et al, 1995). Bivalent domains of specific residues of histones can also exist including lysine 9

of histone H3 (H3K9), which is modified by acetylation and associated with gene transcription in contrast to H3K9 methylation associated with gene repression (Rice & Allis, 2001). The functional and genetic consequence of both methylation and acetylation on individual genes is not known (Soliman et al, 2013).

Previous studies have focused on understanding histone acetylation sites and the regulation of chromatin in brain cells; however have not completed comparisons of the epigenetic markers of whole brain radial glia and astrocyte precursors. For example, prior experiments have explored histone acetylation during normal brain development with or without pharmacological or genetic manipulation and intervention (Cho et al, 2011; Malik et al, 2014; Mitrousis et al, 2015). Specifically, studies have shown that proper brain development and radial glial proliferation is mediated by Histone Deacetylase 1 (HDAC1) and HDAC3, enzymes shown to be important for regulating acetylation of H4K12 and H4K16 in *Xenopus* (Gao et al, 2016; Tao et al, 2015). A possible mechanism of this deacetylation-mediated proliferation and appropriate neurogenesis may be due to control of differentiation signaling pathways, like bone morphogenetic protein (BMP) signaling in mouse radial glial cells, where pharmacological approaches show that HDACs transcriptionally inhibit Bmp2 (Shaked et al, 2008). Astrocyte differentiation is also suppressed by HDAC3 and may compete with an acetylation enzyme, p300, to modulate H3K27 acetylation in the enhancer region of genes associated with oligodendrocyte lineage (Norwood et al, 2014; Zhang et al, 2016a).

While the acetylation-mediated gene regulation and control of proliferation or differentiation has been shown on different lysine residues of histone core proteins, acetylation of histone H3 has been the most extensively studied in astrocytes. Potent HDAC inhibitors have resulted in an increased astrocyte differentiation in P2 to P4 rat brains which coincides with increased H3 acetylation at the same dose (Lee et al, 2016). This may be important for the transcription factor binding of STAT3 to H3 acetylated regions in the promoter of Gfap, a marker of astrocyte differentiation (Asano et al, 2009). It has been shown that STAT3 binds along with p300 to the promoter region and exon 1 of the Gfap gene when H3K9 acetylation occurs following differentiation (Cheng et al, 2011). During the proliferation of rat astroglioma cells *in vitro,* H3K9 hyperacetylated regions and a corresponding increase of transcription factor binding of EGR-1 are found at the promoter region of a neurotrophic factor gene, Gdnf (Yu et al, 2014). Also, H3K9 acetylation, EGR-1 binding and Gdnf expression and mediated proliferation was decreased when treated with HDAC inhibitors (Zhang et al, 2014a). Finally, to understand the neuroprotective mechanisms of acetate supplementation in different inflammatory brain conditions, increase of H3K9 acetylation was seen in acetate-treated astrocyte cultures, likely linked to the upregulation of anti-inflammatory gene transcription (Soliman et al, 2013). These studies have indicated evidence for the basis that histone acetylation is associated in radial glial proliferation and modulation of astrocyte differentiation. However, a full analysis has not been completed during the stages of proliferation and differentiation of radial glial cells and astrocyte precursors.

Since previous studies have shown that H3K9 acetylation is an important regulatory element during the differentiation of astrocytes, understanding genes associated with this post-translational histone modification will help to better understand the potential mechanism of gene regulation of important factors during the differentiation of radial glia and astrocytes in brain development. Chromatin immunoprecipitation using an antibody against H3K9 acetylation coupled with high throughput sequencing (ChIP-seq) analysis has been shown to be a powerful tool to identify acetylated sites of genes (Furey, 2012; Park, 2009). This analysis, along with prior RNA-seq studies will facilitate robustness in classification of important regulation and transcription of genes and pathways that are critical in astrocytes.

ChIP with AcH3K9 antibody immunoprecipitates active gene regions

Initial publications have shown the post-translational acetylation of H3K9 to regulate several genes in astrocytes. These preliminary studies have not reported whole genome H3K9 acetylated regions. Prior to sequencing acetylated regions of the whole genome, an initial study was needed to validate genes that are known to be active or inactive from the current samples. Chromatin from radial glial cells and astrocyte precursors was isolated by ChIP experiments. Replicate ChIP-qPCR experiments show that AcH3K9 IP antibodies bind and pull down high and medium expressing housekeeping genes (Gapdh and Cdkn1a, respectively) but not untranslated regions of chromosome 6 (Untr6) gene desert in both cell types (Figure 28). Since binding events indicate that high and medium expressing genes and a negative control region for H3K9 acetylation association are

appropriate and reproducible, these samples support the hypothesis that H3K9 acetylation corresponds to upregulation of gene expression.

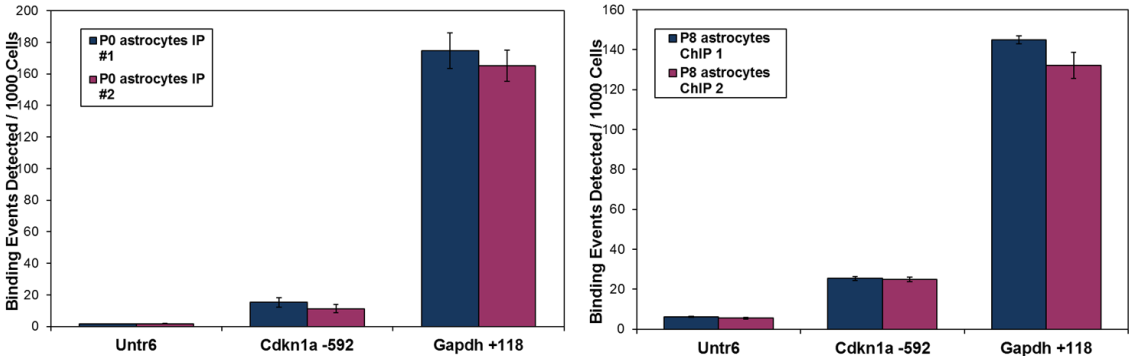

Figure 28: ChIP-qPCR validation.
Control experiments comparing AcH3K9 binding in regions that are known to be active or inactive. Binding events per 1000 cells were detected and plotted in duplicate for each sample for untranslated regions of chromosome 6 (Untr6), cyclin dependant kinase inhibitor 1a (Cdkn1a) and glyceraldehyde 3 phosphate dehydrogenase (Gapdh).

Alignment of active regions in Radial glia and Astrocyte precursors

To distinguish the open chromatin regions within murine radial glial and astrocyte precursors, chromatin immunoprecipitation was performed using the AcH3K9 antibody tested above. A sequence analysis of 50 nucleotide reads was completed along with alignment using the BWA algorithm with a purity filter (Illumina Hi-Seq) and duplicate removal. The density of fragments was determined in continuous 32 nucleotide-long bins following *in silico* 3' extension to 150 – 250.

Quantification and genome-wide distribution of active regions in radial glial and astrocyte precursor cells

To quantify the peaks found following mapping and aligning of each gene, SICER (Zang et al, 2009), a peak calling algorithm typically used to study extended regions of the genome with histone modifications, was used to identify significant enrichment in AcH3K9 immunoprecipitated samples compared to random background. The IgG input control peaks were used to determine false positive ChIP peaks and estimate background for each sample of radial glial and astrocyte precursor cell. Numbers of active regions (overlapping intervals of fragment density above threshold) were counted based on their proximity within 10,000 nucleotides of the annotated genomic locations. Genes with active regions were compared and unique gene lists were compiled for radial glial cells and astrocyte precursor cells. Replicate samples show high overlap of genes with active regions, a 93% commonality in active regions of radial glial cells and 92% in astrocyte precursor cells. Also, among all samples, active regions are mostly found within the gene at 56% as opposed to upstream or downstream non-coding regions, with 57% and 64% in radial glial and astrocyte precursor cells, respectively.

It is crucial for acetylation of H3K9 distribution to be present near the promoter and transcription start site for the initiation of transcription (Guenther et al, 2007). Interestingly, a visual representation of this genome-wide distribution indicates active regions are found near the transcription start site in both radial glial and astrocyte precursor genes (Figure 29). In fact, when calculating the percent of active regions, 79% and 76% of active regions were found at the transcription start site or within 2000 base pairs downstream.

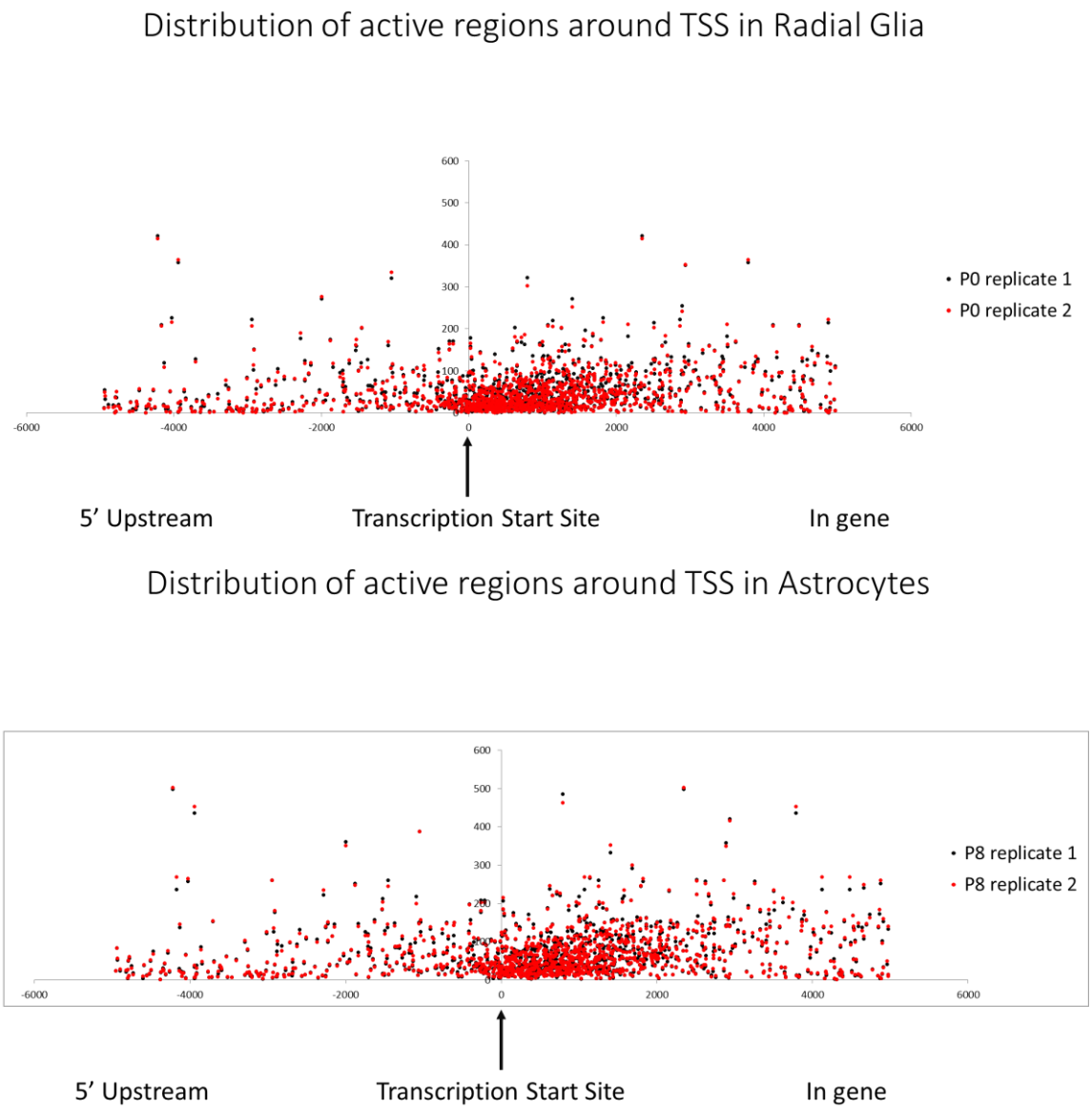

Figure 29: Active acetylated H3K9 regions throughout the genome. Regional location and peak density (y axis) surrounding the transcriptional start site (0) by16,000 base pairs for both replicates (red and black dots) in the radial glia (P0 cells) and astrocytes (P8 cells) represented by a scatter plot. Analysis completed by Sadhna Rao.

Comparison of Radial glial cells and Astrocyte precursors

To understand the differences of genes associated with H3K9 regulatory elements in radial glial cells compared to astrocyte precursor cells, the number of genes with

associated H3K9 active regions above background levels were totaled and overlap of the list of genes were reported between radial glial cells and astrocyte precursors. The ChIP-seq analysis revealed14,798 total genes with H3K9 active regions in the GLAST positive cells, however 566 radial glial genes and 396 astrocyte precursor genes were unique to each of these cell types, suggesting that there are subsets of genes that are epigenetically regulated differently with H3K9 acetylation in radial glial cells and astrocyte precursors (Figure 30). Since previous RNA-seq experiments have been completed using the same cell types used during ChIP-seq experiments, differences in the overlap of genes can be compared between the 2 techniques. To understand the differences of genes associated with H3K9 active regions to the gene transcripts of radial glial cells and astrocyte precursor cells, the RNA-seq and ChIP-seq gene lists were compared. When comparing this gene list for radial glial cells 10,325 genes were commonly acetylated and transcribed, however 5,039 genes were only H3K9 acetylated and a different set of 3,634 genes were transcribed. Also, a comparison of genes from astrocyte precursors that are H3K9 acetylated and transcribed shows 10,271. However, 4,923 genes were H3K9 acetylated, but not transcribed and 3,372 genes were transcribed but not acetylated (Figure 31) Although over half of the genes in radial glial cells and astrocyte precursors are H3K9 acetylated and transcribed, many genes are H3K9 acetylated, but not transcribed. Conversely, there are sets of genes in both radial glial cells and astrocyte precursor cells that are transcribed, but not H3K9 acetylated. This data would suggest that H3K9 regulatory elements are associated with some genes that are expressed, however, this marker is not sufficient to induce gene expression nor does it define gene

expression. This data supports the hypothesis that the regulatory control of the expression of DNA at these stages dynamic, complex and are not well defined.

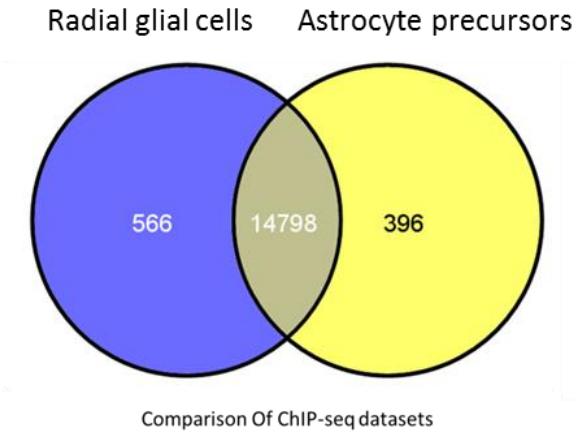

Figure 30: Comparison of H3K9 acetylation of radial glial and astrocyte precursor cells
Venn diagram of the number of common (brown) and unique genes associated with H3K9 active regions for radial glia (blue) and astrocyte precursor (yellow) datasets.

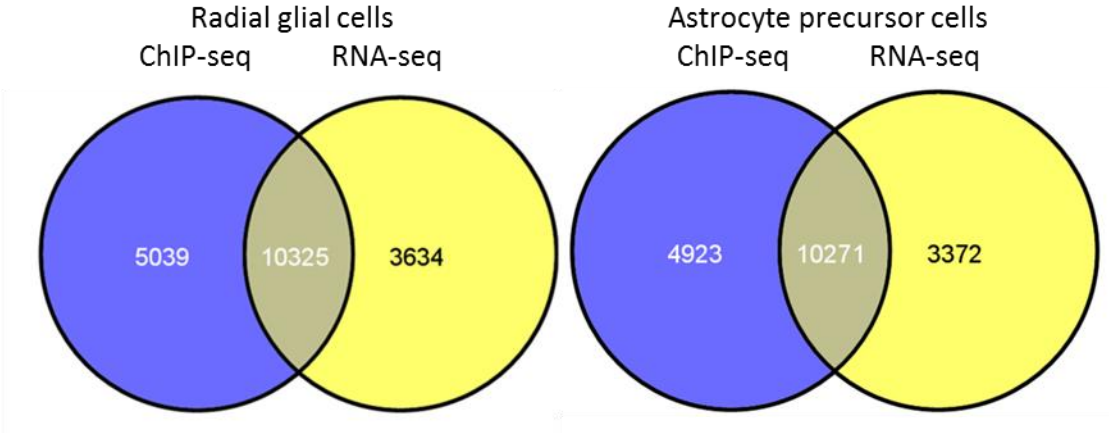

Figure 31: Comparison of ChIP-seq and RNA-seq datasets
Venn diagrams of the number of common (brown) and unique genes between ChIP-seq active regions (blue) and RNA-seq genes (yellow).

A subset of genes were viewed in the Integrated Genome Browser (IGB) to confirm active region peaks for individual genes show representative peaks at transcriptional start sites and have measurable peak densities for differential comparisons. Several genes of

interest were examined including a radial glial gene like, Nfatc2 and an astrocyte precursor gene like Tlr9 (Figure 32)

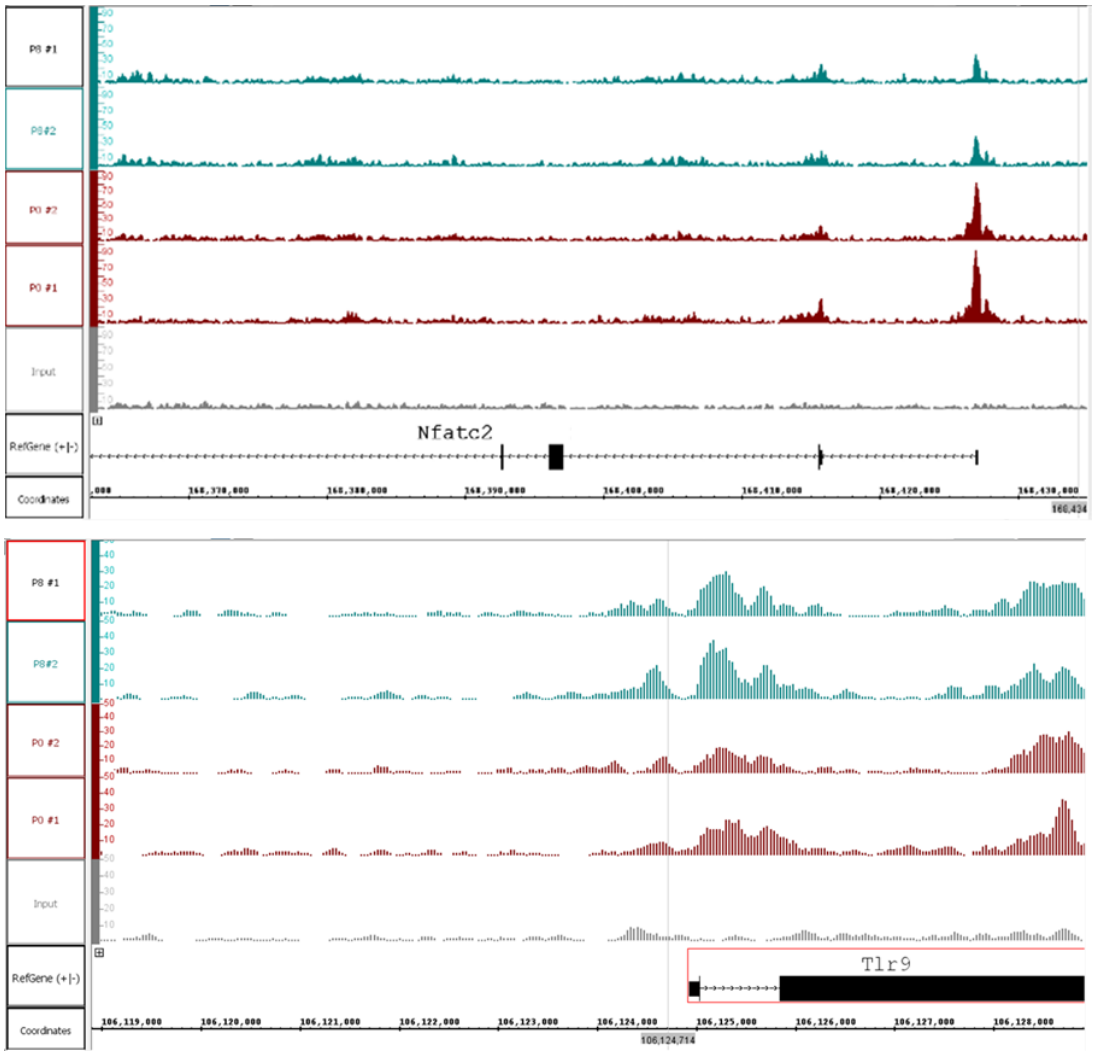

Figure 32: Interactive Genome Browser (IGB) view of example active regions. Duplicate sample peaks shown in blue are from astrocyte precursor cells and duplicate sample peaks shown in red are radial glial cells. Input IgG negative control peaks are shown in grey. Nfatc2 gene is mapped on the antisense strand so that the 5' region is on the right of the diagram. Note the increase in peak density in Nfatc2 proximal promoter at the far 5' end of the gene of radial glial samples compared to lower astrocyte precursor peaks.Tlr9 gene is mapped to the sense strand so that the 5' region is left of the coding region (black rectangle). Note the increase in peak density in Tlr9 proximal promoter at the 5' end of the gene in astrocyte precursor samples compared to lower radial glial peaks. Increased peaks are displayed in Tlr9 gene of astrocyte precursor samples compared to radial glial cell samples.

Pathway analysis genes with H3K9 acetylated regions in Radial glial cells and Astrocyte precursor cells

Since many transcription factors play major roles in signaling pathways and are shown to be important in this dataset, it is important to analyze pathways associated with these factors. To further the understanding of molecular functions of genes with active regions in radial glia or astrocyte precursors, we performed pathway analysis using the Ingenuity Pathway Analysis tool to identify the canonical pathways based on datasets from radial glial cells and astrocyte precursor cells. Regulated genes revealed the highly statistically significant pathways based on a p-value less than 0.05 and FDR less than 0.5 (Table 12). Well-known growth factor signaling pathways in the radial glial cells, including calcium signaling, Wnt signaling, GNRH signaling and CREB signaling matched a significant number of genes with active regions. Genes in astrocyte precursor cells were identified as playing a role in inflammatory pathways, including NF-κB signaling, Toll-like receptor signaling and IL-8 signaling were detected (Table 12).

Table 12: Ingenuity pathway analysis of differential active regions in radial glial and astrocyte precursor cells.

	Pathway	Genes in pathway	Genes matched	P Value	FDR	Hits.Symbol
P0	Calcium Signaling	197	5	0.00010	0.02424	CAMK2A,NFATC2,TRPC4,PRKAR1B, CACNG7
P0	Wnt Signaling pathway	149	3	0.00221	0.10521	WNT7B,CAMK2A,NFATC2
P0	Protein Kinase C Signaling	148	3	0.00275	0.14529	CAMK2A,NFATC2,CACNG7
P0	Gonadotropin-releasing hormone Signaling	156	3	0.00333	0.14529	CAMK2A,PRKAR1B,CACNG7
P0	Protein Kinase A Signaling	309	4	0.00715	0.16087	CAMK2A,NFATC2,PRKAR1B,H1FX
P0	CREB Signaling	203	3	0.00849	0.16087	CAMK2A,PRKAR1B,CACNG7
P8	Insulin Signaling	138	4	0.00009	0.00913	PRKAG3,HK3,PPP1R3D,PIK3CD
P8	Aldosterone Signaling	154	4	0.00020	0.03180	GNA15,PIK3CD,HSPB2,CRYAB
P8	NF-kB Signaling	162	4	0.00025	0.03180	PIK3CD,TLR6,FLT1,TLR9
P8	Toll-like receptor Signaling pathway	102	3	0.00037	0.02103	PIK3CD,TLR6,TLR9
P8	ERK/MAPK Signaling	208	4	0.00080	0.05794	ESR1,PPP1R3D,PIK3CD,HSPB2
P8	Relaxin Signaling	136	3	0.00139	0.06105	GNA15,PIK3CD,PDE8A
P8	Endothelin-1 Signaling	164	3	0.00277	0.07365	GNA15,PIK3CD,LCAT
P8	IL-8 Signaling	185	3	0.00429	0.07365	GNA15,PIK3CD,FLT1

Transcription factor binding analysis of genes with active regions

To identify upstream factors that may interact with H3K9 acetylated chromatin on the promoter region, transcription factor analysis was completed to understand the transcriptional regulators that potentially may bind to consensus site genes within these target datasets. The entire gene list of H3K9 acetylated genes were used to identify

transcription factors that bind to these genes. Transcription factor identification was completed using the Transcription Regulation algorithm from the commercial software MetaCore (GeneGo, Inc, St. Joseph, MI) which is based on manual curation. This algorithm generated networks of our gene lists centered on transcription factors known to directly bind these genes. Transcription factors were ranked according to their p-value and number of genes in our list compared to total genes that it may bind (seed nodes). The top 25 statistically significant transcription factors that have been shown to regulate genes in radial glial cells (Table 13) or astrocyte precursors (Table 14) were indicate by the MetaCore Transcription Factor analysis. Interestingly, many of the transcription factors identified as potential regulators of the genes in H3K9 active regions were similar between radial glial and astrocyte precursors. These factors were marked with a "(C)". There were some differences in potential transcription factors, which suggest differences in the cofactor binding and interactions of transcription factors for the expression of these genes.

Table 13: Metacore transcription factor regulation analysis of active regions from radial glial cells

Network	Seed nodes	p-Value
CREB1 (C)	122	2.71E-264
SP1 (C)	65	9.18E-139
ESR1 (nuclear) (C)	64	1.37E-136
c-Myc (C)	59	9.65E-126
c-Jun (C)	50	2.81E-106
P53 (C)	45	1.68E-95
GCR-alpha (C)	42	4.76E-89
NRSF	42	4.76E-89
Oct-3/4 (C)	41	6.71E-87
Androgen receptor (C)	38	1.85E-80
c-Fos	36	3.58E-76
RelA (p65 NF-kB subunit) (C)	34	6.86E-72
WT1	33	9.46E-70
STAT1 (C)	32	1.30E-67
JunB	32	1.30E-67
HNF3-beta	32	1.30E-67
NANOG	31	5.62E-67
C/EBPbeta (C)	31	1.78E-65
HNF4-alpha	31	1.78E-65
GATA-4	31	1.78E-65
TITF1	30	7.92E-65

Table 14: Metacore transcription factor regulation analysis of active regions from astrocyte precursor cells

Network	Seed nodes	p-Value
CREB1 (C)	94	1.59E-211
SP1 (C)	48	1.82E-106
GCR-alpha (C)	40	1.80E-88
p53 (C)	31	2.50E-68
ESR1 (nuclear) (C)	28	1.22E-61
c-Myc (C)	26	3.44E-57
RelA (p65 NF-kB subunit) (C)	26	3.44E-57
Androgen receptor (C)	24	9.58E-53
STAT1 (C)	24	9.58E-53
c-Jun (C)	22	2.62E-48
GATA-3	18	1.86E-39
C/EBPbeta (C)	18	1.86E-39
SMAD3	17	3.01E-37
STAT3	16	4.83E-35
SP3	15	7.70E-33
PU.1	15	7.70E-33
YY1	15	7.70E-33
Oct-3/4 (C)	15	7.70E-33
NF-kB1 (p50)	15	7.70E-33
LHX2	14	1.22E-30
HIF1A	14	1.22E-30

Discussion

Since aforementioned experiments have shown that H3K9 acetylation is important for gene expression during the differentiation of astrocytes, a genome-wide analysis of this regulatory element will help to better understand the potential mechanism of gene regulation of important astrocyte differentiation factors in brain development. In these studies, ChIP of H3K9 acetylation was shown to appropriately isolate control regions/genes. Also, it is possible to map and align H3K9 active regions to the genome and define the distribution of active regions to quantify the density of the peaks. Within

the coding regions of the genes, H3K9 acetylation modifications are mainly enriched in the near the transcription start site.

Pathway analysis of this data has bolstered the idea that genes identified to play a role in inflammatory pathways are also important factors during astrogenesis stages. Many previous reports corroborate the pathways from the current study. In radial glial cells, Wnt signaling is required for stabilizing vascular networks, self-renewal and neurogenesis following spinal cord injury (Briona et al, 2015; Gan et al, 2014; Ma et al, 2013). CREB signaling has shown to be neuroprotective in reactive glia (Pardo et al, 2016) along with decreases calcium excitability (Eraso-Pichot et al, 2016). Calcium signaling is controlled by TRPC in radial glia and regulates neurogenesis and migration of neurons (Molnar et al, 2016; Rash et al, 2016). Evidence of direct gonadotrophin-releasing hormone interaction with astroglial cells has been shown along with localization of protein kinase C, modulated by MARCKS during postnatal brain development (Baroncini et al, 2007; Chen & Hillman, 1994; Weimer et al, 2009). In astrocyte precursors, nuclear factor-κB-dependent inflammation is a major pathway in Parkinson's disease, Alzheimer's disease and Huntington's disease (Ben Haim et al, 2015; Hsiao et al, 2013; Pal et al, 2016). Also, the IL-8 inflammation pathway in astrocytes correlates with seizure frequency in brain tissue (Pernhorst et al, 2013). Endothelin-1 and its receptors are not normally expressed in astrocytes, however when they adapt to reactive phenotypes, high levels are expressed (Hostenbach et al, 2016). Finally, many pathways converge in to ERK/MAPK signaling and have crucial roles in

demyelinating inflammation and other astrocyte diseases in the central nervous system (Okazaki et al, 2016).

Transcription factor regulation analysis of this data has identified factors important in both radial glial cells and astrocyte precursors, however, interestingly there are factors potentially differentially regulating radial glial genes or astrocyte precursor genes. Factors potentially binding and regulating radial glial cells include WT1 (Wilm's Tumor 1) and NANOG. WT1 has been shown to be overexpressed in primary astrocytic tumors, however this protein expression cannot distinguish between proliferating tumor cells and reactive astrocytes (Bourne et al, 2010; Oji et al, 2004). NANOG, similarly to Wnt signaling regulates astrocyte proliferation following spinal cord injury (Gu et al, 2016). Also, NANOG has the ability, as a stemness marker, to induce dedifferentiation of p53-deficient mouse astrocytes into glioma cells (Moon et al, 2011). Both of these factors have the ability to induce proliferation in certain context, however have been shown to be involved in disease states. Factors potentially binding and regulating astrocyte precursor cells include STAT3 and SMAD3. STAT3 as mentioned above, has a direct role in gene regulation in astrocytes. It is not surprising that our analysis also detected potential STAT3 regulation of astrocyte genes. This transcription factor has been identified as playing a role in IL-6 inflammatory pathways, however, it has other roles in cell growth, differentiation and survival as well (Hirano et al, 2000; Hong & Song, 2014). SMAD3 is a factor that is identified to play a role in inflammatory pathways and also important factors during astrogenesis stages. SMAD3 is associated with the TGF-β pathway that controls differentiation of radial glia into astrocytes (Stipursky et al, 2012). SMAD3

deficiency increases cortical and hippocampal neuronal loss following traumatic brain injury and increases Parkinson's disease pathology (Tapia-Gonzalez et al, 2011; Villapol et al, 2013). Both of these factors have the ability to induce differentiation of astrocytes, however have been shown to have a more direct involvement with inflammatory brain diseases. Many of the other transcription factors are identified as playing a role in inflammatory pathways as well including, CREB1, STAT1 and NFκB. These factors do not seem to have the potential of differentially regulating radial glia or astrocyte precursor gene expression however, a combination of these may have differential roles in proliferation and differentiation (Cheng et al, 2013). Further experiments to understand acetylation during these events and the associated regulatory factors will give better insight to how the complexity of transcription is regulated during brain development.

CHAPTER 7: PHOSPHODIESTERASE 10A INHIBITOR, MP-10 (PF-2545920), PRODUCES GREATER INDUCTION OF C-FOS IN DOPAMINE D2 NEURONS THAN IN D1 NEURONS IN THE NEOSTRIATUM

Introduction

In previous chapters, this dissertation has focused on the regulation of glial cell phenotypes by α-synuclein and genomic alterations associated with astrogenesis. As mentioned earlier, the modulation of inflammatory processes within glial cells are a key feature of PD, but do not directly account for the hallmark symptoms of PD. To better understand deficits in locomotor activity, understanding the cellular signaling processes in different cell types within the basal ganglia is necessary. Pathology of dopamine neurons in the SN of the basal ganglia defines PD (Ehringer & Hornykiewicz, 1960; Hirsch et al, 1988) and the loss of these cells discontinues delivery of dopamine to post-synaptic cells, such as the medium spiny neurons, causing motor symptoms (Damier et al, 1999). However, distinct cell populations with different dopamine receptor activity, stimulatory and inhibitory pathways, defined by D1 receptors and D2 receptors respectively, are present (Gerfen, 1992). During normal function, these cells require balanced activation, and in PD, the loss of SN dopamine neurons leads to disinhibition of the indirect pathway and the loss of stimulation of the direct pathway, which results in the overall decrease in basal ganglia output. One enzyme downstream of the dopamine receptor signaling pathway, PDE10A, has been shown to be uniformly expressed in all medium spiny neurons and show decreased protein levels in PD (Kleiman et al, 2011;

Niccolini et al, 2015; Seeger et al, 2003). When this enzyme is inhibited, an unbalanced induction of medium spiny neuron activity was seen (Strick et al, 2010). Studies such as these are needed to further characterize and confirm the molecules with unbalanced activation in the basal ganglia circuitry. Therefore, the following studies were completed to identify mechanisms that regulate basal ganglia cell activity and may affect PD pathology and the overall decrease of motor circuitry.

The medium spiny neurons (MSN) of the neostriatum are the primary target of antipsychotic and anti-parkinsonian medications. Specifically, these drugs target the Gαi-coupled dopamine D2 family of G protein-coupled receptors on the MSNs (Perreault et al, 2011). Morphological and functional studies have shown that the D2 receptor-expressing MSNs constitute the striatopallidal pathway whereas the Gαs-coupled D1 expressing cells form the striatonigral pathway (Gerfen, 1992). Classical antipsychotic drugs are thought to produce their efficacy by antagonizing the D2 receptors (Kapur & Mamo, 2003). However, these drugs also induce extrapyramidal motor side effects by reducing basal ganglia output (Parr-Brownlie & Hyland, 2005). Although the newer, so-called atypical antipsychotics have a reduced liability to trigger extrapyramidal side effects, they induce intolerable metabolic side effects (Manu et al, 2012). Therefore, it remains critical to identify additional therapeutic mechanisms for treatment of psychotic symptoms associated with schizophrenia and other psychiatric disorders.

Phosphodiesterases (PDEs) are a family of enzymes that cleave cyclic nucleotides and thereby regulate second messenger signaling casacades (Sharma et al, 2013). PDE10A,

like several other PDEs, cleaves both cyclic adenosine monophosphate (cAMP) and cyclic guanosine monophosphate (cGMP) to AMP and GMP, respectively (Wilson & Brandon, 2014). PDE10A is particularly relevant to the basal ganglia system because it is highly enriched in MSNs (Kleiman et al, 2011; Seeger et al, 2003). MP-10 (also known as PF-2545920; 2-((4-(1-methyl-4-(pyridin-4-yl)-1H-pyrazol-3-yl)phenoxy)methyl)quinoline) is a potent and selective PDE10A inhibitor (PDE10i) both *in vitro* and *in vivo* (Schulke et al, 2014). Treatment with MP-10 increases intracellular concentrations of cAMP/cGMP, augmenting dopamine D2 receptor antagonist- and dopamine D1 receptor agonist-mediated effects (Grauer et al, 2009; Schmidt et al, 2008). Given that dopamine D2 receptor inhibition is a pharmacological activity shared by all antipsychotic drugs, PDE10i have been proposed as a new class of therapeutics to treat psychoses (Strick et al, 2010).

The PDE10A knockout mice show reduced locomotor activity (Siuciak et al, 2006; Siuciak et al, 2008). Hence, we hypothesize that although PDE10i will affect activity of all MSNs, it may induce relatively greater activation of D2(+) MSNs. The present set of studies tested this hypothesis using MP-10 as a pharmacological probe. We assessed c-Fos immunoreactivity as a marker of increased neuronal activity in two sub-regions of the neostriatum, the dorsolateral and dorsomedial striatum, preferentially regulated by dopamine D2 and D1 receptors, respectively (Merchant et al, 1994). The regional pattern of c-Fos induction by MP-10 was compared to that produced by acute treatment with prototypical D2 antagonist, haloperidol and D1 agonist, SKF82958. Finally, to directly confirm this effect, we utilized the bacterial artificial chromosome (BAC) transgenic

Drd1a-tdTomato mice line 6 (Ade et al, 2011) to assess co-localization of c-Fos immunoreactivity in MSN populations that express the D1 receptor or those without the D1 receptor. In these mice, the expression of the fluorescent reporter tdTomato is under the regulation of the *Drd1a* gene and the reporter is expressed with high selectivity and specificity only in D1(+) MSNs (Ade et al, 2011), thereby providing a direct method to assess the induction of c-Fos in both the D1 or D2-expressing sub-populations of MSNs.

MP-10 dose-dependently increased c-Fos expression in the rat striatum

Figure 33A shows the c-Fos immunopositive cells at two different magnifications following MP-10 at 30 mg/kg, PO, to rats. A statistically significant, dose-dependent increase in c-Fos immunopositive cells was observed in both the DLS and DMS at 10 and 30 mg/kg of MP-10 (Figure 33B). Notably, the c-Fos signal density was higher in the DLS than the DMS at both 10 and 30 mg/kg doses. The c-Fos dominance index derived by subtracting the DMS signal from that in the DLS confirmed that MP-10 treatment at 10 and 30 mg/kg significantly produced a DLS-dominant effect (Figure 33C). There was no significant induction of c-Fos in additional brain regions examined (Figure 33D). Hence, all subsequent studies focused on the DLS and DMS c-Fos expression.

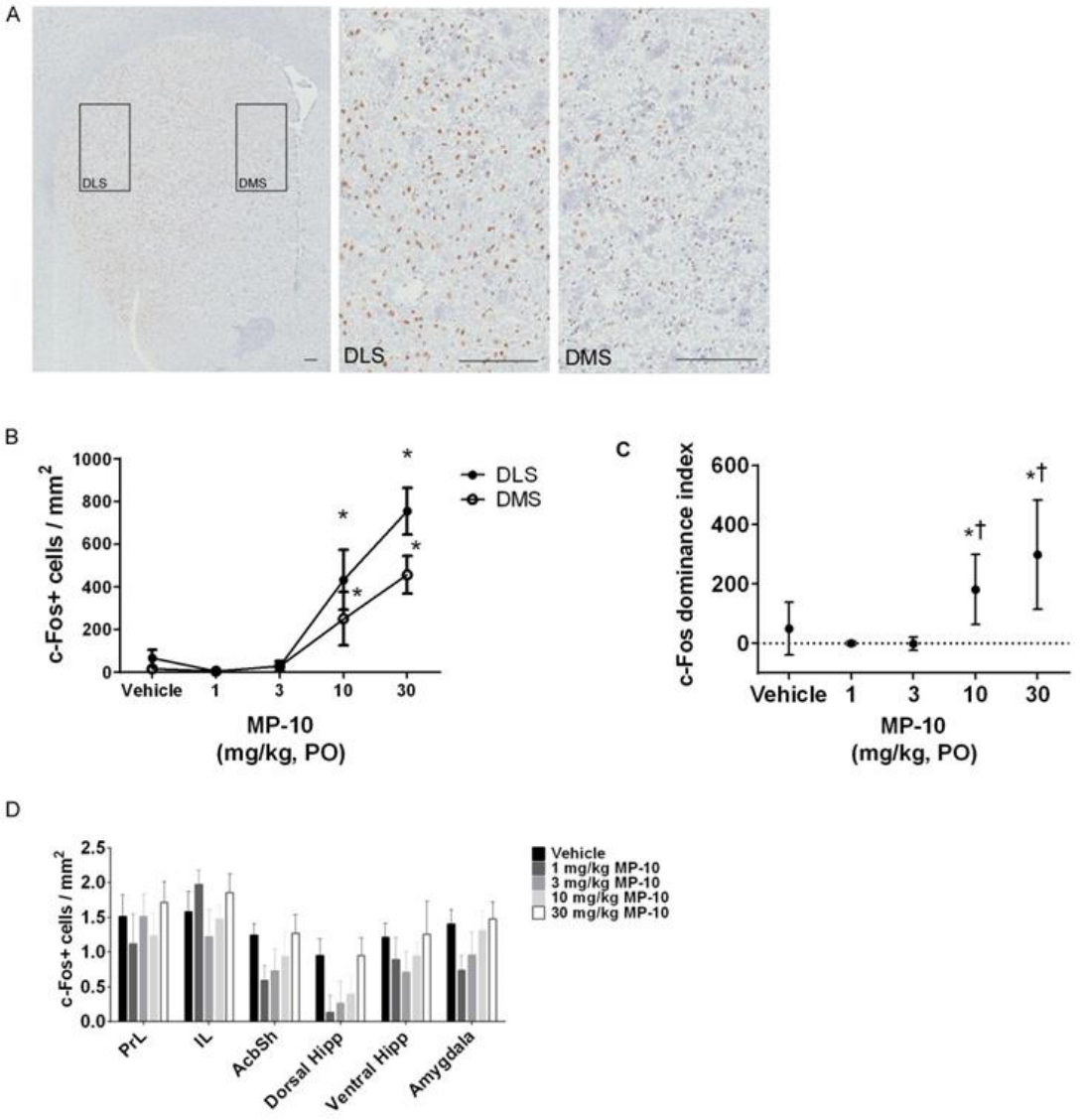

Figure 33: MP-10 dose-dependently and selectively induces c-Fos expression in the rat neostriatum.

A) Representative micrographs of c-Fos immunopositive nuclei in the neostriatum of a rat treated with MP-10 at 30 mg/kg, PO. The left panel shows the neostriatum with DLS and DMS, outlined. The two right panels show c-Fos-positive nuclei in the DLS and DMS at higher magnification. Magnification bars = 200 μm. B) Quantitative analysis of c-Fos immunoreactive cell density in the DLS and DMS. Each point represents the group mean ± SEM. * $p<0.05$ versus the vehicle. C) The c-Fos dominance index derived from data in Figure 1B is shown as adjusted mean ± 95% confidence interval for each group. *$p<0.05$ versus the vehicle. †$p<0.05$ versus the DMS signal. D) Quantitative analysis of c-Fos signal density in other brain regions following treatment with MP-10. Each bar represents the group mean ± SEM. PrL, Prelimbic Cortex; IL, Infralimbic Cortex; AcbSh, Accumbens Shell; Hipp, Hippocampus.

Dopamine D2 receptor inhibition and D1 receptor activation show a regional preference in c-Fos expression

SD rats treated with haloperidol (0.3, 1 or 3 mg/kg, PO) or SKF82958 (0.5, 1 or 2 mg/kg, PO) dose-dependently induced c-Fos in the DLS and DMS. The c-Fos dominance index demonstrated that like MP-10, the dopamine D2 receptor antagonist, haloperidol, favored the activation of the DLS (Figure 34A and 34B), whereas the dopamine D1 receptor agonist, SKF82958, favored that in the DMS (Figure 34C and 34D).

The cross-rodent species consistency of the c-Fos dominance index was established in the C57BL/6 mouse striatum in which haloperidol (2 mg/kg, IP) or SKF82958 (3 mg/kg, IP) produced an identical regional pattern of c-Fos induction (Figure 34E-G).

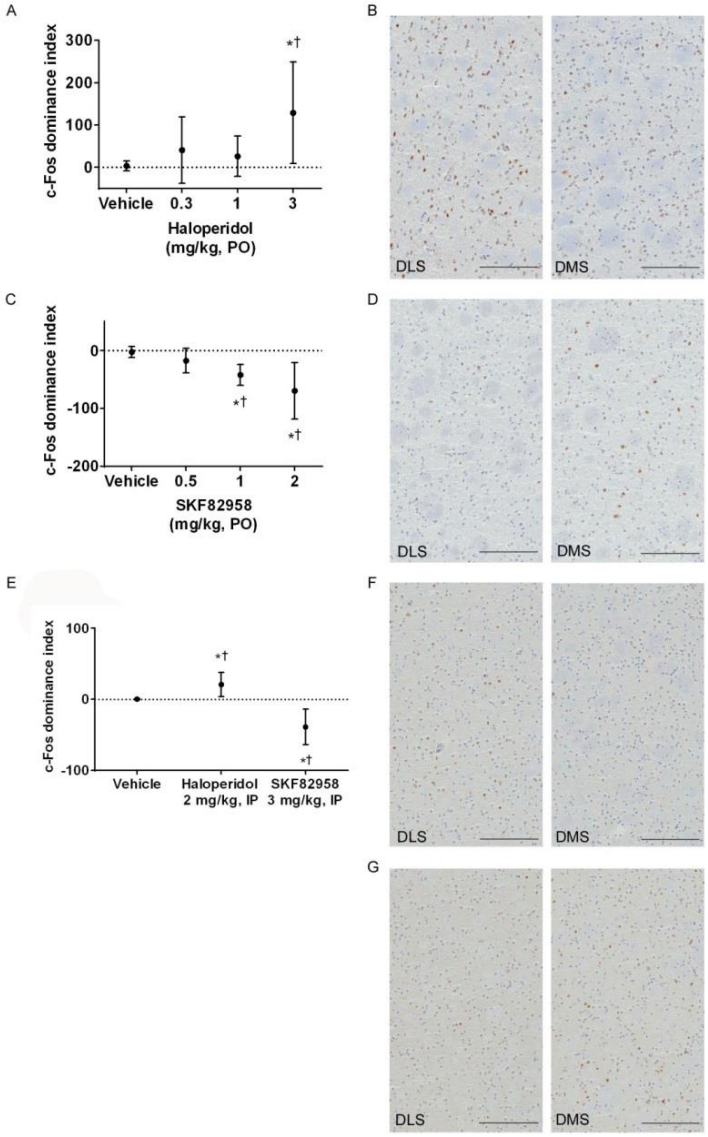

Figure 34: c-Fos induction in the DLS and DMS by haloperidol or SKF82958. Panels A and C compare c-Fos dominance index in the rat neostriatum by haloperidol (0.3, 1 or 3 mg/kg, PO; Panel A) or SKF82958 (0.5, 1 or 2 mg/kg, PO; Panel C) and their respective vehicle. Data are shown as adjusted mean ± 95% confidence interval. *$p<0.05$ versus the vehicle. †$p<0.05$ versus the DMS signal. Panels B and D show representative photomicrographs of c-Fos positive nuclei in the DLS and DMS following treatment with haloperidol (3 mg/kg, PO; Panel B) or SKF82958 (2 mg/kg, PO; Panel D). Magnification bars = 200 μm. E) c-Fos dominance index following treatment of C57BL/6 mice with vehicle (IP), haloperidol (2 mg/kg, IP) or SKF82958 (3 mg/kg, IP) shown as adjusted mean ± 95% confidence interval. *$p<0.05$ versus the vehicle, †$p<0.05$ versus the DMS. Panels F and G show representative photomicrographs corresponding to the data in Figure 2E for effects of haloperidol (Panel F) and SKF82958 (Panel G). Magnification bars = 200 μm.

MP-10-induced c-Fos expression is greater in D2+ MSNs than in D1+ MSNs of the Drd1a-tdTomato mouse

To directly assess MP-10-induced c-Fos expression within the D1(+) and D1(-) (i.e., primarily D2(+)) MSN populations, colocalization experiments were conducted in BAC transgenic Drd1a-tdTomato mice treated with MP-10 (3 or 10 mg/kg, IP). We removed the regional bias of our analyses by comprehensive assessment of the c-Fos signal in five fields encompassing the entire dorsal striatum (Figure 35C). MP-10 increased the percent of c-Fos expressing cells in both D1(-) and D1(+) cells, when compared to vehicle treatment, but there was no statistical difference between the doses of MP-10 assessed (Figure 35A and 35B). At 3 mg/kg, 45% of D1(+) cells expressed c-Fos and at 10 mg/kg, 44% of D1(+) cells were c-Fos positive. On the other hand, 54% and 58% of D1(-) were c-Fos positive at 3 and 10 mg/kg of MP-10, respectively. The percent of c-Fos induction within D1(-) neurons was significantly greater than that in D1(+) neurons, following 10 mg/kg of MP-10; although a similar trend appeared at 3 mg/kg of MP-10 ($p = 0.071$) (Figure 35C).

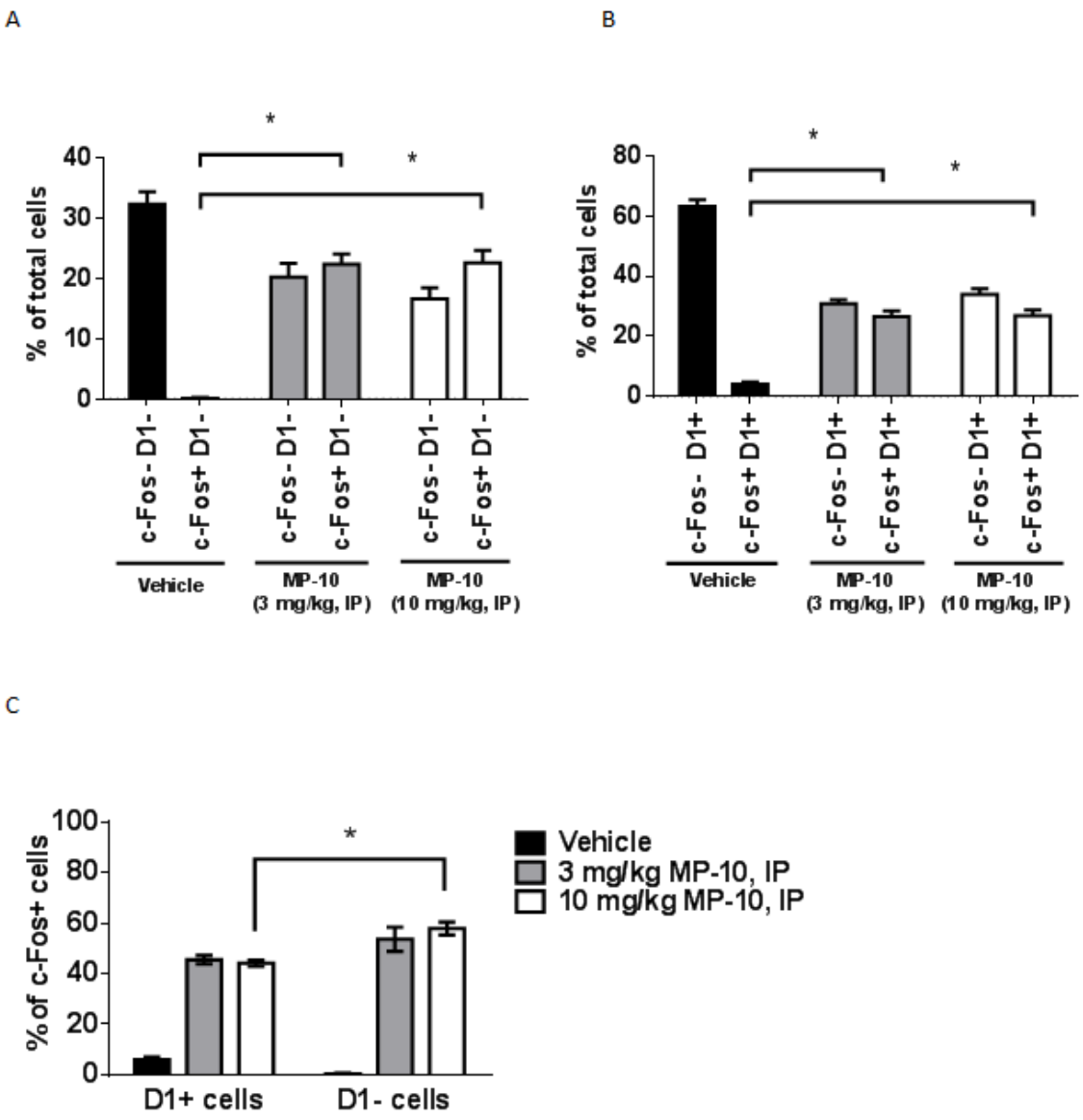

Figure 35: MP-10 produces greater induction of c-Fos in D1(-) cells in the dorsal neostriatum of the BAC transgenic Drd1a-tdTomato mouse.

A and B) The mean ± SEM for the percent of D1(-) and D1(+) cells with and without c-Fos are reported for each treatment group. *p<0.05 versus the vehicle. C) c-Fos positive cell counts were normalized to D1(+) cells or D1(-) cells. The adjusted mean percent of c-Fos positive cells and ± SEM are reported for each dose group. *p<0.05 indicates a statistically increase in c-Fos in D1(-) cells when compared to D1(+) cells.

Discussion

The present studies utilized a combination of pharmacological and genetic tools to test the hypothesis that PDE10A inhibition produces greater activation of D2(+) striatopallidal pathway than D1(+) striatonigral pathway. Using c-Fos as a marker of neuronal activation and a selective PDE10i tool, MP-10, we provide two major but complementary lines of evidence in support of this hypothesis. First, like the effects of the D2 inhibitory ligand, haloperidol, the effects of MP-10 were greater in the DLS than in the DMS in both the rat and the mouse. Second, and more directly, MP-10 treatment produced greater induction of c-Fos in D1(-) MSN neurons in a BAC transgenic mouse where only D1(+) cells are fluorescently labelled. Since MSNs represent 95% of cells in the striatum, it can be deduced that D1(-) cells are predominantly D2(+) cells (Kemp & Powell, 1971), which respond to a greater extent to PDE10A inhibition by MP-10.

MP-10 is a well-characterized pharmacological tool for PDE10A inhibition (Schmidt et al, 2008). At doses used in the present set of experiments, MP-10 is shown to produce robust biochemical and behavioral alterations in the rat and the mouse (Grauer et al, 2009; Megens et al, 2014; Sotty et al, 2009). Characterization of the c-Fos induction within sub-regions of the striatum was performed on the basis of the previously reported greater sensitivity of the DLS to D2 antagonism and the DMS to D1 agonism (Merchant et al, 1994). Although the focus on DLS and DMS may have introduced a regional bias in our initial results, we ultimately removed any confounds of regional selection by broadly surveying the dorsal striatum in the Drd1a-tdTomato mouse study (vide infra). Indeed, MP-10 produces significantly greater c-Fos induction in the DLS than the DMS, a pattern

similar to that produced by the prototypical D2 antagonist, haloperidol, at doses that selectively occupy the D2 receptor. On the other hand, the activation of the D1 receptor by SKF82958 favored c-Fos induction in the DMS. These data are in agreement with a recent report (Gentzel et al, 2015) demonstrating greater sensitivity of the DLS to MP-10-mediated activation of c-fos, arc, and egr-1 mRNA.

To directly assess MP-10 induced c-Fos in D1(+) versus D2(+) MSNs, we took advantage of the BAC transgenic mice expressing a fluorescent reporter (td-Tomato) exclusively in the D1(+) MSNs with negligible rates (0.7%) of false negativity of the transgenic reporter (Ade et al, 2011). Nearly 60% of total cells counted were positive for td-Tomato in vehicle-treated animals. Since >95% of neostriatal cells are MSNs, we presumed that td-Tomato negative cells are predominantly dopamine D2 receptor containing MSNs. Thus, a single mouse line allowed us to assess MP-10-induced c-Fos expression in D1(+) and D2(+) MSNs. The percent of D1(+) neurons did not differ among five fields examined. Since the mouse metabolizes MP-10 at a faster rate after oral administration (data not shown), we tested MP-10 effects via the IP route at doses that produce significant behavioral effects. From the percent of c-Fos-expressing cells in D1(+) and D1(-) MSN population, we conclude that MP-10 produces greater activation of the D2(+) cells. This effect was statistically significant at 10 mg/kg, IP, but missed significance at 3 mg/kg, IP, due to higher variability in this dose group. Numerically, the dose-response relationship was not robust in this study where a limited dose-range was tested. On the other hand, a statistically significant response was only observed at 10 mg/kg. Future tests of a wider dose range would further assess a dose-dependent effect.

The small, but significantly greater effect of PDE10i in D2(+) cells is observed despite similar levels of Pde10a mRNA in the D1(+) and D2(+) MSNs (Fujishige et al, 1999; Heiman et al, 2008). Whether PDE10A protein levels or enzyme activity are different in the two MSN cell types is not known. Thus it appears that despite the presence of PDE10A in all MSNs of the neostriatum (Seeger et al, 2003), the basal tone of the enzyme is higher in the D2 containing striatopallidal pathway. This could be due to the relatively higher basal activity of the D2(+) than the D1(+) MSNs (Day et al, 2008).

Our data are consistent with and extend the behavioral observations of Siuciak *et al*. (Siuciak et al, 2006) in PDE10A knockout mice. These investigators noted that PDE10A-deficient mice display suppressed locomotor output without any reduction in striatal dopamine levels or dopamine turnover. They hypothesized that although PDE10A is expressed at similar levels in all MSNs, inhibition of PDE10A preferentially increases the activity of the inhibitory indirect pathway and thereby reduces motor output. This is somewhat borne out by the results of Strick *et al*. (Strick et al, 2010), who reported greater induction in enkephalin mRNA (a marker of striatopallidal MSN activation), than substance P mRNA (a marker of striatonigral MSN activation) by MP-10 treatment, although their method did not directly quantitate the effect of PDE10A inhibition in the two MSN efferent pathways. More importantly, Nishi *et al*. reported that PDE10A inhibition produces higher levels of DARPP-32 phosphorylation in striatopallidal MSNs than in the striatonigral neurons (Nishi et al, 2008). Direct assessment of MSN activity showed that PDE10A inhibition augmented cortically evoked spike activity only in striatopallidal and not in striatonigral MSNs (Threlfell et al, 2009). On the other hand, a

recent study by Gentzel *et al*. determined the effects of MP-10 on the two MSN populations by analyzing co-expression of egr-1 and substance P (i.e., striatonigral MSNs) or egr-1 and enkephalin (i.e., striatopallidal MSNs) and failed to see preferential activation of the striatopallidal pathway (Gentzel et al, 2015). The reasons underlying the somewhat discrepant results remain unclear but we believe that the Drd1-tdTomato mouse provides the most direct method to determine the relative engagement of the two MSN populations by a PDE10i. Overall, the preponderance of evidence from the current study and those cited above indicate that acute PDE10 inhibition increases the activity of both striatopallidal and striatonigral projections, but with a small but significant preference for the striatopallidal projections. Although this signature of pharmacological activity supports the investigation of this mechanism in psychotic disorders, it also raises a concern whether medically relevant antipsychotic efficacy may be produced in the absence of extrapyramidal side effects.

In contrast to acute activation of MSNs induced by MP-10, PDE10A-deficient mice show overall decreased striatal excitability (Piccart et al, 2014). However, the activity of D1(+) versus D2(+) MSNs in PDE10A deficient mice was not assessed. Furthermore, it is possible that the effects of acute, short-term inhibition of PDE10A inhibition are distinct from a developmental deletion of PDE10A. Future studies assessing chronic effects of a PDE10i in wild-type mouse may further our understanding of the PDE10A-mediated regulation of the striatal output.

It is noteworthy that we failed to observe significant c-Fos induction in regions other than the neostriatum. Gentzel *et al*. reported MP-10 induced increase in c-fos but not egr-1 mRNA in the nucleus accumbens but the effects were greater in the DLS (Gentzel et al, 2015). Seeger *et al*. also failed to show activation of the nucleus accumbens shell by a PDE10i, despite high levels of expression of PDE10A in this nucleus (Seeger et al, 2003). These data indicate that basal activity of PDE10A is regulated in a region and cell-type specific manner.

It is important to point out that PDE10a is not expressed in presynaptic dopamine cells or striatal glutamate terminals, so there are no direct effects of MP-10 on dopamine release via the autoregulatory presynaptic D2 receptors or glutamate activation. Previous reports have interrogated other striatal-enriched PDEs and have hypothesized that PDE1B or PDE4 favorably increase activity in D1(+) cells (Nishi et al, 2008; Reed et al, 2002). However, our unpublished data indicate that unlike PDE10A, the basal tone of PDE1B in rodents is minimal such that acute inhibition of PDE1B fails to induce c-Fos in the neostriatum or other forebrain regions.

Although these studies have provided important evidence of apparently distinct basal tone of PDE10A in different brain regions and neuronal subtypes, a key limitation of the studies is that the effects of the PDE10i were assessed in young, healthy rodents. It is possible that in a model of a basal ganglia disorder such as Parkinson's disease, Huntington's disease or schizophrenia, a PDE10i may produce a distinct profile of MSN activation. The dynamic regulation of PDEs is indicated by a recent animal study

showing an increase in PDE10A expression after acute stress and protracted alcohol withdrawal (Logrip & Zorrilla, 2014). In future studies, it is critical to assess the pharmacology of PDE10A and other PDE inhibitors and their interactions in appropriate disease models to elucidate the role of this important family of druggable enzymes. Although definitive clinical implications of PDE10i effects observed in rodents are not fully clear, the profound activation of direct and indirect pathways indicates potential utility of PDE10i in the treatment of Huntington's disease. It remains to be seen whether this profile of MSN activation underlies the reported antipsychotic activity or dystonia-like side-effects of MP-10 in schizophrenic patients (Schmidt, 2012).

Conclusion

In summary, through a combination of pharmacological and genetic tools, we provide convergent evidence of D2 pathway dominant effects of PDE10A inhibition in rodents. These data augment the existing literature implicating the role of PDE10A in regulation of basal ganglia output and provide further insights into functional implications of modulation of PDE10A, an enzyme actively targeted for therapeutic development.

FUTURE DIRECTIONS

The work presented here has added significant understanding toward the characterization of neuroinflammatory cells, like microglia and astrocytes, which cause neuroinflammation during the pathophysiology of PD. Fibrillar α-synuclein initiates classical activation and their pro-inflammatory state, which in turn may affect an inflammatory cascade including astrocyte reactivity and proliferation. This work is foundational to identifying key mechanisms of inflammation during the treatment of α-synuclein. Based on this data, future experiments should block or decrease fibrillar α-synuclein interactions with microglia or astrocytes. Understanding whether fibrils can be blocked by a therapeutic antibody (Masliah et al, 2011) or decrease interaction with a putative receptor (Mao et al, 2016) while testing the resulting modulation of reactivity within glial cell culture would inform further experiments *in vivo* and the future PD therapies.

Neuroinflammatory mechanisms within activated microglia and proliferating astrocytes, in response to α-synuclein is a major pathology in PD. Future work in this area should focus on a viable therapy for both the blocking of α-synuclein aggregation/propagation using antibodies (Wrasidlo et al, 2016) along with the use of inhibitors to neuroinflammatory effects (Barnum et al, 2014) and possibly enhancing the neuroprotective/anti-inflammatory effects (Le et al, 2016). Neuroinflammatory effects of cytokines can be devastating to the surrounding cell population (McCoy et al, 2011). Blocking these cytokines can have attenuating effect of activation of glial cells along

with associated decreasing dopamine cell death (Barnum et al, 2014). The validation and utilization of an *in vitro* propagation neuronal cell assay would be important in addition to antibodies against both α-synuclein and neuroinflammatory cytokines, or addition of anti-inflammatory cytokines. Further *in vitro* experiments modeling α-synuclein propagation in the context of inflammation will help to understand if robust increases of transmission are seen when in the presence of inflammation. Decreasing acute pro-inflammatory cytokines like TNFα during the initial stages of cell-to-cell transfer may help to slow propagation of α-synuclein and possibly decrease neuronal death and patient decline, however later in the disease process when patients are presenting symptoms, only dopamine cell regeneration or other dopamine therapies would help chronic patients.

A prognostic biomarker that measures fast and slow progressors of disease would help to inform the correct individualized therapy for these PD patients. It is unknown whether patients with increased CSF cytokines progress faster than patients with baseline levels of inflammatory markers. Collection and evaluation of CSF constituents should be measured using clinically validated assays. The measurement of a CSF cytokine, like TNFα, would be informative of the pro-inflammatory cytokine levels and possibly the state of neuroinflammation in the brain. When cytokine levels in CSF are understood, correlations to progression of disease of individual patients can be made. If significant statistical correlations are found, the rate of disease progression can be monitored by CSF biopsy and evaluation of cytokine levels.

Another future direction for PD and microglia would involve Trem2 activity. A Trem2 therapy may be of interest for the clearance of Lewy bodies. An agonist of Trem2 has been shown to promote phagocytosis of other misfolded proteins like Aβ plaques (Yeh et al, 2016). Future experiments should study the effects of Trem2 function in PD related models. For instance, internalization of α-synuclein following the modulation of Trem2 levels in microglia would help to understand the role of Trem2 in α-synuclein clearance. Current data show that microglia react to α-synuclein by an increase in phagocytosis action. Both reactions of increased cytokine and uptake when in contact with α-synuclein would be ideal, as long as the process does not chronically ensue, as the duality of mechanisms are initially beneficial for neuronal survival (Barnum & Tansey, 2011). Also, the current data suggest that as the quantity of aggregated α-synuclein increases, cytokines increase. Further experiments should modulate the levels of α-synuclein prior to measuring phagocytosis function *in vitro* to understand the levels of particles that microglia can engulf at steady state. Other future experiments modulating many phagocytosis receptors in microglia will be beneficial toward the understanding of eat-me signaling, the connection to the intracellular inflammasome trigger and function of microglia mediated clearance (Codolo et al, 2013). Although other cell types were not studied in this work, phagocytosis of other cell types should be studied. Astrocytes are phagocytizing cells in non-stimulated resting states (Chung et al, 2013; Yamamoto et al, 2013). Signaling pathways regulating astrocyte uptake such as P2X7, MERTK and MEGF10 signaling receptors should be modulated following aggregated α-synuclein treatments to confirm uptake and understand the role of these receptors.

Since both microglia and astrocytes responded to fibrillar α-synuclein by releasing TNFα, further studies should understand how these cells increase pro-inflammatory state in PD. Learning about the molecules and pathways involved in these glial cells may help to discover brain specific therapies for neuroinflammation. Recently, a brain specific activator of LXRs, a pathway shown to be important for microglia and astrocyte reactivity (Theofilopoulos et al, 2013) may promote midbrain neurogenesis. Although no differential expression of LXRs are seen in post-mortem dementia brains and a related nuclear receptor, RXR seems to increase with other markers of reactive astrocytes (Akram et al, 2010). LXRβ KO mice have defective development of the early midbrain (Sacchetti et al, 2009). Also, treatment of human embryonic stem cells with LXR agonists increased neurogenesis of mature dopamine neurons, and protects dopamine neurons in a mouse model of PD suggesting a novel therapeutic application of LXR ligands in PD (Steffensen et al, 2013). Also, it has been shown in another model of neurodegeneration that nuclear receptor agonists increase tissue repair mechanisms, increase phagocytosis receptors (MERTK, AXL, TREM2) and suppress pro-inflammation (Savage et al, 2015). Based on current data in the P0 GLAST positive cells that show this pathway to be differentially upregulated, it would be of interest to understanding treatment effects of LXR agonists on the proliferation and differentiation in glial cells as well as the effect of this agonist on the pro-inflammatory state of glial cells.

The current data show astrocyte proliferation is mediated by inflammatory signaling pathways and transcriptional activation of known inflammatory genes. Known

inflammation mechanisms have been demonstrated during proliferation stages of astrocyte development, a recapitulation of the mechanisms seen in reactivity and gliosis. This disordered state and feed-forward pathogenic mechanism of inflammatory modulating cells within the basal ganglia of the brain may cause further propagation of PD pathology and dopamine neuron cell death. Genetic validation of astrocyte involvement in PD has come from CLU and SORL1 without any mechanistic evidence (Gao et al, 2011; Sasaki et al, 2002). Grasping a better understanding of genetic markers such as these and many others from the current dataset is key to understanding neuroinflammation in PD. BMP and Notch signaling pathways are highly expressed using genetic techniques and have plenty of mechanistic experimental results, although low levels of astroglial cell type markers like GFAP, vimentin and heat shock protein 27 in PD relative to α-synuclein may indicate a deficient reactivity in this disease (Tong et al, 2015). The current unique dataset of ChIP sequencing and RNA sequencing and future validation can add to the expression pattern changes previously seen in astrocytes. A main question pertaining to SMADs and Notch signaling transcriptional regulation and their potential cross-talk with other known inflammatory signaling factors like JAK/STAT pathways would help to elucidate the neuroinflammatory component seen during proliferation. Also, astrocyte markers at different stages of development and disease are sparse. Validation of radial glia and astrocyte markers in active regions of acetylated H3K9 regions would help to bolster our knowledge of these cells along with ontologies of genes within these regions that are differentially acetylated. It is unknown if there is a motif or promoter region that has been differentially acetylated within these cells.

PDE10A is modulated during the process of PD and affects dopamine signaling pathways, preferentially in D2 expressing neurons in the indirect pathway within the striatum. The current studies characterize and confirm an unbalanced activation of basal ganglia circuitry based on PDE10A inhibition. This circuitry is also affected by PD pathology and results in the overall decrease of motor circuitry. Although information has been elucidated PDE10A biology in the context of PD, further studies can build on this work to better understand PD pathobiology (Niccolini et al, 2015). Assessment of a broader dose regimen of PDE10i and other PDE inhibitors in disease models will help to elucidate the role these enzymes. It is unknown how this inhibitor may affect striatal cell types when PDE10A expression has declined. During the disease state, further expression analysis should be completed to understand if PDE10A decreases preferentially in either D1 expressing cells or D2 expressing cells. Long term experiments determining PDE10i mediated effects on chronic neuronal activation in D1 and D2 dopamine pathways, for instance, would increase our understanding of the activation of cells in the basal ganglia affecting chronic PD patients.

REFERENCES

Adachi T, Takanaga H, Kunimoto M, Asou H (2005) Influence of LIF and BMP-2 on differentiation and development of glial cells in primary cultures of embryonic rat cerebral hemisphere. *Journal of neuroscience research* **79:** 608-615

Ade KK, Wan Y, Chen M, Gloss B, Calakos N (2011) An Improved BAC Transgenic Fluorescent Reporter Line for Sensitive and Specific Identification of Striatonigral Medium Spiny Neurons. *Frontiers in systems neuroscience* **5:** 32

Ahmad M, Attoub S, Singh MN, Martin FL, El-Agnaf OM (2007) Gamma-synuclein and the progression of cancer. *The FASEB journal : official publication of the Federation of American Societies for Experimental Biology* **21:** 3419-3430

Ahn TB, Langston JW, Aachi VR, Dickson DW (2012) Relationship of neighboring tissue and gliosis to alpha-synuclein pathology in a fetal transplant for Parkinson's disease. *American journal of neurodegenerative disease* **1:** 49-59

Akram A, Schmeidler J, Katsel P, Hof PR, Haroutunian V (2010) Increased expression of RXRalpha in dementia: an early harbinger for the cholesterol dyshomeostasis? *Molecular neurodegeneration* **5:** 36

Alim MA, Ma QL, Takeda K, Aizawa T, Matsubara M, Nakamura M, Asada A, Saito T, Kaji H, Yoshii M, Hisanaga S, Ueda K (2004) Demonstration of a role for alpha-synuclein as a functional microtubule-associated protein. *Journal of Alzheimer's disease : JAD* **6:** 435-442; discussion 443-439

Allfrey VG, Faulkner R, Mirsky AE (1964) Acetylation and Methylation of Histones and Their Possible Role in the Regulation of Rna Synthesis. *Proceedings of the National Academy of Sciences of the United States of America* **51:** 786-794

Annunziato AT, Eason MB, Perry CA (1995) Relationship between methylation and acetylation of arginine-rich histones in cycling and arrested HeLa cells. *Biochemistry* **34:** 2916-2924

Asano H, Aonuma M, Sanosaka T, Kohyama J, Namihira M, Nakashima K (2009) Astrocyte differentiation of neural precursor cells is enhanced by retinoic acid through a change in epigenetic modification. *Stem Cells* **27:** 2744-2752

Ayoub AE, Oh S, Xie Y, Leng J, Cotney J, Dominguez MH, Noonan JP, Rakic P (2011) Transcriptional programs in transient embryonic zones of the cerebral cortex defined by high-resolution mRNA sequencing. *Proceedings of the National Academy of Sciences of the United States of America* **108:** 14950-14955

Bandeira F, Lent R, Herculano-Houzel S (2009) Changing numbers of neuronal and non-neuronal cells underlie postnatal brain growth in the rat. *Proceedings of the National Academy of Sciences of the United States of America* **106:** 14108-14113

Barnabe-Heider F, Wasylnka JA, Fernandes KJ, Porsche C, Sendtner M, Kaplan DR, Miller FD (2005) Evidence that embryonic neurons regulate the onset of cortical gliogenesis via cardiotrophin-1. *Neuron* **48:** 253-265

Barnum CJ, Chen X, Chung J, Chang J, Williams M, Grigoryan N, Tesi RJ, Tansey MG (2014) Peripheral administration of the selective inhibitor of soluble tumor necrosis factor (TNF) XPro(R)1595 attenuates nigral cell loss and glial activation in 6-OHDA hemiparkinsonian rats. *Journal of Parkinson's disease* **4:** 349-360

Barnum CJ, Tansey MG (2011) The duality of TNF signaling outcomes in the brain: potential mechanisms? *Experimental neurology* **229:** 198-200

Baroncini M, Allet C, Leroy D, Beauvillain JC, Francke JP, Prevot V (2007) Morphological evidence for direct interaction between gonadotrophin-releasing hormone neurones and astroglial cells in the human hypothalamus. *Journal of neuroendocrinology* **19:** 691-702

Barrett PJ, Timothy Greenamyre J (2015) Post-translational modification of alpha-synuclein in Parkinson's disease. *Brain Res* **1628:** 247-253

Bartels AL, Leenders KL (2007) Neuroinflammation in the pathophysiology of Parkinson's disease: evidence from animal models to human in vivo studies with [11C]-PK11195 PET. *Movement disorders : official journal of the Movement Disorder Society* **22:** 1852-1856

Beckervordersandforth R, Tripathi P, Ninkovic J, Bayam E, Lepier A, Stempfhuber B, Kirchhoff F, Hirrlinger J, Haslinger A, Lie DC, Beckers J, Yoder B, Irmler M, Gotz M (2010) In vivo fate mapping and expression analysis reveals molecular hallmarks of prospectively isolated adult neural stem cells. *Cell stem cell* **7:** 744-758

Ben Haim L, Ceyzeriat K, Carrillo-de Sauvage MA, Aubry F, Auregan G, Guillermier M, Ruiz M, Petit F, Houitte D, Faivre E, Vandesquille M, Aron-Badin R, Dhenain M, Deglon N, Hantraye P, Brouillet E, Bonvento G, Escartin C (2015) The JAK/STAT3 pathway is a common inducer of astrocyte reactivity in Alzheimer's and Huntington's diseases. *The Journal of neuroscience : the official journal of the Society for Neuroscience* **35:** 2817-2829

Bengoechea-Alonso MT, Ericsson J (2016) The phosphorylation-dependent regulation of nuclear SREBP1 during mitosis links lipid metabolism and cell growth. *Cell Cycle* **15:** 2753-2765

Benjamini Y, Hochberg Y (1995) Controlling the False Discovery Rate: A Practical and Powerful Approach to Multiple Testing. *J R Stat Soc B* **57:** 289-300

Beraud D, Hathaway HA, Trecki J, Chasovskikh S, Johnson DA, Johnson JA, Federoff HJ, Shimoji M, Mhyre TR, Maguire-Zeiss KA (2013) Microglial activation and antioxidant responses induced by the Parkinson's disease protein alpha-synuclein. *Journal of neuroimmune pharmacology : the official journal of the Society on NeuroImmune Pharmacology* **8:** 94-117

Beraud D, Twomey M, Bloom B, Mittereder A, Ton V, Neitzke K, Chasovskikh S, Mhyre TR, Maguire-Zeiss KA (2011) alpha-Synuclein Alters Toll-Like Receptor Expression. *Frontiers in neuroscience* **5:** 80

Blasi E, Barluzzi R, Bocchini V, Mazzolla R, Bistoni F (1990) Immortalization of murine microglial cells by a v-raf/v-myc carrying retrovirus. *Journal of neuroimmunology* **27:** 229-237

Bollen E, Prickaerts J (2012) Phosphodiesterases in neurodegenerative disorders. *IUBMB life* **64:** 965-970

Bourne TD, Elias WJ, Lopes MB, Mandell JW (2010) WT1 is not a reliable marker to distinguish reactive from neoplastic astrocyte populations in the central nervous system. *Brain Pathol* **20:** 1090-1095

Boza-Serrano A, Reyes JF, Rey NL, Leffler H, Bousset L, Nilsson U, Brundin P, Venero JL, Burguillos MA, Deierborg T (2014) The role of Galectin-3 in alpha-synuclein-induced microglial activation. *Acta neuropathologica communications* **2:** 156

Braak H, Del Tredici K, Rub U, de Vos RA, Jansen Steur EN, Braak E (2003) Staging of brain pathology related to sporadic Parkinson's disease. *Neurobiology of aging* **24:** 197-211

Braidy N, Gai WP, Xu YH, Sachdev P, Guillemin GJ, Jiang XM, Ballard JW, Horan MP, Fang ZM, Chong BH, Chan DK (2013) Uptake and mitochondrial dysfunction of alpha-synuclein in human astrocytes, cortical neurons and fibroblasts. *Translational neurodegeneration* **2:** 20

Breese MR, Liu Y (2013) NGSUtils: a software suite for analyzing and manipulating next-generation sequencing datasets. *Bioinformatics* **29:** 494-496

Briona LK, Poulain FE, Mosimann C, Dorsky RI (2015) Wnt/ss-catenin signaling is required for radial glial neurogenesis following spinal cord injury. *Developmental biology* **403:** 15-21

Brooks DJ (2005) Positron emission tomography and single-photon emission computed tomography in central nervous system drug development. *NeuroRx : the journal of the American Society for Experimental NeuroTherapeutics* **2:** 226-236

Bruck D, Wenning GK, Stefanova N, Fellner L (2016) Glia and alpha-synuclein in neurodegeneration: A complex interaction. *Neurobiol Dis* **85:** 262-274

Brunne B, Franco S, Bouche E, Herz J, Howell BW, Pahle J, Muller U, May P, Frotscher M, Bock HH (2013) Role of the postnatal radial glial scaffold for the development of the dentate gyrus as revealed by Reelin signaling mutant mice. *Glia* **61:** 1347-1363

Cahoy JD, Emery B, Kaushal A, Foo LC, Zamanian JL, Christopherson KS, Xing Y, Lubischer JL, Krieg PA, Krupenko SA, Thompson WJ, Barres BA (2008) A transcriptome database for astrocytes, neurons, and oligodendrocytes: a new resource for understanding brain development and function. *The Journal of neuroscience : the official journal of the Society for Neuroscience* **28:** 264-278

Cammer W, Zhang H (1992) Carbonic anhydrase in distinct precursors of astrocytes and oligodendrocytes in the forebrains of neonatal and young rats. *Brain research Developmental brain research* **67:** 257-263

Campioni S, Mannini B, Zampagni M, Pensalfini A, Parrini C, Evangelisti E, Relini A, Stefani M, Dobson CM, Cecchi C, Chiti F (2010) A causative link between the structure of aberrant protein oligomers and their toxicity. *Nature chemical biology* **6:** 140-147

Carrero I, Gonzalo MR, Martin B, Sanz-Anquela JM, Arevalo-Serrano J, Gonzalo-Ruiz A (2012) Oligomers of beta-amyloid protein (Abeta1-42) induce the activation of cyclooxygenase-2 in astrocytes via an interaction with interleukin-1beta, tumour necrosis factor-alpha, and a nuclear factor kappa-B mechanism in the rat brain. *Experimental neurology* **236:** 215-227

Chambel SS, Santos-Goncalves A, Duarte TL (2015) The Dual Role of Nrf2 in Nonalcoholic Fatty Liver Disease: Regulation of Antioxidant Defenses and Hepatic Lipid Metabolism. *BioMed research international* **2015:** 597134

Chaudhry FA, Lehre KP, van Lookeren Campagne M, Ottersen OP, Danbolt NC, Storm-Mathisen J (1995) Glutamate transporters in glial plasma membranes: highly differentiated localizations revealed by quantitative ultrastructural immunocytochemistry. *Neuron* **15:** 711-720

Chen S, Hillman DE (1994) Immunohistochemical localization of protein kinase C delta during postnatal development of the cerebellum. *Brain research Developmental brain research* **80:** 19-25

Chen SW, Drakulic S, Deas E, Ouberai M, Aprile FA, Arranz R, Ness S, Roodveldt C, Guilliams T, De-Genst EJ, Klenerman D, Wood NW, Knowles TP, Alfonso C, Rivas G, Abramov AY, Valpuesta JM, Dobson CM, Cremades N (2015) Structural characterization of toxic oligomers that are kinetically trapped during alpha-synuclein fibril formation. *Proceedings of the National Academy of Sciences of the United States of America* **112:** E1994-2003

Cheng P, Alberts I, Li X (2013) The role of ERK1/2 in the regulation of proliferation and differentiation of astrocytes in developing brain. *International journal of developmental neuroscience : the official journal of the International Society for Developmental Neuroscience* **31:** 783-789

Cheng PY, Lin YP, Chen YL, Lee YC, Tai CC, Wang YT, Chen YJ, Kao CF, Yu J (2011) Interplay between SIN3A and STAT3 mediates chromatin conformational changes and GFAP expression during cellular differentiation. *PLoS One* **6:** e22018

Cho B, Kim HJ, Kim H, Sun W (2011) Changes in the Histone Acetylation Patterns during the Development of the Nervous System. *Experimental neurobiology* **20:** 81-84

Chung WS, Clarke LE, Wang GX, Stafford BK, Sher A, Chakraborty C, Joung J, Foo LC, Thompson A, Chen C, Smith SJ, Barres BA (2013) Astrocytes mediate synapse elimination through MEGF10 and MERTK pathways. *Nature* **504:** 394-400

Cimini A, Ceru MP (2008) Emerging roles of peroxisome proliferator-activated receptors (PPARs) in the regulation of neural stem cells proliferation and differentiation. *Stem cell reviews* **4:** 293-303

Codolo G, Plotegher N, Pozzobon T, Brucale M, Tessari I, Bubacco L, de Bernard M (2013) Triggering of inflammasome by aggregated alpha-synuclein, an inflammatory response in synucleinopathies. *PLoS One* **8:** e55375

Cole NB, Murphy DD, Lebowitz J, Di Noto L, Levine RL, Nussbaum RL (2005) Metal-catalyzed oxidation of alpha-synuclein: helping to define the relationship between oligomers, protofibrils, and filaments. *The Journal of biological chemistry* **280:** 9678-9690

Colonna M, Wang Y (2016) TREM2 variants: new keys to decipher Alzheimer disease pathogenesis. *Nature reviews Neuroscience* **17:** 201-207

Conway KA, Lee SJ, Rochet JC, Ding TT, Williamson RE, Lansbury PT, Jr. (2000) Acceleration of oligomerization, not fibrillization, is a shared property of both alpha-synuclein mutations linked to early-onset Parkinson's disease: implications for pathogenesis and therapy. *Proceedings of the National Academy of Sciences of the United States of America* **97:** 571-576

Conway KA, Rochet JC, Bieganski RM, Lansbury PT, Jr. (2001) Kinetic stabilization of the alpha-synuclein protofibril by a dopamine-alpha-synuclein adduct. *Science* **294:** 1346-1349

Cookson MR, Hardy J, Lewis PA (2008) Genetic neuropathology of Parkinson's disease. *International journal of clinical and experimental pathology* **1:** 217-231

Cremades N, Cohen SI, Deas E, Abramov AY, Chen AY, Orte A, Sandal M, Clarke RW, Dunne P, Aprile FA, Bertoncini CW, Wood NW, Knowles TP, Dobson CM, Klenerman D (2012) Direct observation of the interconversion of normal and toxic forms of alpha-synuclein. *Cell* **149:** 1048-1059

Croisier E, Graeber MB (2006) Glial degeneration and reactive gliosis in alpha-synucleinopathies: the emerging concept of primary gliodegeneration. *Acta neuropathologica* **112:** 517-530

Cyster JG, Dang EV, Reboldi A, Yi T (2014) 25-Hydroxycholesterols in innate and adaptive immunity. *Nature reviews Immunology* **14:** 731-743

Damier P, Hirsch EC, Agid Y, Graybiel AM (1999) The substantia nigra of the human brain. II. Patterns of loss of dopamine-containing neurons in Parkinson's disease. *Brain : a journal of neurology* **122 (Pt 8):** 1437-1448

Daniele SG, Beraud D, Davenport C, Cheng K, Yin H, Maguire-Zeiss KA (2015) Activation of MyD88-dependent TLR1/2 signaling by misfolded alpha-synuclein, a protein linked to neurodegenerative disorders. *Science signaling* **8:** ra45

Dauer W, Przedborski S (2003) Parkinson's disease: mechanisms and models. *Neuron* **39:** 889-909

Day M, Wokosin D, Plotkin JL, Tian X, Surmeier DJ (2008) Differential excitability and modulation of striatal medium spiny neuron dendrites. *The Journal of neuroscience : the official journal of the Society for Neuroscience* **28:** 11603-11614

de Chevigny A, Cooper O, Vinuela A, Reske-Nielsen C, Lagace DC, Eisch AJ, Isacson O (2008) Fate mapping and lineage analyses demonstrate the production of a large number of striatal neuroblasts after transforming growth factor alpha and noggin striatal infusions into the dopamine-depleted striatum. *Stem Cells* **26:** 2349-2360

Dehay B, Bourdenx M, Gorry P, Przedborski S, Vila M, Hunot S, Singleton A, Olanow CW, Merchant KM, Bezard E, Petsko GA, Meissner WG (2015) Targeting alpha-synuclein for treatment of Parkinson's disease: mechanistic and therapeutic considerations. *Lancet neurology* **14:** 855-866

Deneen B, Ho R, Lukaszewicz A, Hochstim CJ, Gronostajski RM, Anderson DJ (2006) The transcription factor NFIA controls the onset of gliogenesis in the developing spinal cord. *Neuron* **52:** 953-968

Dennis G, Jr., Sherman BT, Hosack DA, Yang J, Gao W, Lane HC, Lempicki RA (2003) DAVID: Database for Annotation, Visualization, and Integrated Discovery. *Genome biology* **4:** P3

Dexter DT, Jenner P (2013) Parkinson disease: from pathology to molecular disease mechanisms. *Free radical biology & medicine* **62:** 132-144

Ding W, Ding LJ, Li FF, Han Y, Mu L (2015) Neurodegeneration and cognition in Parkinson's disease: a review. *European review for medical and pharmacological sciences* **19:** 2275-2281

Dixon JE, Allegrucci C, Redwood C, Kump K, Bian Y, Chatfield J, Chen YH, Sottile V, Voss SR, Alberio R, Johnson AD (2010) Axolotl Nanog activity in mouse embryonic stem cells demonstrates that ground state pluripotency is conserved from urodele amphibians to mammals. *Development* **137:** 2973-2980

Dragunow M, Faull R (1989) The use of c-fos as a metabolic marker in neuronal pathway tracing. *Journal of neuroscience methods* **29:** 261-265

Duan Z, Ma C, Han Y, Li Y, Zhou H (2013) Nanog attenuates lipopolysaccharide-induced inflammatory responses by blocking nuclear factor-kappaB transcriptional activity in BV-2 cells. *Neuroreport* **24:** 718-723

Ehringer H, Hornykiewicz O (1960) [Distribution of noradrenaline and dopamine (3-hydroxytyramine) in the human brain and their behavior in diseases of the extrapyramidal system]. *Klinische Wochenschrift* **38:** 1236-1239

Eraso-Pichot A, Larramona-Arcas R, Vicario-Orri E, Villalonga R, Pardo L, Galea E, Masgrau R (2016) CREB decreases astrocytic excitability by modifying subcellular calcium fluxes via the sigma-1 receptor. *Cellular and molecular life sciences : CMLS*

Fan G, Martinowich K, Chin MH, He F, Fouse SD, Hutnick L, Hattori D, Ge W, Shen Y, Wu H, ten Hoeve J, Shuai K, Sun YE (2005) DNA methylation controls the timing of astrogliogenesis through regulation of JAK-STAT signaling. *Development* **132:** 3345-3356

Fang Z, Cui X (2011) Design and validation issues in RNA-seq experiments. *Briefings in bioinformatics* **12:** 280-287

Fellner L, Irschick R, Schanda K, Reindl M, Klimaschewski L, Poewe W, Wenning GK, Stefanova N (2013) Toll-like receptor 4 is required for alpha-synuclein dependent activation of microglia and astroglia. *Glia* **61:** 349-360

Fujishige K, Kotera J, Omori K (1999) Striatum- and testis-specific phosphodiesterase PDE10A isolation and characterization of a rat PDE10A. *European journal of biochemistry / FEBS* **266:** 1118-1127

Fujita M, Sekigawa A, Sekiyama K, Takamatsu Y, Hashimoto M (2012) Possible Alterations in beta-Synuclein, the Non-Amyloidogenic Homologue of alpha-Synuclein, during Progression of Sporadic alpha-Synucleinopathies. *International journal of molecular sciences* **13:** 11584-11592

Furey TS (2012) ChIP-seq and beyond: new and improved methodologies to detect and characterize protein-DNA interactions. *Nature reviews Genetics* **13:** 840-852

Gadient RA, Otten UH (1997) Interleukin-6 (IL-6)--a molecule with both beneficial and destructive potentials. *Progress in neurobiology* **52:** 379-390

Galvagnion C, Buell AK, Meisl G, Michaels TC, Vendruscolo M, Knowles TP, Dobson CM (2015) Lipid vesicles trigger alpha-synuclein aggregation by stimulating primary nucleation. *Nature chemical biology* **11:** 229-234

Gan L, Vargas MR, Johnson DA, Johnson JA (2012) Astrocyte-specific overexpression of Nrf2 delays motor pathology and synuclein aggregation throughout the CNS in the alpha-synuclein mutant (A53T) mouse model. *The Journal of neuroscience : the official journal of the Society for Neuroscience* **32:** 17775-17787

Gan Q, Lee A, Suzuki R, Yamagami T, Stokes A, Nguyen BC, Pleasure D, Wang J, Chen HW, Zhou CJ (2014) Pax6 mediates ss-catenin signaling for self-renewal and neurogenesis by neocortical radial glial stem cells. *Stem Cells* **32:** 45-58

Gao HM, Hong JS (2011) Gene-environment interactions: key to unraveling the mystery of Parkinson's disease. *Progress in neurobiology* **94:** 1-19

Gao HM, Kotzbauer PT, Uryu K, Leight S, Trojanowski JQ, Lee VM (2008) Neuroinflammation and oxidation/nitration of alpha-synuclein linked to dopaminergic neurodegeneration. *The Journal of neuroscience : the official journal of the Society for Neuroscience* **28:** 7687-7698

Gao J, Huang X, Park Y, Hollenbeck A, Chen H (2011) An exploratory study on CLU, CR1 and PICALM and Parkinson disease. *PLoS One* **6:** e24211

Gao J, Ruan H, Qi X, Tao Y, Guo X, Shen W (2016) HDAC3 But not HDAC2 Mediates Visual Experience-Dependent Radial Glia Proliferation in the Developing Xenopus Tectum. *Frontiers in cellular neuroscience* **10:** 221

Gardet A, Benita Y, Li C, Sands BE, Ballester I, Stevens C, Korzenik JR, Rioux JD, Daly MJ, Xavier RJ, Podolsky DK (2010) LRRK2 is involved in the IFN-gamma response and host response to pathogens. *J Immunol* **185:** 5577-5585

Ge W, Martinowich K, Wu X, He F, Miyamoto A, Fan G, Weinmaster G, Sun YE (2002) Notch signaling promotes astrogliogenesis via direct CSL-mediated glial gene activation. *Journal of neuroscience research* **69:** 848-860

Ge WP, Jia JM (2016) Local production of astrocytes in the cerebral cortex. *Neuroscience* **323:** 3-9

Ge WP, Miyawaki A, Gage FH, Jan YN, Jan LY (2012) Local generation of glia is a major astrocyte source in postnatal cortex. *Nature* **484:** 376-380

Gentzel RC, Toolan D, Roberts R, Koser AJ, Kandebo M, Hershey J, Renger JJ, Uslaner J, Smith SM (2015) The PDE10A inhibitor MP-10 and haloperidol produce distinct gene expression profiles in the striatum and influence cataleptic behavior in rodents. *Neuropharmacology* **99:** 256-263

Gerfen CR (1992) The neostriatal mosaic: multiple levels of compartmental organization. *Journal of neural transmission Supplementum* **36:** 43-59

Gerhard A, Pavese N, Hotton G, Turkheimer F, Es M, Hammers A, Eggert K, Oertel W, Banati RB, Brooks DJ (2006) In vivo imaging of microglial activation with [11C](R)-PK11195 PET in idiopathic Parkinson's disease. *Neurobiol Dis* **21:** 404-412

Gilgun-Sherki Y, Djaldetti R, Melamed E, Offen D (2004) Polymorphism in candidate genes: implications for the risk and treatment of idiopathic Parkinson's disease. *The pharmacogenomics journal* **4:** 291-306

Glass CK, Ogawa S (2006) Combinatorial roles of nuclear receptors in inflammation and immunity. *Nature reviews Immunology* **6:** 44-55

Gomez-Lopez S, Wiskow O, Favaro R, Nicolis SK, Price DJ, Pollard SM, Smith A (2011) Sox2 and Pax6 maintain the proliferative and developmental potential of gliogenic neural stem cells In vitro. *Glia* **59:** 1588-1599

Goritz C, Mauch DH, Nagler K, Pfrieger FW (2002) Role of glia-derived cholesterol in synaptogenesis: new revelations in the synapse-glia affair. *Journal of physiology, Paris* **96:** 257-263

Goritz C, Mauch DH, Pfrieger FW (2005) Multiple mechanisms mediate cholesterol-induced synaptogenesis in a CNS neuron. *Mol Cell Neurosci* **29:** 190-201

Gotz M, Sirko S, Beckers J, Irmler M (2015) Reactive astrocytes as neural stem or progenitor cells: In vivo lineage, In vitro potential, and Genome-wide expression analysis. *Glia* **63:** 1452-1468

Grauer SM, Pulito VL, Navarra RL, Kelly MP, Kelley C, Graf R, Langen B, Logue S, Brennan J, Jiang L, Charych E, Egerland U, Liu F, Marquis KL, Malamas M, Hage T, Comery TA, Brandon NJ (2009) Phosphodiesterase 10A inhibitor activity in preclinical models of the positive, cognitive, and negative symptoms of schizophrenia. *The Journal of pharmacology and experimental therapeutics* **331:** 574-590

Gregg C, Weiss S (2005) CNTF/LIF/gp130 receptor complex signaling maintains a VZ precursor differentiation gradient in the developing ventral forebrain. *Development* **132:** 565-578

Gu J, Ni Y, Xu L, Xu H, Cai Z (2016) Nanog interact with CDK6 to regulates astrocyte cells proliferation following spinal cord injury. *Biochemical and biophysical research communications* **469:** 1097-1103

Gu XL, Long CX, Sun L, Xie C, Lin X, Cai H (2010) Astrocytic expression of Parkinson's disease-related A53T alpha-synuclein causes neurodegeneration in mice. *Molecular brain* **3:** 12

Guenther MG, Levine SS, Boyer LA, Jaenisch R, Young RA (2007) A chromatin landmark and transcription initiation at most promoters in human cells. *Cell* **130:** 77-88

Guo F, Ma J, McCauley E, Bannerman P, Pleasure D (2009) Early postnatal proteolipid promoter-expressing progenitors produce multilineage cells in vivo. *The Journal of neuroscience : the official journal of the Society for Neuroscience* **29:** 7256-7270

Guo JL, Lee VM (2011) Seeding of normal Tau by pathological Tau conformers drives pathogenesis of Alzheimer-like tangles. *The Journal of biological chemistry* **286:** 15317-15331

Halassa MM, Fellin T, Haydon PG (2007) The tripartite synapse: roles for gliotransmission in health and disease. *Trends in molecular medicine* **13:** 54-63

Hallett PJ, Standaert DG (2004) Rationale for and use of NMDA receptor antagonists in Parkinson's disease. *Pharmacology & therapeutics* **102:** 155-174

Halliday GM, McCann H (2010) The progression of pathology in Parkinson's disease. *Annals of the New York Academy of Sciences* **1184:** 188-195

Hashimoto M, Kawahara K, Bar-On P, Rockenstein E, Crews L, Masliah E (2004) The Role of alpha-synuclein assembly and metabolism in the pathogenesis of Lewy body disease. *Journal of molecular neuroscience : MN* **24:** 343-352

Hashimoto M, Kobayashi K, Yamazaki M, Kazuki Y, Takehara S, Oshimura M, Chiba K (2016) Cyp3a deficiency enhances androgen receptor activity and cholesterol synthesis in the mouse prostate. *The Journal of steroid biochemistry and molecular biology* **163:** 121-128

Hebbes TR, Thorne AW, Crane-Robinson C (1988) A direct link between core histone acetylation and transcriptionally active chromatin. *The EMBO journal* **7:** 1395-1402

Heiman M, Schaefer A, Gong S, Peterson JD, Day M, Ramsey KE, Suarez-Farinas M, Schwarz C, Stephan DA, Surmeier DJ, Greengard P, Heintz N (2008) A translational profiling approach for the molecular characterization of CNS cell types. *Cell* **135:** 738-748

Helin K (1998) Regulation of cell proliferation by the E2F transcription factors. *Current opinion in genetics & development* **8:** 28-35

Hermanson O, Jepsen K, Rosenfeld MG (2002) N-CoR controls differentiation of neural stem cells into astrocytes. *Nature* **419:** 934-939

Hindle JV (2010) Ageing, neurodegeneration and Parkinson's disease. *Age and ageing* **39:** 156-161

Hirano T, Ishihara K, Hibi M (2000) Roles of STAT3 in mediating the cell growth, differentiation and survival signals relayed through the IL-6 family of cytokine receptors. *Oncogene* **19:** 2548-2556

Hirsch E, Graybiel AM, Agid YA (1988) Melanized dopaminergic neurons are differentially susceptible to degeneration in Parkinson's disease. *Nature* **334:** 345-348

Hishikawa N, Hashizume Y, Yoshida M, Niwa J, Tanaka F, Sobue G (2005) Tuft-shaped astrocytes in Lewy body disease. *Acta neuropathologica* **109:** 373-380

Hoenen C, Gustin A, Birck C, Kirchmeyer M, Beaume N, Felten P, Grandbarbe L, Heuschling P, Heurtaux T (2016) Alpha-Synuclein Proteins Promote Pro-Inflammatory Cascades in Microglia: Stronger Effects of the A53T Mutant. *PLoS One* **11:** e0162717

Hokenson MJ, Uversky VN, Goers J, Yamin G, Munishkina LA, Fink AL (2004) Role of individual methionines in the fibrillation of methionine-oxidized alpha-synuclein. *Biochemistry* **43:** 4621-4633

Hong S, Song MR (2014) STAT3 but not STAT1 is required for astrocyte differentiation. *PLoS One* **9:** e86851

Hostenbach S, D'Haeseleer M, Kooijman R, De Keyser J (2016) The pathophysiological role of astrocytic endothelin-1. *Progress in neurobiology* **144:** 88-102

Hsiao HY, Chen YC, Chen HM, Tu PH, Chern Y (2013) A critical role of astrocyte-mediated nuclear factor-kappaB-dependent inflammation in Huntington's disease. *Human molecular genetics* **22:** 1826-1842

Hsu LJ, Sagara Y, Arroyo A, Rockenstein E, Sisk A, Mallory M, Wong J, Takenouchi T, Hashimoto M, Masliah E (2000) alpha-synuclein promotes mitochondrial deficit and oxidative stress. *The American journal of pathology* **157:** 401-410

Imayoshi I, Kageyama R (2014) bHLH factors in self-renewal, multipotency, and fate choice of neural progenitor cells. *Neuron* **82:** 9-23

Ishimoto K, Tachibana K, Hanano I, Yamasaki D, Nakamura H, Kawai M, Urano Y, Tanaka T, Hamakubo T, Sakai J, Kodama T, Doi T (2010) Sterol-regulatory-element-binding protein 2 and nuclear factor Y control human farnesyl diphosphate synthase expression and affect cell proliferation in hepatoblastoma cells. *The Biochemical journal* **429:** 347-357

Islam O, Gong X, Rose-John S, Heese K (2009) Interleukin-6 and neural stem cells: more than gliogenesis. *Molecular biology of the cell* **20:** 188-199

Ito D, Imai Y, Ohsawa K, Nakajima K, Fukuuchi Y, Kohsaka S (1998) Microglia-specific localisation of a novel calcium binding protein, Iba1. *Brain research Molecular brain research* **57:** 1-9

Iwai A, Masliah E, Yoshimoto M, Ge N, Flanagan L, de Silva HA, Kittel A, Saitoh T (1995) The precursor protein of non-A beta component of Alzheimer's disease amyloid is a presynaptic protein of the central nervous system. *Neuron* **14:** 467-475

Jakes R, Spillantini MG, Goedert M (1994) Identification of two distinct synucleins from human brain. *FEBS letters* **345:** 27-32

Jo S, Yarishkin O, Hwang YJ, Chun YE, Park M, Woo DH, Bae JY, Kim T, Lee J, Chun H, Park HJ, Lee DY, Hong J, Kim HY, Oh SJ, Park SJ, Lee H, Yoon BE, Kim Y, Jeong Y, Shim I, Bae YC, Cho J, Kowall NW, Ryu H, Hwang E, Kim D, Lee CJ (2014) GABA from reactive astrocytes impairs memory in mouse models of Alzheimer's disease. *Nature medicine* **20:** 886-896

Johnson MB, Wang PP, Atabay KD, Murphy EA, Doan RN, Hecht JL, Walsh CA (2015) Single-cell analysis reveals transcriptional heterogeneity of neural progenitors in human cortex. *Nature neuroscience* **18:** 637-646

Joo SH, Kwon KJ, Kim JW, Hasan MR, Lee HJ, Han SH, Shin CY (2010) Regulation of matrix metalloproteinase-9 and tissue plasminogen activator activity by alpha-synuclein in rat primary glial cells. *Neuroscience letters* **469:** 352-356

Juan L, Wang G, Radovich M, Schneider BP, Clare SE, Wang Y, Liu Y (2013) Potential roles of microRNAs in regulating long intergenic noncoding RNAs. *BMC medical genomics* **6 Suppl 1:** S7

Jungblut M, Tiveron MC, Barral S, Abrahamsen B, Knobel S, Pennartz S, Schmitz J, Perraut M, Pfrieger FW, Stoffel W, Cremer H, Bosio A (2012) Isolation and characterization of living primary astroglial cells using the new GLAST-specific monoclonal antibody ACSA-1. *Glia* **60:** 894-907

Kapur S, Mamo D (2003) Half a century of antipsychotics and still a central role for dopamine D2 receptors. *Progress in neuro-psychopharmacology & biological psychiatry* **27:** 1081-1090

Kemp JM, Powell TP (1971) The structure of the caudate nucleus of the cat: light and electron microscopy. *Philosophical transactions of the Royal Society of London Series B, Biological sciences* **262:** 383-401

Kettenmann H, Kirchhoff F, Verkhratsky A (2013) Microglia: new roles for the synaptic stripper. *Neuron* **77:** 10-18

Khakh BS, Sofroniew MV (2015) Diversity of astrocyte functions and phenotypes in neural circuits. *Nature neuroscience* **18:** 942-952

Kierdorf K, Prinz M (2013) Factors regulating microglia activation. *Frontiers in cellular neuroscience* **7:** 44

Kim C, Ho DH, Suk JE, You S, Michael S, Kang J, Joong Lee S, Masliah E, Hwang D, Lee HJ, Lee SJ (2013) Neuron-released oligomeric alpha-synuclein is an endogenous agonist of TLR2 for paracrine activation of microglia. *Nature communications* **4:** 1562

Kim KH, Lee GY, Kim JI, Ham M, Won Lee J, Kim JB (2010) Inhibitory effect of LXR activation on cell proliferation and cell cycle progression through lipogenic activity. *Journal of lipid research* **51:** 3425-3433

Klegeris A, Giasson BI, Zhang H, Maguire J, Pelech S, McGeer PL (2006) Alpha-synuclein and its disease-causing mutants induce ICAM-1 and IL-6 in human astrocytes and astrocytoma cells. *The FASEB journal : official publication of the Federation of American Societies for Experimental Biology* **20:** 2000-2008

Klegeris A, McGeer EG, McGeer PL (2007) Therapeutic approaches to inflammation in neurodegenerative disease. *Current opinion in neurology* **20:** 351-357

Kleiman RJ, Kimmel LH, Bove SE, Lanz TA, Harms JF, Romegialli A, Miller KS, Willis A, des Etages S, Kuhn M, Schmidt CJ (2011) Chronic suppression of phosphodiesterase 10A alters striatal expression of genes responsible for neurotransmitter synthesis, neurotransmission, and signaling pathways implicated in Huntington's disease. *The Journal of pharmacology and experimental therapeutics* **336:** 64-76

Klein C, Ziegler A (2011) From GWAS to clinical utility in Parkinson's disease. *Lancet* **377:** 613-614

Koob AO, Paulino AD, Masliah E (2010) GFAP reactivity, apolipoprotein E redistribution and cholesterol reduction in human astrocytes treated with alpha-synuclein. *Neuroscience letters* **469:** 11-14

Kouzarides T (2007) Chromatin modifications and their function. *Cell* **128:** 693-705

Kowal SL, Dall TM, Chakrabarti R, Storm MV, Jain A (2013) The current and projected economic burden of Parkinson's disease in the United States. *Movement disorders : official journal of the Movement Disorder Society* **28:** 311-318

Kramer ML, Schulz-Schaeffer WJ (2007) Presynaptic alpha-synuclein aggregates, not Lewy bodies, cause neurodegeneration in dementia with Lewy bodies. *The Journal of neuroscience : the official journal of the Society for Neuroscience* **27:** 1405-1410

Labhart P, Karmakar S, Salicru EM, Egan BS, Alexiadis V, O'Malley BW, Smith CL (2005) Identification of target genes in breast cancer cells directly regulated by the SRC-3/AIB1 coactivator. *Proceedings of the National Academy of Sciences of the United States of America* **102:** 1339-1344

Laflamme N, Soucy G, Rivest S (2001) Circulating cell wall components derived from gram-negative, not gram-positive, bacteria cause a profound induction of the gene-encoding Toll-like receptor 2 in the CNS. *Journal of neurochemistry* **79:** 648-657

Lai JJ, Lai KP, Zeng W, Chuang KH, Altuwaijri S, Chang C (2012) Androgen receptor influences on body defense system via modulation of innate and adaptive immune systems: lessons from conditional AR knockout mice. *The American journal of pathology* **181:** 1504-1512

Lashuel HA, Overk CR, Oueslati A, Masliah E (2013) The many faces of alpha-synuclein: from structure and toxicity to therapeutic target. *Nature reviews Neuroscience* **14:** 38-48

Le W, Wu J, Tang Y (2016) Protective Microglia and Their Regulation in Parkinson's Disease. *Frontiers in molecular neuroscience* **9:** 89

Lee EJ, Woo MS, Moon PG, Baek MC, Choi IY, Kim WK, Junn E, Kim HS (2010a) Alpha-synuclein activates microglia by inducing the expressions of matrix metalloproteinases and the subsequent activation of protease-activated receptor-1. *J Immunol* **185:** 615-623

Lee HJ, Bae EJ, Lee SJ (2014) Extracellular alpha--synuclein-a novel and crucial factor in Lewy body diseases. *Nature reviews Neurology* **10:** 92-98

Lee HJ, Dreyfus C, DiCicco-Bloom E (2016) Valproic acid stimulates proliferation of glial precursors during cortical gliogenesis in developing rat. *Developmental neurobiology* **76:** 780-798

Lee HJ, Kim C, Lee SJ (2010b) Alpha-synuclein stimulation of astrocytes: Potential role for neuroinflammation and neuroprotection. *Oxidative medicine and cellular longevity* **3:** 283-287

Lee HJ, Suk JE, Patrick C, Bae EJ, Cho JH, Rho S, Hwang D, Masliah E, Lee SJ (2010c) Direct transfer of alpha-synuclein from neuron to astroglia causes inflammatory responses in synucleinopathies. *The Journal of biological chemistry* **285:** 9262-9272

Lehre KP, Levy LM, Ottersen OP, Storm-Mathisen J, Danbolt NC (1995) Differential expression of two glial glutamate transporters in the rat brain: quantitative and immunocytochemical observations. *The Journal of neuroscience : the official journal of the Society for Neuroscience* **15:** 1835-1853

Lemberger T, Parkitna JR, Chai M, Schutz G, Engblom D (2008) CREB has a context-dependent role in activity-regulated transcription and maintains neuronal cholesterol homeostasis. *The FASEB journal : official publication of the Federation of American Societies for Experimental Biology* **22:** 2872-2879

Lensu S, Miettinen R, Pohjanvirta R, Linden J, Tuomisto J (2006) Assessment by c-Fos immunostaining of changes in brain neural activity induced by 2,3,7,8-tetrachlorodibenzo-p-dioxin (TCDD) and leptin in rats. *Basic & clinical pharmacology & toxicology* **98:** 363-371

Leverenz JB, Umar I, Wang Q, Montine TJ, McMillan PJ, Tsuang DW, Jin J, Pan C, Shin J, Zhu D, Zhang J (2007) Proteomic identification of novel proteins in cortical lewy bodies. *Brain Pathol* **17:** 139-145

Lewis MM, Watts VJ, Lawler CP, Nichols DE, Mailman RB (1998) Homologous desensitization of the D1A dopamine receptor: efficacy in causing desensitization dissociates from both receptor occupancy and functional potency. *The Journal of pharmacology and experimental therapeutics* **286:** 345-353

Li H, Durbin R (2009) Fast and accurate short read alignment with Burrows-Wheeler transform. *Bioinformatics (Oxford, England)* **25:** 1754-1760

Li X, Newbern JM, Wu Y, Morgan-Smith M, Zhong J, Charron J, Snider WD (2012) MEK Is a Key Regulator of Gliogenesis in the Developing Brain. *Neuron* **75:** 1035-1050

Lim S, Chun Y, Lee JS, Lee SJ (2016) Neuroinflammation in Synucleinopathies. *Brain Pathol* **26:** 404-409

Logrip ML, Zorrilla EP (2014) Differential changes in amygdala and frontal cortex Pde10a expression during acute and protracted withdrawal. *Frontiers in integrative neuroscience* **8:** 30

Lorenzen N, Nielsen SB, Buell AK, Kaspersen JD, Arosio P, Vad BS, Paslawski W, Christiansen G, Valnickova-Hansen Z, Andreasen M, Enghild JJ, Pedersen JS, Dobson CM, Knowles TP, Otzen DE (2014) The role of stable alpha-synuclein oligomers in the molecular events underlying amyloid formation. *Journal of the American Chemical Society* **136:** 3859-3868

Luk KC, Kehm V, Carroll J, Zhang B, O'Brien P, Trojanowski JQ, Lee VM (2012a) Pathological alpha-synuclein transmission initiates Parkinson-like neurodegeneration in nontransgenic mice. *Science* **338:** 949-953

Luk KC, Kehm VM, Zhang B, O'Brien P, Trojanowski JQ, Lee VM (2012b) Intracerebral inoculation of pathological alpha-synuclein initiates a rapidly progressive neurodegenerative alpha-synucleinopathy in mice. *The Journal of experimental medicine* **209:** 975-986

Luna E, Luk KC (2015) Bent out of shape: alpha-Synuclein misfolding and the convergence of pathogenic pathways in Parkinson's disease. *FEBS letters* **589:** 3749-3759

Ma J, Cui B, Ding X, Wei J, Cui L (2015) Over-Expression of Cyclin D1 Promotes NSCs Proliferation and Induces the Differentiation into Astrocytes Via Jak-STAT3 Pathways. *Neurochemical research* **40:** 1681-1690

Ma S, Kwon HJ, Johng H, Zang K, Huang Z (2013) Radial glial neural progenitors regulate nascent brain vascular network stabilization via inhibition of Wnt signaling. *PLoS biology* **11:** e1001469

Magavi S, Friedmann D, Banks G, Stolfi A, Lois C (2012) Coincident generation of pyramidal neurons and protoplasmic astrocytes in neocortical columns. *The Journal of neuroscience : the official journal of the Society for Neuroscience* **32:** 4762-4772

Malik AN, Vierbuchen T, Hemberg M, Rubin AA, Ling E, Couch CH, Stroud H, Spiegel I, Farh KK, Harmin DA, Greenberg ME (2014) Genome-wide identification and characterization of functional neuronal activity-dependent enhancers. *Nature neuroscience* **17:** 1330-1339

Manu P, Correll CU, van Winkel R, Wampers M, De Hert M (2012) Prediabetes in patients treated with antipsychotic drugs. *The Journal of clinical psychiatry* **73:** 460-466

Mao X, Ou MT, Karuppagounder SS, Kam TI, Yin X, Xiong Y, Ge P, Umanah GE, Brahmachari S, Shin JH, Kang HC, Zhang J, Xu J, Chen R, Park H, Andrabi SA, Kang SU, Goncalves RA, Liang Y, Zhang S, Qi C, Lam S, Keiler JA, Tyson J, Kim D, Panicker N, Yun SP, Workman CJ, Vignali DA, Dawson VL, Ko HS, Dawson TM (2016) Pathological alpha-synuclein transmission initiated by binding lymphocyte-activation gene 3. *Science* **353**

Marques O, Outeiro TF (2012) Alpha-synuclein: from secretion to dysfunction and death. *Cell death & disease* **3:** e350

Masliah E, Rockenstein E, Mante M, Crews L, Spencer B, Adame A, Patrick C, Trejo M, Ubhi K, Rohn TT, Mueller-Steiner S, Seubert P, Barbour R, McConlogue L, Buttini M, Games D, Schenk D (2011) Passive immunization reduces behavioral and neuropathological deficits in an alpha-synuclein transgenic model of Lewy body disease. *PLoS One* **6:** e19338

Masuda T, Prinz M (2016) Microglia: A Unique Versatile Cell in the Central Nervous System. *ACS chemical neuroscience*

Mauch DH, Nagler K, Schumacher S, Goritz C, Muller EC, Otto A, Pfrieger FW (2001) CNS synaptogenesis promoted by glia-derived cholesterol. *Science* **294:** 1354-1357

McCoy MK, Ruhn KA, Blesch A, Tansey MG (2011) TNF: a key neuroinflammatory mediator of neurotoxicity and neurodegeneration in models of Parkinson's disease. *Advances in experimental medicine and biology* **691:** 539-540

Medeiros R, LaFerla FM (2013) Astrocytes: conductors of the Alzheimer disease neuroinflammatory symphony. *Experimental neurology* **239:** 133-138

Megens AA, Hendrickx HM, Mahieu MM, Wellens AL, de Boer P, Vanhoof G (2014) PDE10A inhibitors stimulate or suppress motor behavior dependent on the relative activation state of the direct and indirect striatal output pathways. *Pharmacology research & perspectives* **2:** e00057

Melnikova VO, Dobroff AS, Zigler M, Villares GJ, Braeuer RR, Wang H, Huang L, Bar-Eli M (2010) CREB inhibits AP-2alpha expression to regulate the malignant phenotype of melanoma. *PLoS One* **5:** e12452

Mengel D, Thelen M, Balzer-Geldsetzer M, Soling C, Bach JP, Schaeffer E, Herold C, Becker T, Liepelt I, Becker J, Riedel-Heller S, Scherer M, Jessen F, Maier W, Dodel R, Ramirez A (2016) TREM2 rare variant p.R47H is not associated with Parkinson's disease. *Parkinsonism & related disorders* **23:** 109-111

Merchant KM, Hanson GR, Dorsa DM (1994) Induction of neurotensin and c-fos mRNA in distinct subregions of rat neostriatum after acute methamphetamine: comparison with acute haloperidol effects. *The Journal of pharmacology and experimental therapeutics* **269:** 806-812

Mitrousis N, Tropepe V, Hermanson O (2015) Post-Translational Modifications of Histones in Vertebrate Neurogenesis. *Frontiers in neuroscience* **9:** 483

Moehle MS, West AB (2015) M1 and M2 immune activation in Parkinson's Disease: Foe and ally? *Neuroscience* **302:** 59-73

Molnar T, Yarishkin O, Iuso A, Barabas P, Jones B, Marc RE, Phuong TT, Krizaj D (2016) Store-Operated Calcium Entry in Muller Glia Is Controlled by Synergistic Activation of TRPC and Orai Channels. *The Journal of neuroscience : the official journal of the Society for Neuroscience* **36:** 3184-3198

Molofsky AV, Deneen B (2015) Astrocyte development: A Guide for the Perplexed. *Glia* **63:** 1320-1329

Molofsky AV, Glasgow SM, Chaboub LS, Tsai HH, Murnen AT, Kelley KW, Fancy SP, Yuen TJ, Madireddy L, Baranzini S, Deneen B, Rowitch DH, Oldham MC (2013) Expression profiling of Aldh1l1-precursors in the developing spinal cord reveals glial lineage-specific genes and direct Sox9-Nfe2l1 interactions. *Glia* **61:** 1518-1532

Molofsky AV, Krencik R, Ullian EM, Tsai HH, Deneen B, Richardson WD, Barres BA, Rowitch DH (2012) Astrocytes and disease: a neurodevelopmental perspective. *Genes & development* **26:** 891-907

Montgomery SL, Bowers WJ (2012) Tumor necrosis factor-alpha and the roles it plays in homeostatic and degenerative processes within the central nervous system. *Journal of neuroimmune pharmacology : the official journal of the Society on NeuroImmune Pharmacology* **7:** 42-59

Moon JH, Kwon S, Jun EK, Kim A, Whang KY, Kim H, Oh S, Yoon BS, You S (2011) Nanog-induced dedifferentiation of p53-deficient mouse astrocytes into brain cancer stem-like cells. *Biochemical and biophysical research communications* **412:** 175-181

Mougenot AL, Nicot S, Bencsik A, Morignat E, Verchere J, Lakhdar L, Legastelois S, Baron T (2012) Prion-like acceleration of a synucleinopathy in a transgenic mouse model. *Neurobiology of aging* **33:** 2225-2228

Mukherjee J, Christian BT, Narayanan TK, Shi B, Mantil J (2001) Evaluation of dopamine D-2 receptor occupancy by clozapine, risperidone, and haloperidol in vivo in the rodent and nonhuman primate brain using 18F-fallypride. *Neuropsychopharmacology : official publication of the American College of Neuropsychopharmacology* **25:** 476-488

Nagao M, Sugimori M, Nakafuku M (2007) Cross talk between notch and growth factor/cytokine signaling pathways in neural stem cells. *Molecular and cellular biology* **27:** 3982-3994

Nakajima-Koyama M, Lee J, Ohta S, Yamamoto T, Nishida E (2015) Induction of Pluripotency in Astrocytes through a Neural Stem Cell-like State. *The Journal of biological chemistry* **290:** 31173-31188

Nakamura K, Mori F, Kon T, Tanji K, Miki Y, Tomiyama M, Kurotaki H, Toyoshima Y, Kakita A, Takahashi H, Yamada M, Wakabayashi K (2016) Accumulation of phosphorylated alpha-synuclein in subpial and periventricular astrocytes in multiple system atrophy of long duration. *Neuropathology : official journal of the Japanese Society of Neuropathology* **36:** 157-167

Nakashima K, Yanagisawa M, Arakawa H, Taga T (1999) Astrocyte differentiation mediated by LIF in cooperation with BMP2. *FEBS letters* **457:** 43-46

Naukkarinen J, Gentile M, Soro-Paavonen A, Saarela J, Koistinen HA, Pajukanta P, Taskinen MR, Peltonen L (2005) USF1 and dyslipidemias: converging evidence for a functional intronic variant. *Human molecular genetics* **14:** 2595-2605

Niccolini F, Foltynie T, Reis Marques T, Muhlert N, Tziortzi AC, Searle GE, Natesan S, Kapur S, Rabiner EA, Gunn RN, Piccini P, Politis M (2015) Loss of phosphodiesterase 10A expression is associated with progression and severity in Parkinson's disease. *Brain : a journal of neurology* **138:** 3003-3015

Nishi A, Kuroiwa M, Miller DB, O'Callaghan JP, Bateup HS, Shuto T, Sotogaku N, Fukuda T, Heintz N, Greengard P, Snyder GL (2008) Distinct roles of PDE4 and PDE10A in the regulation of cAMP/PKA signaling in the striatum. *The Journal of neuroscience : the official journal of the Society for Neuroscience* **28:** 10460-10471

Norris EH, Giasson BI, Hodara R, Xu S, Trojanowski JQ, Ischiropoulos H, Lee VM (2005) Reversible inhibition of alpha-synuclein fibrillization by dopaminochrome-mediated conformational alterations. *The Journal of biological chemistry* **280:** 21212-21219

Norwood J, Franklin JM, Sharma D, D'Mello SR (2014) Histone deacetylase 3 is necessary for proper brain development. *The Journal of biological chemistry* **289:** 34569-34582

Obayashi S, Tabunoki H, Kim SU, Satoh J (2009) Gene expression profiling of human neural progenitor cells following the serum-induced astrocyte differentiation. *Cellular and molecular neurobiology* **29:** 423-438

Oh J, McCloskey MA, Blong CC, Bendickson L, Nilsen-Hamilton M, Sakaguchi DS (2010) Astrocyte-derived interleukin-6 promotes specific neuronal differentiation of neural progenitor cells from adult hippocampus. *Journal of neuroscience research* **88:** 2798-2809

Oji Y, Yano M, Nakano Y, Abeno S, Nakatsuka S, Ikeba A, Yasuda T, Fujiwara Y, Takiguchi S, Yamamoto H, Fujita S, Kanato K, Ito K, Jomgeow T, Kawakami M, Tsuboi A, Shirakata T, Nishida S, Hosen N, Oka Y, Aozasa K, Monden M, Sugiyama H (2004) Overexpression of the Wilms' tumor gene WT1 in esophageal cancer. *Anticancer research* **24:** 3103-3108

Okazaki R, Doi T, Hayakawa K, Morioka K, Imamura O, Takishima K, Hamanoue M, Sawada Y, Nagao M, Tanaka S, Ogata T (2016) The crucial role of Erk2 in demyelinating inflammation in the central nervous system. *Journal of neuroinflammation* **13:** 235

Ottolini D, Cali T, Szabo I, Brini M (2017) Alpha-synuclein at the intracellular and the extracellular side: functional and dysfunctional implications. *Biological chemistry* **398:** 77-100

Painter MM, Atagi Y, Liu CC, Rademakers R, Xu H, Fryer JD, Bu G (2015) TREM2 in CNS homeostasis and neurodegenerative disease. *Molecular neurodegeneration* **10:** 43

Pal R, Tiwari PC, Nath R, Pant KK (2016) Role of neuroinflammation and latent transcription factors in pathogenesis of Parkinson's disease. *Neurological research* **38:** 1111-1122

Pardo L, Schluter A, Valor LM, Barco A, Giralt M, Golbano A, Hidalgo J, Jia P, Zhao Z, Jove M, Portero-Otin M, Ruiz M, Gimenez-Llort L, Masgrau R, Pujol A, Galea E (2016) Targeted activation of CREB in reactive astrocytes is neuroprotective in focal acute cortical injury. *Glia* **64:** 853-874

Park JY, Paik SR, Jou I, Park SM (2008) Microglial phagocytosis is enhanced by monomeric alpha-synuclein, not aggregated alpha-synuclein: implications for Parkinson's disease. *Glia* **56:** 1215-1223

Park PJ (2009) ChIP-seq: advantages and challenges of a maturing technology. *Nature reviews Genetics* **10:** 669-680

Parr-Brownlie LC, Hyland BI (2005) Bradykinesia induced by dopamine D2 receptor blockade is associated with reduced motor cortex activity in the rat. *The Journal of neuroscience : the official journal of the Society for Neuroscience* **25:** 5700-5709

Paxinos G, Watson C (2004) *The rat brain in stereotaxic coordinates*, Fifth edn.: 5th ed. Elsevier Academic Press.

Pernhorst K, Herms S, Hoffmann P, Cichon S, Schulz H, Sander T, Schoch S, Becker AJ, Grote A (2013) TLR4, ATF-3 and IL8 inflammation mediator expression correlates with seizure frequency in human epileptic brain tissue. *Seizure* **22:** 675-678

Perreault ML, Hasbi A, O'Dowd BF, George SR (2011) The dopamine d1-d2 receptor heteromer in striatal medium spiny neurons: evidence for a third distinct neuronal pathway in Basal Ganglia. *Frontiers in neuroanatomy* **5:** 31

Perry C, Sklan EH, Soreq H (2004) CREB regulates AChE-R-induced proliferation of human glioblastoma cells. *Neoplasia* **6:** 279-286

Pfrieger FW, Ungerer N (2011) Cholesterol metabolism in neurons and astrocytes. *Progress in lipid research* **50:** 357-371

Piccart E, De Backer JF, Gall D, Lambot L, Raes A, Vanhoof G, Schiffmann S, D'Hooge R (2014) Genetic deletion of PDE10A selectively impairs incentive salience attribution and decreases medium spiny neuron excitability. *Behavioural brain research* **268:** 48-54

Pickering M, O'Connor JJ (2007) Pro-inflammatory cytokines and their effects in the dentate gyrus. *Progress in brain research* **163:** 339-354

Pieri L, Chafey P, Le Gall M, Clary G, Melki R, Redeker V (2016) Cellular response of human neuroblastoma cells to alpha-synuclein fibrils, the main constituent of Lewy bodies. *Biochimica et biophysica acta* **1860:** 8-19

Pieri L, Madiona K, Bousset L, Melki R (2012) Fibrillar alpha-synuclein and huntingtin exon 1 assemblies are toxic to the cells. *Biophysical journal* **102:** 2894-2905

Pollen AA, Nowakowski TJ, Chen J, Retallack H, Sandoval-Espinosa C, Nicholas CR, Shuga J, Liu SJ, Oldham MC, Diaz A, Lim DA, Leyrat AA, West JA, Kriegstein AR (2015) Molecular identity of human outer radial glia during cortical development. *Cell* **163:** 55-67

Pollen AA, Nowakowski TJ, Shuga J, Wang X, Leyrat AA, Lui JH, Li N, Szpankowski L, Fowler B, Chen P, Ramalingam N, Sun G, Thu M, Norris M, Lebofsky R, Toppani D, Kemp DW, 2nd, Wong M, Clerkson B, Jones BN, Wu S, Knutsson L, Alvarado B, Wang J, Weaver LS, May AP, Jones RC, Unger MA, Kriegstein AR, West JA (2014) Low-coverage single-cell mRNA sequencing reveals cellular heterogeneity and activated signaling pathways in developing cerebral cortex. *Nature biotechnology* **32:** 1053-1058

Radford R, Rcom-H'cheo-Gauthier A, Wong MB, Eaton ED, Quilty M, Blizzard C, Norazit A, Meedeniya A, Vickers JC, Gai WP, Guillemin GJ, West AK, Dickson TC, Chung R, Pountney DL (2015) The degree of astrocyte activation in multiple system atrophy is inversely proportional to the distance to alpha-synuclein inclusions. *Mol Cell Neurosci* **65:** 68-81

Rannikko EH, Weber SS, Kahle PJ (2015) Exogenous alpha-synuclein induces toll-like receptor 4 dependent inflammatory responses in astrocytes. *BMC neuroscience* **16:** 57

Rash BG, Ackman JB, Rakic P (2016) Bidirectional radial Ca(2+) activity regulates neurogenesis and migration during early cortical column formation. *Science advances* **2:** e1501733

Rayaprolu S, Mullen B, Baker M, Lynch T, Finger E, Seeley WW, Hatanpaa KJ, Lomen-Hoerth C, Kertesz A, Bigio EH, Lippa C, Josephs KA, Knopman DS, White CL, 3rd, Caselli R, Mackenzie IR, Miller BL, Boczarska-Jedynak M, Opala G, Krygowska-Wajs A, Barcikowska M, Younkin SG, Petersen RC, Ertekin-Taner N, Uitti RJ, Meschia JF, Boylan KB, Boeve BF, Graff-Radford NR, Wszolek ZK, Dickson DW, Rademakers R, Ross OA (2013) TREM2 in neurodegeneration: evidence for association of the p.R47H variant with frontotemporal dementia and Parkinson's disease. *Molecular neurodegeneration* **8:** 19

Reed TM, Repaske DR, Snyder GL, Greengard P, Vorhees CV (2002) Phosphodiesterase 1B knock-out mice exhibit exaggerated locomotor hyperactivity and DARPP-32 phosphorylation in response to dopamine agonists and display impaired spatial learning. *The Journal of neuroscience : the official journal of the Society for Neuroscience* **22:** 5188-5197

Reiprich S, Wegner M (2015) From CNS stem cells to neurons and glia: Sox for everyone. *Cell and tissue research* **359:** 111-124

Rice JC, Allis CD (2001) Histone methylation versus histone acetylation: new insights into epigenetic regulation. *Current opinion in cell biology* **13:** 263-273

Robel S, Berninger B, Gotz M (2011) The stem cell potential of glia: lessons from reactive gliosis. *Nature reviews Neuroscience* **12:** 88-104

Robinson MD, McCarthy DJ, Smyth GK (2010) edgeR: a Bioconductor package for differential expression analysis of digital gene expression data. *Bioinformatics* **26:** 139-140

Rossi D, Volterra A (2009) Astrocytic dysfunction: insights on the role in neurodegeneration. *Brain research bulletin* **80:** 224-232

Russo I, Berti G, Plotegher N, Bernardo G, Filograna R, Bubacco L, Greggio E (2015) Leucine-rich repeat kinase 2 positively regulates inflammation and down-regulates NF-kappaB p50 signaling in cultured microglia cells. *Journal of neuroinflammation* **12:** 230

Sacchetti P, Sousa KM, Hall AC, Liste I, Steffensen KR, Theofilopoulos S, Parish CL, Hazenberg C, Richter LA, Hovatta O, Gustafsson JA, Arenas E (2009) Liver X receptors and oxysterols promote ventral midbrain neurogenesis in vivo and in human embryonic stem cells. *Cell stem cell* **5:** 409-419

Sacino AN, Brooks M, McGarvey NH, McKinney AB, Thomas MA, Levites Y, Ran Y, Golde TE, Giasson BI (2013) Induction of CNS alpha-synuclein pathology by fibrillar and non-amyloidogenic recombinant alpha-synuclein. *Acta neuropathologica communications* **1:** 38

Sanchez-Guajardo V, Barnum CJ, Tansey MG, Romero-Ramos M (2013a) Neuroimmunological processes in Parkinson's disease and their relation to alpha-synuclein: microglia as the referee between neuronal processes and peripheral immunity. *ASN neuro* **5:** 113-139

Sanchez-Guajardo V, Barnum CJ, Tansey MG, Romero-Ramos M (2013b) Neuroimmunological processes in Parkinson's disease and their relation to alpha-synuclein: microglia as the referee between neuronal processes and peripheral immunity. *ASN neuro*

Sanchez-Guajardo V, Tentillier N, Romero-Ramos M (2015) The relation between alpha-synuclein and microglia in Parkinson's disease: Recent developments. *Neuroscience* **302:** 47-58

Sasaki K, Doh-ura K, Wakisaka Y, Iwaki T (2002) Clusterin/apolipoprotein J is associated with cortical Lewy bodies: immunohistochemical study in cases with alpha-synucleinopathies. *Acta neuropathologica* **104:** 225-230

Saunders A, Faiola F, Wang J (2013) Concise review: pursuing self-renewal and pluripotency with the stem cell factor Nanog. *Stem Cells* **31:** 1227-1236

Savage JC, Jay T, Goduni E, Quigley C, Mariani MM, Malm T, Ransohoff RM, Lamb BT, Landreth GE (2015) Nuclear receptors license phagocytosis by trem2+ myeloid cells in mouse models of Alzheimer's disease. *The Journal of neuroscience : the official journal of the Society for Neuroscience* **35:** 6532-6543

Schindelin J, Arganda-Carreras I, Frise E, Kaynig V, Longair M, Pietzsch T, Preibisch S, Rueden C, Saalfeld S, Schmid B, Tinevez JY, White DJ, Hartenstein V, Eliceiri K, Tomancak P, Cardona A (2012) Fiji: an open-source platform for biological-image analysis. *Nature methods* **9:** 676-682

Schlierf B, Friedrich RP, Roerig P, Felsberg J, Reifenberger G, Wegner M (2007) Expression of SoxE and SoxD genes in human gliomas. *Neuropathol Appl Neurobiol* **33:** 621-630

Schmidt CJ (2012) Inhibition of Phosphodiesterase10A for the treatment of Schizophrenia: Preclinical Rationale and Clinical Evaluation [Abstract]. *ACNP 51st Annual Meeting*

Schmidt CJ, Chapin DS, Cianfrogna J, Corman ML, Hajos M, Harms JF, Hoffman WE, Lebel LA, McCarthy SA, Nelson FR, Proulx-LaFrance C, Majchrzak MJ, Ramirez AD, Schmidt K, Seymour PA, Siuciak JA, Tingley FD, 3rd, Williams RD, Verhoest PR, Menniti FS (2008) Preclinical characterization of selective phosphodiesterase 10A inhibitors: a new therapeutic approach to the treatment of schizophrenia. *The Journal of pharmacology and experimental therapeutics* **325:** 681-690

Schneider CA, Rasband WS, Eliceiri KW (2012) NIH Image to ImageJ: 25 years of image analysis. *Nature methods* **9:** 671-675

Scholze AR, Foo LC, Mulinyawe S, Barres BA (2014) BMP signaling in astrocytes downregulates EGFR to modulate survival and maturation. *PLoS One* **9:** e110668

Schroeder A, Mueller O, Stocker S, Salowsky R, Leiber M, Gassmann M, Lightfoot S, Menzel W, Granzow M, Ragg T (2006) The RIN: an RNA integrity number for assigning integrity values to RNA measurements. *BMC molecular biology* **7:** 3

Schulke JP, McAllister LA, Geoghegan KF, Parikh V, Chappie TA, Verhoest PR, Schmidt CJ, Johnson DS, Brandon NJ (2014) Chemoproteomics Demonstrates Target Engagement and Exquisite Selectivity of the Clinical Phosphodiesterase 10A Inhibitor MP-10 in Its Native Environment. *ACS chemical biology* **9:** 2823-2832

Scott DA, Tabarean I, Tang Y, Cartier A, Masliah E, Roy S (2010) A pathologic cascade leading to synaptic dysfunction in alpha-synuclein-induced neurodegeneration. *The Journal of neuroscience : the official journal of the Society for Neuroscience* **30:** 8083-8095

Seeger TF, Bartlett B, Coskran TM, Culp JS, James LC, Krull DL, Lanfear J, Ryan AM, Schmidt CJ, Strick CA, Varghese AH, Williams RD, Wylie PG, Menniti FS (2003) Immunohistochemical localization of PDE10A in the rat brain. *Brain Res* **985:** 113-126

Sehgal R, Sheibani N, Rhodes SJ, Belecky Adams TL (2009) BMP7 and SHH regulate Pax2 in mouse retinal astrocytes by relieving TLX repression. *Developmental biology* **332:** 429-443

Sery O, Sultana N, Kashem MA, Pow DV, Balcar VJ (2015) GLAST But Not Least--Distribution, Function, Genetics and Epigenetics of L-Glutamate Transport in Brain--Focus on GLAST/EAAT1. *Neurochemical research* **40:** 2461-2472

Shaked M, Weissmuller K, Svoboda H, Hortschansky P, Nishino N, Wolfl S, Tucker KL (2008) Histone deacetylases control neurogenesis in embryonic brain by inhibition of BMP2/4 signaling. *PLoS One* **3:** e2668

Sharma S, Kumar K, Deshmukh R, Sharma PL (2013) Phosphodiesterases: Regulators of cyclic nucleotide signals and novel molecular target for movement disorders. *European journal of pharmacology* **714:** 486-497

Shemer A, Erny D, Jung S, Prinz M (2015) Microglia Plasticity During Health and Disease: An Immunological Perspective. *Trends in immunology* **36:** 614-624

Shibata T, Yamada K, Watanabe M, Ikenaka K, Wada K, Tanaka K, Inoue Y (1997) Glutamate transporter GLAST is expressed in the radial glia-astrocyte lineage of developing mouse spinal cord. *The Journal of neuroscience : the official journal of the Society for Neuroscience* **17:** 9212-9219

Shrivastava AN, Redeker V, Fritz N, Pieri L, Almeida LG, Spolidoro M, Liebmann T, Bousset L, Renner M, Lena C, Aperia A, Melki R, Triller A (2015) alpha-synuclein assemblies sequester neuronal alpha3-Na+/K+-ATPase and impair Na+ gradient. *The EMBO journal* **34:** 2408-2423

Shrivastava AN, Redeker V, Fritz N, Pieri L, Almeida LG, Spolidoro M, Liebmann T, Bousset L, Renner M, Lena C, Aperia A, Melki R, Triller A (2016) Data in support of the identification of neuronal and astrocyte proteins interacting with extracellularly applied oligomeric and fibrillar alpha-synuclein assemblies by mass spectrometry. *Data in brief* **7:** 221-228

Simard M, Nedergaard M (2004) The neurobiology of glia in the context of water and ion homeostasis. *Neuroscience* **129:** 877-896

Simon-Sanchez J, Singleton A (2008) Genome-wide association studies in neurological disorders. *Lancet neurology* **7:** 1067-1072

Singleton AB, Farrer M, Johnson J, Singleton A, Hague S, Kachergus J, Hulihan M, Peuralinna T, Dutra A, Nussbaum R, Lincoln S, Crawley A, Hanson M, Maraganore D, Adler C, Cookson MR, Muenter M, Baptista M, Miller D, Blancato J, Hardy J, Gwinn-Hardy K (2003) alpha-Synuclein locus triplication causes Parkinson's disease. *Science* **302:** 841

Sirko S, Irmler M, Gascon S, Bek S, Schneider S, Dimou L, Obermann J, De Souza Paiva D, Poirier F, Beckers J, Hauck SM, Barde YA, Gotz M (2015) Astrocyte reactivity after brain injury-: The role of galectins 1 and 3. *Glia* **63:** 2340-2361

Siuciak JA (2008) The role of phosphodiesterases in schizophrenia : therapeutic implications. *CNS drugs* **22:** 983-993

Siuciak JA, McCarthy SA, Chapin DS, Fujiwara RA, James LC, Williams RD, Stock JL, McNeish JD, Strick CA, Menniti FS, Schmidt CJ (2006) Genetic deletion of the striatum-enriched phosphodiesterase PDE10A: evidence for altered striatal function. *Neuropharmacology* **51:** 374-385

Siuciak JA, McCarthy SA, Chapin DS, Martin AN, Harms JF, Schmidt CJ (2008) Behavioral characterization of mice deficient in the phosphodiesterase-10A (PDE10A) enzyme on a C57/Bl6N congenic background. *Neuropharmacology* **54:** 417-427

Skoff RP, Knapp PE (1991) Division of astroblasts and oligodendroblasts in postnatal rodent brain: evidence for separate astrocyte and oligodendrocyte lineages. *Glia* **4:** 165-174

Soliman ML, Combs CK, Rosenberger TA (2013) Modulation of inflammatory cytokines and mitogen-activated protein kinases by acetate in primary astrocytes. *Journal of neuroimmune pharmacology : the official journal of the Society on NeuroImmune Pharmacology* **8:** 287-300

Sotty F, Montezinho LP, Steiniger-Brach B, Nielsen J (2009) Phosphodiesterase 10A inhibition modulates the sensitivity of the mesolimbic dopaminergic system to D-amphetamine: involvement of the D1-regulated feedback control of midbrain dopamine neurons. *Journal of neurochemistry* **109:** 766-775

Spillantini MG, Crowther RA, Jakes R, Hasegawa M, Goedert M (1998) alpha-Synuclein in filamentous inclusions of Lewy bodies from Parkinson's disease and dementia with lewy bodies. *Proceedings of the National Academy of Sciences of the United States of America* **95:** 6469-6473

Stefanova N, Fellner L, Reindl M, Masliah E, Poewe W, Wenning GK (2011) Toll-like receptor 4 promotes alpha-synuclein clearance and survival of nigral dopaminergic neurons. *The American journal of pathology* **179:** 954-963

Steffensen KR, Jakobsson T, Gustafsson JA (2013) Targeting liver X receptors in inflammation. *Expert opinion on therapeutic targets* **17:** 977-990

Stipursky J, Francis D, Gomes FC (2012) Activation of MAPK/PI3K/SMAD pathways by TGF-beta(1) controls differentiation of radial glia into astrocytes in vitro. *Developmental neuroscience* **34:** 68-81

Stolp HB (2013) Neuropoietic cytokines in normal brain development and neurodevelopmental disorders. *Mol Cell Neurosci* **53:** 63-68

Stolt CC, Lommes P, Sock E, Chaboissier MC, Schedl A, Wegner M (2003) The Sox9 transcription factor determines glial fate choice in the developing spinal cord. *Genes & development* **17:** 1677-1689

Strick CA, James LC, Fox CB, Seeger TF, Menniti FS, Schmidt CJ (2010) Alterations in gene regulation following inhibition of the striatum-enriched phosphodiesterase, PDE10A. *Neuropharmacology* **58:** 444-451

Su X, Federoff HJ, Maguire-Zeiss KA (2009) Mutant alpha-synuclein overexpression mediates early proinflammatory activity. *Neurotoxicity research* **16:** 238-254

Su X, Maguire-Zeiss KA, Giuliano R, Prifti L, Venkatesh K, Federoff HJ (2008) Synuclein activates microglia in a model of Parkinson's disease. *Neurobiology of aging* **29:** 1690-1701

Subramanian L, Sarkar A, Shetty AS, Muralidharan B, Padmanabhan H, Piper M, Monuki ES, Bach I, Gronostajski RM, Richards LJ, Tole S (2011) Transcription factor Lhx2 is necessary and sufficient to suppress astrogliogenesis and promote neurogenesis in the developing hippocampus. *Proceedings of the National Academy of Sciences of the United States of America* **108:** E265-274

Sun F, He Z (2010) Neuronal intrinsic barriers for axon regeneration in the adult CNS. *Current opinion in neurobiology* **20:** 510-518

Sundquist SJ, Nisenbaum LK (2005) Fast Fos: rapid protocols for single- and double-labeling c-Fos immunohistochemistry in fresh frozen brain sections. *Journal of neuroscience methods* **141:** 9-20

Tabata H (2015) Diverse subtypes of astrocytes and their development during corticogenesis. *Frontiers in neuroscience* **9:** 114

Tanaka T, Murakami K, Bando Y, Yoshida S (2015) Interferon regulatory factor 7 participates in the M1-like microglial polarization switch. *Glia* **63:** 595-610

Tansey MG, Goldberg MS (2010) Neuroinflammation in Parkinson's disease: its role in neuronal death and implications for therapeutic intervention. *Neurobiol Dis* **37:** 510-518

Tao Y, Ruan H, Guo X, Li L, Shen W (2015) HDAC1 regulates the proliferation of radial glial cells in the developing Xenopus tectum. *PLoS One* **10:** e0120118

Tapia-Gonzalez S, Giraldez-Perez RM, Cuartero MI, Casarejos MJ, Mena MA, Wang XF, Sanchez-Capelo A (2011) Dopamine and alpha-synuclein dysfunction in Smad3 null mice. *Molecular neurodegeneration* **6:** 72

Taschenberger G, Garrido M, Tereshchenko Y, Bahr M, Zweckstetter M, Kugler S (2012) Aggregation of alphaSynuclein promotes progressive in vivo neurotoxicity in adult rat dopaminergic neurons. *Acta neuropathologica* **123:** 671-683

Taylor MK, Yeager K, Morrison SJ (2007) Physiological Notch signaling promotes gliogenesis in the developing peripheral and central nervous systems. *Development* **134:** 2435-2447

Theofilopoulos S, Wang Y, Kitambi SS, Sacchetti P, Sousa KM, Bodin K, Kirk J, Salto C, Gustafsson M, Toledo EM, Karu K, Gustafsson JA, Steffensen KR, Ernfors P, Sjovall J, Griffiths WJ, Arenas E (2013) Brain endogenous liver X receptor ligands selectively promote midbrain neurogenesis. *Nature chemical biology* **9:** 126-133

Thomsen ER, Mich JK, Yao Z, Hodge RD, Doyle AM, Jang S, Shehata SI, Nelson AM, Shapovalova NV, Levi BP, Ramanathan S (2016) Fixed single-cell transcriptomic characterization of human radial glial diversity. *Nature methods* **13:** 87-93

Thrash JC, Torbett BE, Carson MJ (2009) Developmental regulation of TREM2 and DAP12 expression in the murine CNS: implications for Nasu-Hakola disease. *Neurochemical research* **34:** 38-45

Threlfell S, Sammut S, Menniti FS, Schmidt CJ, West AR (2009) Inhibition of Phosphodiesterase 10A Increases the Responsiveness of Striatal Projection Neurons to Cortical Stimulation. *The Journal of pharmacology and experimental therapeutics* **328:** 785-795

Todd AG, Lin H, Ebert AD, Liu Y, Androphy EJ (2013) COPI transport complexes bind to specific RNAs in neuronal cells. *Human molecular genetics* **22:** 729-736

Tong J, Ang LC, Williams B, Furukawa Y, Fitzmaurice P, Guttman M, Boileau I, Hornykiewicz O, Kish SJ (2015) Low levels of astroglial markers in Parkinson's disease: relationship to alpha-synuclein accumulation. *Neurobiol Dis* **82:** 243-253

Toulorge D, Schapira AH, Hajj R (2016) Molecular changes in the postmortem parkinsonian brain. *Journal of neurochemistry*

Tousi NS, Buck DJ, Curtis JT, Davis RL (2012) alpha-Synuclein potentiates interleukin-1beta-induced CXCL10 expression in human A172 astrocytoma cells. *Neuroscience letters* **507:** 133-136

Trapnell C, Pachter L, Salzberg SL (2009) TopHat: discovering splice junctions with RNA-Seq. *Bioinformatics* **25:** 1105-1111

Trojanowski JQ, Lee VM (2002) Parkinson's disease and related synucleinopathies are a new class of nervous system amyloidoses. *Neurotoxicology* **23:** 457-460

Valera E, Ubhi K, Mante M, Rockenstein E, Masliah E (2014) Antidepressants reduce neuroinflammatory responses and astroglial alpha-synuclein accumulation in a transgenic mouse model of multiple system atrophy. *Glia* **62:** 317-337

Vazquez-Chona FR, Swan A, Ferrell WD, Jiang L, Baehr W, Chien WM, Fero M, Marc RE, Levine EM (2011) Proliferative reactive gliosis is compatible with glial metabolic support and neuronal function. *BMC neuroscience* **12:** 98

Villapol S, Wang Y, Adams M, Symes AJ (2013) Smad3 deficiency increases cortical and hippocampal neuronal loss following traumatic brain injury. *Experimental neurology* **250:** 353-365

Wakabayashi K, Hayashi S, Yoshimoto M, Kudo H, Takahashi H (2000) NACP/alpha-synuclein-positive filamentous inclusions in astrocytes and oligodendrocytes of Parkinson's disease brains. *Acta neuropathologica* **99:** 14-20

Wang Q, Liu Y, Zhou J (2015) Neuroinflammation in Parkinson's disease and its potential as therapeutic target. *Translational neurodegeneration* **4:** 19

Waterston RH, Lindblad-Toh K, Birney E, Rogers J, Abril JF, Agarwal P, Agarwala R, Ainscough R, Alexandersson M, An P, Antonarakis SE, Attwood J, Baertsch R, Bailey J, Barlow K, Beck S, Berry E, Birren B, Bloom T, Bork P, Botcherby M, Bray N, Brent MR, Brown DG, Brown SD, Bult C, Burton J, Butler J, Campbell RD, Carninci P, Cawley S, Chiaromonte F, Chinwalla AT, Church DM, Clamp M, Clee C, Collins FS, Cook LL, Copley RR, Coulson A, Couronne O, Cuff J, Curwen V, Cutts T, Daly M, David R, Davies J, Delehaunty KD, Deri J, Dermitzakis ET, Dewey C, Dickens NJ, Diekhans M, Dodge S, Dubchak I, Dunn DM, Eddy SR, Elnitski L, Emes RD, Eswara P, Eyras E, Felsenfeld A, Fewell GA, Flicek P, Foley K, Frankel WN, Fulton LA, Fulton RS, Furey TS, Gage D, Gibbs RA, Glusman G, Gnerre S, Goldman N, Goodstadt L, Grafham D, Graves TA, Green ED, Gregory S, Guigo R, Guyer M, Hardison RC, Haussler D, Hayashizaki Y, Hillier LW, Hinrichs A, Hlavina W, Holzer T, Hsu F, Hua A, Hubbard T, Hunt A, Jackson I, Jaffe DB, Johnson LS, Jones M, Jones TA, Joy A, Kamal M, Karlsson EK, Karolchik D, Kasprzyk A, Kawai J, Keibler E, Kells C, Kent WJ, Kirby A, Kolbe DL, Korf I, Kucherlapati RS, Kulbokas EJ, Kulp D, Landers T, Leger JP, Leonard S, Letunic I, Levine R, Li J, Li M, Lloyd C, Lucas S, Ma B, Maglott DR, Mardis ER, Matthews L, Mauceli E, Mayer JH, McCarthy M, McCombie WR, McLaren S, McLay K, McPherson JD, Meldrim J, Meredith B, Mesirov JP, Miller W, Miner TL, Mongin E, Montgomery KT, Morgan M, Mott R, Mullikin JC, Muzny DM, Nash WE, Nelson JO, Nhan MN, Nicol R, Ning Z, Nusbaum C, O'Connor MJ, Okazaki Y, Oliver K, Overton-Larty E, Pachter L, Parra G, Pepin KH, Peterson J, Pevzner P, Plumb R, Pohl CS, Poliakov A, Ponce TC, Ponting CP, Potter S, Quail M, Reymond A, Roe BA, Roskin KM,

Rubin EM, Rust AG, Santos R, Sapojnikov V, Schultz B, Schultz J, Schwartz MS, Schwartz S, Scott C, Seaman S, Searle S, Sharpe T, Sheridan A, Shownkeen R, Sims S, Singer JB, Slater G, Smit A, Smith DR, Spencer B, Stabenau A, Stange-Thomann N, Sugnet C, Suyama M, Tesler G, Thompson J, Torrents D, Trevaskis E, Tromp J, Ucla C, Ureta-Vidal A, Vinson JP, Von Niederhausern AC, Wade CM, Wall M, Weber RJ, Weiss RB, Wendl MC, West AP, Wetterstrand K, Wheeler R, Whelan S, Wierzbowski J, Willey D, Williams S, Wilson RK, Winter E, Worley KC, Wyman D, Yang S, Yang SP, Zdobnov EM, Zody MC, Lander ES (2002) Initial sequencing and comparative analysis of the mouse genome. *Nature* **420:** 520-562

Weimer JM, Yokota Y, Stanco A, Stumpo DJ, Blackshear PJ, Anton ES (2009) MARCKS modulates radial progenitor placement, proliferation and organization in the developing cerebral cortex. *Development* **136:** 2965-2975

Westphal CH, Chandra SS (2013) Monomeric synucleins generate membrane curvature. *The Journal of biological chemistry* **288:** 1829-1840

Wilson LS, Brandon NJ (2014) 'Emerging Biology of PDE10A'. *Current pharmaceutical design*

Winner B, Jappelli R, Maji SK, Desplats PA, Boyer L, Aigner S, Hetzer C, Loher T, Vilar M, Campioni S, Tzitzilonis C, Soragni A, Jessberger S, Mira H, Consiglio A, Pham E, Masliah E, Gage FH, Riek R (2011) In vivo demonstration that alpha-synuclein oligomers are toxic. *Proceedings of the National Academy of Sciences of the United States of America* **108:** 4194-4199

Wrasidlo W, Tsigelny IF, Price DL, Dutta G, Rockenstein E, Schwarz TC, Ledolter K, Bonhaus D, Paulino A, Eleuteri S, Skjevik AA, Kouznetsova VL, Spencer B, Desplats P, Gonzalez-Ruelas T, Trejo-Morales M, Overk CR, Winter S, Zhu C, Chesselet MF, Meier D, Moessler H, Konrat R, Masliah E (2016) A de novo compound targeting alpha-synuclein improves deficits in models of Parkinson's disease. *Brain : a journal of neurology*

Wu KC, Liu JJ, Klaassen CD (2012) Nrf2 activation prevents cadmium-induced acute liver injury. *Toxicology and applied pharmacology* **263:** 14-20

Xu P, Guo L, Tang X, Xu H, Fan X (2011) ERbeta may contribute to the maintaining of radial glia cells polarity through cadherins during corticogenesis. *Medical hypotheses* **77:** 974-976

Xu S, Grullon S, Ge K, Peng W (2014) Spatial clustering for identification of ChIP-enriched regions (SICER) to map regions of histone methylation patterns in embryonic stem cells. *Methods Mol Biol* **1150:** 97-111

Yamaguchi M, Seki T, Imayoshi I, Tamamaki N, Hayashi Y, Tatebayashi Y, Hitoshi S (2016) Neural stem cells and neuro/gliogenesis in the central nervous system: understanding the structural and functional plasticity of the developing, mature, and diseased brain. *The journal of physiological sciences : JPS* **66:** 197-206

Yamamoto M, Kamatsuka Y, Ohishi A, Nishida K, Nagasawa K (2013) P2X7 receptors regulate engulfing activity of non-stimulated resting astrocytes. *Biochemical and biophysical research communications* **439:** 90-95

Yeh FL, Wang Y, Tom I, Gonzalez LC, Sheng M (2016) TREM2 Binds to Apolipoproteins, Including APOE and CLU/APOJ, and Thereby Facilitates Uptake of Amyloid-Beta by Microglia. *Neuron* **91:** 328-340

Young AB, Penney JB (1984) Neurochemical anatomy of movement disorders. *Neurologic clinics* **2:** 417-433

Yu T, Cao G, Feng L (2006) Low temperature induced de-differentiation of astrocytes. *Journal of cellular biochemistry* **99:** 1096-1107

Yu ZQ, Zhang BL, Ni HB, Liu ZH, Wang JC, Ren QX, Mo JB, Xiong Y, Yao RQ, Gao DS (2014) Hyperacetylation of histone H3K9 involved in the promotion of abnormally high transcription of the gdnf gene in glioma cells. *Molecular neurobiology* **50:** 914-922

Yuan H, Zhang ZW, Liang LW, Shen Q, Wang XD, Ren SM, Ma HJ, Jiao SJ, Liu P (2010) Treatment strategies for Parkinson's disease. *Neuroscience bulletin* **26:** 66-76

Zamanian JL, Xu L, Foo LC, Nouri N, Zhou L, Giffard RG, Barres BA (2012) Genomic analysis of reactive astrogliosis. *The Journal of neuroscience : the official journal of the Society for Neuroscience* **32:** 6391-6410

Zang C, Schones DE, Zeng C, Cui K, Zhao K, Peng W (2009) A clustering approach for identification of enriched domains from histone modification ChIP-Seq data. *Bioinformatics* **25:** 1952-1958

Zhang BL, Ni HB, Liu J, Lei Y, Li H, Xiong Y, Yao R, Yu ZQ, Gao DS (2014a) Egr-1 participates in abnormally high gdnf gene transcription mediated by histone hyperacetylation in glioma cells. *Biochimica et biophysica acta* **1839:** 1161-1169

Zhang L, He X, Liu L, Jiang M, Zhao C, Wang H, He D, Zheng T, Zhou X, Hassan A, Ma Z, Xin M, Sun Z, Lazar MA, Goldman SA, Olson EN, Lu QR (2016a) Hdac3 Interaction with p300 Histone Acetyltransferase Regulates the Oligodendrocyte and Astrocyte Lineage Fate Switch. *Developmental cell* **36:** 316-330

Zhang Y, Chen K, Sloan SA, Bennett ML, Scholze AR, O'Keeffe S, Phatnani HP, Guarnieri P, Caneda C, Ruderisch N, Deng S, Liddelow SA, Zhang C, Daneman R, Maniatis T, Barres BA, Wu JQ (2014b) An RNA-sequencing transcriptome and splicing database of glia, neurons, and vascular cells of the cerebral cortex. *The Journal of neuroscience : the official journal of the Society for Neuroscience* **34:** 11929-11947

Zhang Y, Reinberg D (2001) Transcription regulation by histone methylation: interplay between different covalent modifications of the core histone tails. *Genes & development* **15:** 2343-2360

Zhang Y, Sloan SA, Clarke LE, Caneda C, Plaza CA, Blumenthal PD, Vogel H, Steinberg GK, Edwards MS, Li G, Duncan JA, 3rd, Cheshier SH, Shuer LM, Chang EF, Grant GA, Gephart MG, Barres BA (2016b) Purification and Characterization of Progenitor and Mature Human Astrocytes Reveals Transcriptional and Functional Differences with Mouse. *Neuron* **89:** 37-53

Zhou M, Schools GP, Kimelberg HK (2006) Development of GLAST(+) astrocytes and NG2(+) glia in rat hippocampus CA1: mature astrocytes are electrophysiologically passive. *Journal of neurophysiology* **95:** 134-143

Zhou W, Long C, Reaney SH, Di Monte DA, Fink AL, Uversky VN (2010a) Methionine oxidation stabilizes non-toxic oligomers of alpha-synuclein through strengthening the auto-inhibitory intra-molecular long-range interactions. *Biochimica et biophysica acta* **1802:** 322-330

Zhou ZD, Kumari U, Xiao ZC, Tan EK (2010b) Notch as a molecular switch in neural stem cells. *IUBMB life* **62:** 618-623

Zhou ZD, Lim TM (2009) Dopamine (DA) induced irreversible proteasome inhibition via DA derived quinones. *Free radical research* **43:** 417-430

Zhu X, Bergles DE, Nishiyama A (2008) NG2 cells generate both oligodendrocytes and gray matter astrocytes. *Development* **135:** 145-157

Zinchuk V, Zinchuk O, Okada T (2007) Quantitative colocalization analysis of multicolor confocal immunofluorescence microscopy images: pushing pixels to explore biological phenomena. *Acta histochemica et cytochemica* **40:** 101-111

VITA

EDUCATION

Doctor of Philosophy, Indiana University-Purdue University Indianapolis, Indianapolis, IN., Graduation May 2017, Developmental Neurobiology, Concentration in Regenerative Neurobiology.

Master of Science, Indiana University-Purdue University Indianapolis, Indianapolis, IN., Graduation May 2007, Developmental and Cell Biology, Concentration in Regenerative Neurobiology.

Bachelor of Science, Marian College, Indianapolis, IN., Graduated May 2005, Major in Biology, Minor in Chemistry

EXPERIENCE

Consultant Biologist, Neuroscience, Eli Lilly and Company, Indianapolis, IN March 2016-Present

Associate Consultant Biologist, Tailored Therapeutics, Eli Lilly and Company, Indianapolis, IN March 2012-Present

Senior Biologist, Translational Science, Eli Lilly and Company, Indianapolis, IN March 2010-March 2012

Senior Toxicologist, Toxicology, Eli Lilly and Company, Indianapolis, IN March 2009-March 2010

Toxicologist, Toxicology, Eli Lilly and Company, Indianapolis, IN October 2007-March 2009

Graduate Researcher, Regenerative and Developmental Neurobiology Laboratory. Department of Biology, Indiana University-Purdue University Indianapolis, Indianapolis, IN. August 2005-October 2007

Teaching Assistant, Department of Biology, Indiana University-Purdue University Indianapolis, Indianapolis, IN. August 2005-May 2007

Research Technician, Regenerative and Developmental Neurobiology Laboratory. Indiana University Center for Regenerative Biology and Medicine, Indiana University-Purdue University Indianapolis, Indianapolis, IN. June 2005-August 2005

Developmental Toxicology-Teratology Internship, Lilly Research Laboratories, Eli Lilly and Co., Greenfield, IN., May 2004-August 2004

Clinical Pathology Laboratory Technician, Lilly Research Laboratories, Eli Lilly and Co., Greenfield, IN., May 2002-August 2002

SELECTED PEER-REVIEWED PUBLICATIONS

Wilson, J.M., Ogden, A.M.L., Loomis, S., Gilmour, G., Baucum II., A.J., Belecky-Adams, T.L., Merchant, K.M. (2015) Phosphodiesterase 10A inhibitor, MP-10 (PF-2545920), produces greater induction of c-Fos in dopamine D2 neurons than in D1 neurons in the neostriatum, Neuropharmacology 99, 379-386.

Smith, Rosamund C., O'Bryan, Linda M., Mitchell, Pamela J., Leung, Donmienne, Ghanem, Mahmoud, Wilson, Jonathan M., Hanson, Jeff C., Sossick, Sandra, Cooper, Jane, Huang, Lihua, Merchant, Kalpana M., Lu, Jirong, O'Neill, Michael J. (2015) Increased Brain Bio-distribution and Chemical Stability and Decreased Immunogenicity of an Engineered Variant of GDNF, Experimental Neurology 267, 165-176.

Yaden BC, Wang Y, Croy J, Milner A, Wilson JM, Shetler P, Dai G, and Krishnan VK (2014) Inhibition of activin A ameliorates skeletal muscle injury and rescues contractile properties in mice. Am. J. Pathol.

Yaden BC, Croy JE, Wang Y, Wilson JM, Datta-Mannan A, Shetler P, Milner A, Andrews J, Bryant HU, Dai G, and Krishnan V. (2014) Follistatin: a novel therapeutic for the improvement of muscle regeneration. Am. J. Pharmacol. And Exp. Therapeutics.

Teri L. Belecky-Adams, Ellen C. Chernoff, Jonathan M. Wilson and Subramanian Dharmarajan (2013). Reactive Muller Glia as Potential Retinal Progenitors, Neural Stem Cells - New Perspectives, Dr. Luca Bonfanti (Ed.), ISBN: 978-953-51-1069-9, InTech, DOI: 10.5772/55150. Available from: http://www.intechopen.com/books/neural-stem-cells-new-perspectives/reactive-muller-glia-as-potential-retinal-progenitors

Smith, Rosamund C., Bryan, Linda M., Farrow, Emily G., Summers, Lelia J., Clinkenbeard, Erica L., Roberts, Jessica L., Cass, Taryn A., Saha, Joy, Broderick, Carol, Ma, Y. Linda, Zeng, Qing Qiang, Kharitonenkov, Alexei, Wilson, Jonathan M., Guo, Qianxu, Sun, Haijun, Allen, Matthew R., Burr, David B., Breyer, Matthew D., White, Kenneth E. (2012). "Circulating αKlotho influences phosphate handling by controlling FGF23 production." J Clin Invest 122(12): 4710-4715

Long GG, Goodman DG, Credille KM, Mann PC, Wilson JM, Cardy R. 2010. Hematopoietic Proliferative Lesions in the Spleen of rasH2 Transgenic Mice Treated with MNU. Toxicol Pathol. Sept: 38(7):1026-1036

Wilson JM, Martinez-De Luna RI, El Hodiri HM, Smith RC, King MW, Mescher AL, Neff AW, Belecky-Adams TL. 2010. RNA helicase Ddx39 is expressed in the developing central nervous system, limb, otic vesicle, branchial arches and facial meneschyme of Xenoupus laevis. Gene Expr Patterns. Jan: 10(1):44-52

Belecky-Adams TL, Haynes T, Wilson JM, Del Rio-Tsonis K. “The Chick as a Model for Retina Development and Regeneration” Animal Models in Eye Research. 2009 Elsevier, Ltd. Chapter 8, 102-115

Wilson JM, Sato K, Chernoff EAG, Belecky-Adams TL. 2007. Expression Patterns of Chick Musashi-1 in the Developing Nervous System. Gene Expr Patterns. Aug: 7(7):817-25

PRESENTATIONS

Wilson JM, Chavali K, Wang H, Belecky-Adams TL, Merchant KM (2016) Fibrillar but not monomeric alpha-synuclein induces pro-inflammatory phenotypes but both conformers increase phagocytosis via the TREM2 receptor in microglial cells. Annual IUPUI Biology Departmental Retreat. Bradford Woods, IN

Wilson JM, Chavali K, Wang H, Belecky-Adams TL, Merchant KM (2016) Fibrillar but not monomeric alpha-synuclein induces pro-inflammatory phenotypes but both conformers increase phagocytosis via the TREM2 receptor in microglial cells. World Parkinson Congress. Portland, OR

Wilson JM (2016) Characterization of Neuroinflammatory Pathophysiology of Parkinson's disease. LRL Grand Rounds Seminar. Indianapolis, IN

Wilson JM (2015) Astrocyte Development and Regulation of Inflammatory Pathways. Oral Platform Presentation. Annual IUPUI Biology Departmental Retreat. Bradford Woods, IN

Hum, JM, O'Bryan L, Tatiparthi A, Johnson RL, Wilson JM, Clinkenbeard EL, Cass TA, Smith RC, White KE (2015) Sustained expression of a soluble form of αKlotho prevents aortic calcification and disease phenotypes during chronic hyperphosphatemia. ASMBR. Seattle, Washington

Wilson JM, Li L, Hayashi ML, Ruble C, Hersley CA, Wang H, Belecky-Adams TL, Merchant KM (2015) α-Synuclein Seeding in Inducible Cell Models With or Without Inflammatory Context. Grand Challenges in Parkinson's Disease: The Role of α-Synuclein, Van Andel Research Institute, Grand Rapids, Michigan

Wilson JM, Rash K, Czilli D, Need A, Eessalu T, Barth V, Ryder J, Chavali B (2015) Absence of Synuclein Pathology in a Toxin-Free Castrated Mouse Model. Grand Challenges in Parkinson's Disease: The Role of α-Synuclein, Van Andel Research Institute, Grand Rapids, Michigan

Hum, JM, O'Bryan L, Tatiparthi A, Johnson RL, Wilson JM, Clinkenbeard EL, Cass TA, Smith RC, White KE (2015) Prevention of aortic calcification and disease phenotypes during chronic hyperphosphatemia by sustained expression of a soluble form of αKlotho. ORS 45th International Sun Valley Workshop: Musculoskeletal Biology. Sun Valley, Idaho

O'Neill MJ, O'Bryan LM, Leung D, Ghanem M, Wilson JM, Hanson JC, Sossick S, Cooper J, Huang L, Merchant KM, Lu J, Smith RC (2014) Increased Chemical Stability, Brain Bio-Distribution and Decreased Immunogenicity of an Engineered Variant of GDNF. Neuroscience 2014. Washington, D.C.

Smith RC, O'Bryan L, Mitchell P, Leung D, Ghanem M, Wilson JM, Hanson JC, Sossick S, Cooper J, Merchant KM, Lu J, O'Neill MJ (2014) Reduction of Heparin Binding of GDNF improves Brain Bio-Distribution while Maintaining In Vitro and In Vivo Activity. Neuroscience 2014. Washington, D.C.

Wilson JM, Rao S, Liu J, Wang Z, Liu Y, Belecky-Adams TL (2014) Genome-Wide Comparison of Acetylated H3K9 Regions of Chromatin in Murine GLAST+ Progenitors and Developing Astrocytes with a Focus on Inflammatory Genes. FASEB SRC 2014. Big Sky, MT

Smith RC, O'Bryan L, Mitchell P, Leung D, Ghanem M, Wilson JM, Hanson JC, Sossick S, Cooper J, Merchant KM, Lu J, O'Neill MJ (2014) Reduction of Heparin Binding of GDNF improves Brain Bio-Distribution while Maintaining In Vitro and In Vivo Activity. 18th International Congress of Parkinson's Disease and Movement Disorders. Stockholm, Sweden

Wang Y, Yaden BC, Wilson JM, Shetler P, Gifondorwa D, Milner A, Ballman K, Bryant H, Krishnan V (2013) IL-15Ra Antibody Preserved Skeletal Muscle Weight and Decrease in Fat Mass Following Denervated Injury. Neuroscience 2013. San Diego, CA

Harlan SM, Yang DD, Wilson JM, Breyer MD, Heuer JG. (2013) Human and Mouse EGF Ligand and Receptor Expression in Chronic Kidney Disease. American Society of Nephrology. Atlanta, GA

Yaden BC, Wang Y, Wilson JM, Ryan A, Skljarevski A, Croy JE, Dai G, Krishnan V (2013) Mac25 Promotes Muscle Hypertrophy by Coordinating both IGFII and TGFb Pathways. American Physical Society. Denver, CO

Wang Y, Yaden BC, Datta-Mannan A, Wilson JM, Croy JE, Shetler P, Milner A, Dai G, Krishnan V (2014) Neutralization of Activin A Improves Skeletal Muscle Regeneration Following Muscle Injury Muscle. Keystone Symposia – Growth and Wasting in Heart and Skeletal Muscle. Santa Fe, NM

Wilson JM, Yaden BC, Belecky-Adams TL, Merchant KM. (2013) The Direct Inflammatory Effects of Alpha-Synuclein on Microglia in Combination with Astrocytes. Annual Biology Departmental Retreat. Bradford Woods, IN

Wilson, JM, Yaden BC, Belecky-Adams TL, Merchant KM. (2013) The Direct Inflammatory Effects of Alpha-Synuclein on Microglia in Combination with Astrocytes. Grand Challenges in Parkinson's Disease. Grand Rapids, MI

Wilson J.M. (2011) "Automated IHC Methodology in Research". The Annual Indiana Society of Histotechnology Meeting. Indianapolis, IN. March 2011.

Wilson J.M., King M.W., Mescher A.L., Neff A.W., Belecky-Adams T.L. (2007) "Ddx39 in developing and regenerating Xenopus retina" The Association for Research in Vision and Ophthalmology 2007 Annual Meeting, Ft. Lauderdale, FL. May 2007.

Wilson J.M., Sato K., Chernoff E.A.G., Belecky-Adams T.L. (2006) "Expression Patterns of Chick Musashi-1 in the Developing Chick Retina" 9th Annual Great Lakes Vision Research Conference, Ann Arbor, MI. November 2006.

Wilson J.M., Sato K., Chernoff E.A.G., Belecky-Adams T.L. (2006) "Expression of RNA binding protein, Msi-1, in developing chick retina" The Association for Research in Vision and Opthalmology 2006 Annual Meeting, Ft. Lauderdale, FL. May 2006.

Wilson J.M., Sato K., Chernoff E.A.G., Belecky-Adams T.L. (2005) "Expression of RNA binding protein, MSI, in developing chick retina" 8th Annual Great Lakes Vision Research Conference, Cincinnati, OH. November 2005.

Wilson, J.M., Astroff, B., (2005) "Chronological Fetal Development in Mice, Rats and Rabbits" 17th Annual Butler Undergraduate Research Conference. April 2005.

Wilson, J.M. (2005). "Greener SN1 Reaction" 1st Annual Marian College Undergraduate Research Symposium in Chemistry. April 2005.
Presentation available at: http://chemphys.marian.edu/greenchem/Sn1.pdf

Wilson, J.M., Fultz, B. (2005) "Relationship between Beaver Canals and Beaver Signs" EcoLab Research Conference on the Campus of Marian College. March 2005.